UNIVERSITY OF BELGRADE
SCHOOL OF ELECTRICAL ENGINEERING

Nemanja M. Lučić

Light propagation in deterministic aperiodic waveguide arrays

Doctoral Dissertation

Belgrade, 2016.

УНИВЕРЗИТЕТ У БЕОГРАДУ
ЕЛЕКТРОТЕХНИЧКИ ФАКУЛТЕТ

Немања М. Лучић

Пропагација светлости у детерминистичким апериодичним низовима таласовода

Докторска дисертација

Београд, 2016.

Committee members

PhD Dejan Gvozdić, thesis advisor
Full Professor
School of Electrical Engineering, University of Belgrade

PhD Jasna Crnjanski, thesis advisor
Assistant Professor
School of Electrical Engineering, University of Belgrade

PhD Dejan Timotijević
Full Research Professor
Institute of Physics, University of Belgrade

PhD Zoran Jakšić
Full Research Professor
Institute of Chemistry, Technology and Metallurgy, University of Belgrade

PhD Slobodan Petričević
Associate Professor
School of Electrical Engineering, University of Belgrade

Day of the defense:

To my friends

Firstly, I would like to express my sincere gratitude to my professors and my thesis committee for the knowledge having been communicated, for their well-minded critics and evidenced patience. My sincere thanks to my colleagues for the help in my work, precious peaces of advice and inspirational discussions. Thanks to my friends for the appreciation and support. Last, but not least, thanks to Senka for giving sense to everything I do.

Nemanja M. Lučić

Belgrade, June 23th, 2016.

Захваљујем се професорима и члановима Комисије на пренесеном знању, добронамерним критикама и показаном стрпљењу. Захваљујем се колегама на помоћи у раду, драгоценим саветима и инспиративним дискусијама. Захваљујем се пријатељима на разумевању и подршци. Захваљујем се Сенки, јер даје смисао свему што радим.

Немања М. Лучић

Београд, 23. јун 2016.

Light propagation in deterministic aperiodic waveguide arrays

Abstract

Over the past two decades, the light transport properties in regular (periodic) and disordered coupled waveguides have been extensively scrutinized. These two, in a sense, opposite types of ordering lead to two different phenomena - discrete diffraction in regular arrays, where light energy spreads linearly along propagation direction, and transverse localization in disordered, where light energy is distributed between finite number of adjacent waveguides. Still an open question remains whether light behavior in intermediate domain is between fully periodic and fully disordered structures - deterministic structures with no periodicity.

In this thesis the impact of deterministic aperiodic one-dimensional (1D) and two-dimensional (2D) coupled waveguide arrays (photonic lattices) on transverse light transport has been investigated both experimentally and numerically. Several types of lattices were considered: 1D and 2D position modulated Fibonacci lattices, 1D refractive index contrast modulated Fibonacci lattice, 1D regular lattice and regular lattice with defect. The aim is to explore the possibility of using these structures as a tool for light diffraction suppression.

In the experiment, waveguide arrays were generated in photorefractive crystals, lithium-niobate and strontium-barium-niobate, by direct laser writing and incoherent Bessel beam induction technique, respectively. Gaussian and Airy beam were used as excitation beams. A series of numerical simulations were conducted using Beam Propagation Method.

It is found that the position modulated Fibonacci lattice can suppress light diffraction in comparison to the regular one. This is more pronounced in 1D than in 2D lattice. In 1D case, for relatively high refractive index contrasts, the propagating beam becomes almost completely localized in transverse plane. In 1D refractive index contrast modulated Fibonacci lattice the similar result is obtained - diffraction is suppressed considerably comparing to regular lattice. Furthermore, the stronger modulation leads to strongly localized states, so the light propagation in Fibonacci

lattice resembles the propagation in disordered one. Besides, it is shown that the slightly disordered Fibonacci lattice with relatively small refractive index contrast modulation enhances diffraction. In addition, it is shown that a regular lattice can reduce a self-bending of Airy beam trajectory.

The research presented in the thesis provides additional standpoint in understanding of light transport in complex optical structures and imposes new ways for control of light diffraction and engineering of the optical response of devices.

Keywords: photonic crystals, deterministic aperiodic structures, discrete diffraction, transverse light localization

Scientific field: Electrical and Computer Engineering

Research area: Nanoelectronics and Photonics

UDC number: 621.3

Пропагација светлости у детерминистичким апериодичним низовима таласовода

Резиме

У претходне две деценије, простирање светлости у регуларним (периодичним) и неуређеним спрегнутим таласоводима је интензивно проучавано. Ова два, на неки начин супротна типа уређења, одговорна су за два различита феномена - дискретну дифракцију у регуларним низовима, где се енергија светлости шири линеарно дуж правца пропагације, и трансверзалну локализацију у неуређеним низовима, где је светлосна енергија распоређена у коначном броју суседних таласовода. Још увек је отворено питање понашања светлости у области између сасвим периодичних и сасвим неуређених структура - детерминистичким структурама без периодичности.

У овој тези је експериментално и нумерички проучаван утицај детерминистичких апериодичних једнодимензионих (1Д) и дводимензионих (2Д) низова спрегнутих таласовода (фотонских решетки) на трансверзалну пропагацију светлости. Разматрано је неколико типова решетки: 1Д и 2Д Фибоначи решетке са модулисаним међусобним растојањем суседних таласовода, 1Д Фибоначи решетка са модулисаним контрастом индекса преламања, 1Д регуларна решетка и регуларна решетка са дефектом. Циљ је да се испита могућност коришћења ових структура као механизма за потискивање дифракције светлости.

У експерименту, низови таласовода су реализовани у фоторефрактивним кристалима, литијум-ниобату и стронцијум-баријум-ниобату, техникама директног ласерског уписивања и некохерентном индукцијом Беселовим зрацима, респективно. Структуре су побуђиване гаусовским и Ејри снопом. Серије нумеричких симулација су спроведене техником пропагације зрака.

Утврђено је да Фибоначи решетка са модулисаним положајем може да потисне дифракцију светлости, у поређењу са регуларном решетком. Овај ефекат је израженији у 1Д него у 2Д решеткама. У 1Д случају, за релативно високе контрасте индекса преламања пропагирајући сноп бива готово сасвим локализован у трансверзалној равни. У 1Д Фибоначи решетки са модулисаним кон-

трастом индексом преламања добија се сличан резултат - дифракција је значајно потиснута у поређењу са регуларном решетком. Такође, јача модулација води до јаче локализације, тако да пропагација светлости у Фибоначи решетки личи на пропагацију у неуређеној решетки. Поред тога, показује се да мала неуређеност у Фибоначи решетки са релативно малом модулацијом контраста индекса преламања појачава дифракцију. Утврђено је и да регуларна решетка може да умањи ефекат савијања трајекторије Ејри зрака.

Истраживање приказано у тези пружа додатне аспекте у разумевању простирања светлости у комплексним оптичким структурама, као и нови приступ у контроли дифракције и дизајну оптичких уређаја.

Кључне речи: фотонски кристали, детерминистичке апериодичне структуре, дискретна дифракција, трансверзална локализација светлости

Научна област: Електротехничко и рачунарско инжењерство

Ужа научна област: Наноелектроника и фотоника

УДК број: 621.3

Contents

List of Figures **xiii**

1 Introduction **1**

2 General properties of deterministic aperiodic structures **14**

2.1 About periodicity, aperiodicity and disorder 14

2.2 Wave propagation in periodic, aperiodic and disordered structures . . 19

3 Diffraction in waveguide arrays **25**

3.1 The coupled-mode theory 26

3.2 The Floquet-Bloch theory 29

3.3 Diffraction in disordered waveguide arrays 30

4 Numerical tools for treatment of light propagation in waveguide arrays **33**

4.1 Basic equation of BPM 34

4.2 Numerical implementation of FD-BPM 36

5 Experimental methods for photonic structures generation and characterization **39**

5.1 Photorefractivity 39

5.1.1 Properties of lithium-niobate and strontium-barium-niobate . 42

5.2 Generation and characterization of waveguide arrays 43

5.2.1 1D arrays 43

5.2.2 2D arrays 47

6 Results and discussion **52**

6.1 Light propagation in position modulated 1D Fibonacci lattice 52

6.2 Light propagation in position modulated 2D Fibonacci lattice 57

6.3 Light propagation in refractive index modulated 1D Fibonacci lattice 61
6.4 Airy beam propagation in 1D regular lattice with defect 63

7 Conclusions and outlook **67**

A Difference equations of implicit FD-BPM based on Crank-Nicolson algorithm **69**

Bibliography **74**

Biography **87**

List of publications **88**

List of Figures

1.1 Extended and localized eigenstates in different media 4
1.2 Diffraction pattern taken from a single grain of the icosahedral phase 6
1.3 Fibonacci dielectric multilayer 7
1.4 The transmission spectrum of a Fibonacci multilayer 8
1.5 Electron micrographs of fabricated 3D icosahedral silicon quasicrystal structure 9
1.6 Transverse electric field and light intensity distribution of 1D Airy beam 10
1.7 1D Airy beam - longitudinal intensity profile 11

2.1 Quasiperiodic function $f(x) = \cos(x) + \cos(\alpha x)$ 16
2.2 Lattices and corresponding diffraction patterns 17
2.3 A lattice spectrum of three different deterministic aperiodic 1D structures 18
2.4 Dispersion relation 21
2.5 Light waves transport through disordered medium 22
2.6 Localized state 23
2.7 Critical wave function one-dimensional Fibonacci lattice 24

3.1 Diffraction in continuous and periodic medium 25
3.2 Anomalous refraction and diffraction in one-dimensional periodic lattice 28
3.3 Reduced band-gap diagram of a typical waveguide array 30
3.4 The beam profile evolution in regular and disordered lattice with off-diagonal disorder 32

4.1 Discretization of a space in finite-difference method 36

5.1 Illustration of 1D waveguide array writing process 43
5.2 Array of the waveguides seen under microscope 44

5.3 Scheme of experimental setup for one-dimensional waveguide array diagnostics . . . 44
5.4 The light intensity distribution acquisition . . . 45
5.5 Scheme of experimental setup for 1D waveguide array excitation by Airy beam . . . 46
5.6 1D Airy beam generation . . . 46
5.7 2D waveguide array writing . . . 49
5.8 Scheme of the experimental setup for 2D waveguide array generation and diagnostics . . . 50
5.9 The excitation of the 2D Fibonacci lattice . . . 51

6.1 The refractive index profile of 1D Fibonacci waveguides array . . . 52
6.2 Light propagation through 1D Fibonacci waveguide array - on-site excitation . . . 53
6.3 Light propagation in 1D Fibonacci waveguide array - between sites excitation . . . 54
6.4 Comparison between beam diffraction in periodic and quasi-periodic waveguide arrays . . . 55
6.5 Light propagation in Fibonacci lattice for a higher refractive index contrast . . . 56
6.6 2D Fibonacci lattice . . . 57
6.7 Light propagation through 2D Fibonacci lattice for three different input positions . . . 58
6.8 The square lattice induced by the Bessel beam multiplexing technique 59
6.9 Exciting beam input positions according to the first neighbors arrangement . . . 60
6.10 The comparison of the effective beam width - 2D Fibonacci lattice vs. square lattice . . . 60
6.11 The refractive index profile of diagonal disordered Fibonacci and random lattice . . . 61
6.12 Effective beam width in 1D Fibonacci and random lattice for different levels of aperiodicity . . . 62
6.13 Effective beam width in 1D Fibonacci lattice for different levels of superimposed disorder . . . 63
6.14 Airy beam propagation - refractive index profiles . . . 64

6.15 Airy beam propagation in homogeneous medium and in the regular lattice 65
6.16 Airy beam propagation in the lattice with negative and positive defect 65

Chapter 1

Introduction

The notion of structural order underlies our understanding of properties of most physical systems. A crystal structure is the best example of a periodically ordered pattern in nature. It consists of a certain atomic configuration (base) which repeats in space according to an underlying periodic pattern (periodic lattice).

The microscopic regularity of crystalline matter was long hypothesized as the obvious way to explain the simple geometric regularities of macroscopic crystals (Aschroft and Mermin, 1976). The first direct experimental confirmation was obtained in 1913 through the work of William Lawrence Bragg and William Henry Bragg (Bragg and Bragg, 1913). They showed in their X-ray diffraction experiment that the patterns of X-radiation scattered from crystalline materials possessed sharp intensity peaks (now known as *Bragg peaks*) for certain sharply defined wavelengths and incident directions, which was an unambiguous verification of a structure periodicity.

Taking the advantage of the simplicity of the periodic order and the quantum mechanical approach, and by treating an electron as a wave (*de Broglie waves*), Felix Bloch explained the electrical conductivity of metal in his groundbreaking paper in 1928 (Bloch, 1928). This approach has paved the way to the development of the band theory of the electronic structure of solids, that explained why electrons of some energies travelled through a periodic potential without scattering[1], and why electrons of some other energies were forbidden to propagate in certain directions. This theory has established the concepts of *energy spectrum*, *energy gap* and *Brillouin zone* as the base for the understanding of physical properties of solids.

From the above mentioned, the impact of the periodicity of the lattice on the

[1] In the case of no defects and impurities were presented.

wave nature of electrons manages the properties of a material. On the other hand, the interplay between waves and periodicity is not the exclusivity of the condensed matter physics. These ideas can be applied to any of elastic or electromagnetic waves in the corresponding periodic media without any restrictions.

In the domain of optics, periodicity refers to a periodic modulation of the refractive index (or, equivalently, dielectric constant) of a medium in one or more spatial dimensions. If the period of modulation is comparable with the wavelength of light, the absorptivity of material low and the refractive index contrast high enough, the *photonic band gaps* are formed, meaning that the propagation of light of certain wavelength in certain directions is prohibited, while for the other wavelengths the structure is almost fully transparent. Here, photons are affected by the structure in much the same way as electrons are by a crystal lattice. Structures formed in this way are denoted as *photonic crystals*. The fact that the photonic band gaps can be formed by the choice in a very simple way, by selecting an adequate period and refractive index contrast of the lattice, gives an opportunity for the full control of a light flow.

The physical mechanism behind this behavior is an interference of a partially reflected light from interfaces of two materials of a different permittivity. The first explanation of this phenomenon has been proposed by Lord Rayleigh in 1917 in his paper about the reflection of light from a stack of alternating layers of transparent materials of different refractive index values (Lord Rayleigh, 1917)[1]. However, the scientific community paid more attention to this topic in the late $1980s$ and the $1990s$. The work of Eli Yablonovitch, see e.g. Yablonovitch (1987) and Yablonovitch and Gmitter (1989), implied the vast potential of this research field and spurred the intense exploring and exploiting of periodicity effects in photonics.

Today, periodic structures are widely used in photonic devices, just to mention Fabry-Perot filters (Joannopoulos *et al.*, 2008), vertical-cavity surface-emitting lasers (Lee *et al.*, 2004), omnidirectional reflectors (Fink *et al.*, 1998), photonic crystal fibers (Russell, 2003).

Despite the immense significance of the periodicity and the energy bands theory in physics, it has a momentous drawback. Namely, the (ideal) periodicity in real life is an exception, rather then the rule. In almost every structure the *disorder* is present in a varying degree. It may be a weakly disordered system, e.g. a monocrystal with

[1]This idea has been introduced by Lord Rayleigh in 1887 considering reflection of mechanical waves. (Lord Rayleigh, 1887)

a few impurities or vacancies, or strongly disordered ones, such as alloys and glassy materials. It turns out that in these systems the concept of energy bands is not valid. Instead of extended Bloch modes, in disordered systems waves are localized within restricted regions.

The concept of the wave localization in a disordered potential is introduced in 1958 by Philip Anderson, in his seminal paper entitled *Absence of diffusion in certain random lattices*, Anderson (1958). The traditional viewpoint had been that scattering by the random potential cause the Bloch waves to lose phase coherence on the length scale of the mean free path [1]. Nevertheless, the wavefunction remains extended throughout the sample (Lagendijk *et al.*, 2009, Lee and Ramakrishnan, 1985). Anderson noticed that if the disorder is strong enough, the wavefunction may become localized. When the electron is placed on one atom, its wavefunction will not expand to cover the whole crystal with time, but it will remain localized around its initial position (Segev *et al.*, 2013). In this situation the electron becomes trapped and the conductivity vanishes.

The Anderson localization is in essence a wave phenomenon, that arises entirely from coherent multiple scattering and interference, so similar behavior should also be observed in other classical coherent wave systems, such as acoustic and electromagnetic (Lagendijk *et al.*, 2009).

There are several experiments that verified a presence of Anderson localization in acoustic systems. He and Maynard demonstrated it in one-dimensional (1D) system, consisting of small lead masses spaced along a long thin steel wire (He and Maynard, 1986). The amplitude of transverse waves along the wire, generated by electromechanical actuator at one end, was measured. If equivalent masses were equidistantly spaced, the Bloch states were obtained. If the positions of masses, or the sizes of masses were randomized, the localized states occurred (cf. Fig.1.1a). Similarly, two-dimensional (2D) localized states were observed in an inhomogeneous 30 centimeter square aluminum plate excited by ultrasound (Weaver, 1990), while localized states in a three-dimensional (3D) system were measured in a 3-D elastic network of aluminum beads excited also by ultrasound (Hu *et al.*, 2008).

Nevertheless, optics appeared as an ideal playground to study localization effects, considering two facts: first, the coherence of optical waves in appropriate dielectric microstructures is naturally preserved (time-invariant structures), and second, photons are bosons, meaning inherently non-interacting particles (Segev *et al.*, 2013).

[1] the average length an electron travels before it collides with a positive ion in metal lattice site

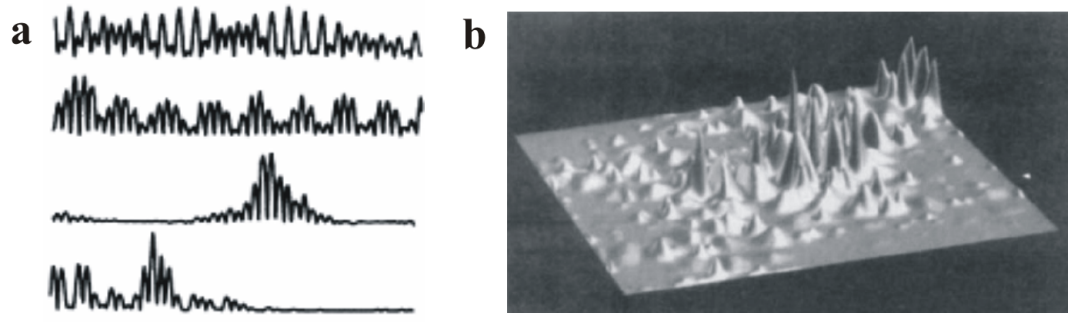

Figure 1.1: Extended and localized states in different media. a) Eigenstate amplitude as a function of position along wire (1D system) - the first two are extended (Bloch) states in regular system and the second two are localized states in disordered system, (He and Maynard, 1986), b) The electric field energy density of microwave radiation localized states in 2D disordered system (Dalichaouch *et al.*, 1991).

The excellent theoretical works of Sajeev John (John, 1984, 1987) initiated the first experiments that investigated propagation of electromagnetic waves in random media. Localized microwave modes were observed in 2D space, a random array of dielectric cylinders placed between a pair of parallel conducting plates (cf. Fig.1.1b) (Dalichaouch *et al.*, 1991). Presence of localized optical waves in tree-dimensional space was confirmed measuring transmission parameters of light passing through samples made of strongly scattering semiconductor powders (Wiersma *et al.*, 1997). In recent years optical systems have been playing an important role in the fundamental understanding and experimental observation of Anderson localization because of many techniques that can be used to *visualize* this phenomenon (Mafi, 2015).

A particularly interesting form of light localization is the so-called *transverse localization*, first introduced in Abdullaev and Abdullaev (1980) and Raedt *et al.* (1989). In this concept, the index of refraction is a random function in xy plane but is uniform in z direction. If a light beam propagates in the z direction, it will expand until the beam diameter becomes of the order of the transverse localization length. From then on, the beam propagates without further expansion. This approach led to the first direct observation of Anderson localization in 2D disordered lattices, reported in Schwartz *et al.* (2007), as well as in 1D disordered lattices, reported in Lahini *et al.* (2008). Besides the pure theoretical importance, the transverse Anderson localization has been appearing as an attractive device-level concept, e.g. in imaging systems (Karbasi *et al.*, 2014).

During the last decades, the structures that cannot be properly described by the concept of periodicity or disorder have emerged. The explanation of their properties

has required a new concept - *order without periodicity*. The building blocks of these structures are arranged according to a *deterministic* rule, but without translational symmetry.

The notion of the *aperiodic order* has been a relevant topic in mathematics for a long time (Sigler, 2002). However, it had almost no impact in all other scientific fields. The aperiodic order gained in importance during the $1940's$, when the nature of genetic material was one of the uppermost scientific topics. Erwin Schrödinger proposed that genetic material should be composed of a long sequence of a few recurring constituents exhibiting a well-defined order without periodic repetition. He termed it as the *aperiodic crystal* (Schrödinger, 1945). To quote the author itself: "Organic chemistry, indeed, in investigating more and more complicated molecules, has come very much nearer to that *aperiodic crystal* which, in my opinion, is the material carrier of life.".

On the contrary, the aperiodic order hadn't been accepted in the condensed matter community for a few more decades. The reason is a sufficiency of the crystalline-amorphous matter dichotomy (i.e. periodic-disordered dichotomy), meaning that the periodicity allowed convenient explanation of the most relevant features of crystals. A deficiency of this concept unambiguously appeared in 1984.

Namely, crystal structures are mathematically described in 3D space by their 32 point-group symmetries. Despite the fact that there are 230 different types of crystallographic space-groups, only 32 of them have translational symmetry[1] (Dal Negro and Boriskina, 2012, Duan and Guojun, 2005). This is one of the most important results of classical crystallography, known as crystallographic restriction. The consequence was that only rotational symmetries of order 2, 3, 4 and 6 were allowed in periodic lattice (Barber, 2009). Hence, e.g. five-fold rotational symmetry, widely found in the living world, could not exist in condensed matter [2].

The major breakthrough in an anticipation of condensed matter happened when Dan Shechtman and coworkers discovered *quasicrystals* (Shechtman *et al.*, 1984). They reported the existence of a five-fold symmetry in certain Al-Mn alloys, as shown in Fig.1.2. An analysis of the obtained spectra indicated the icosahedral point group symmetry, which was inconsistent with lattice translations. On the other hand, the

[1] Point-groups describe the symmetry of finite figures, excluding translation as a symmetry element.

[2] At that time, materials containing icosahedral units, which is not allowed crystal point group, were discovered, but these materials exhibited global symmetries of proper periodic order (Maciá, 2006)

intense sharpness of the diffraction spots indicated the long-range order, as in the case of ordinary crystals. Soon, there followed the theoretical explanation, provided by Levine and Steinhardt in Levine and Steinhardt (1984). There, they introduced the notion of a *quasiperiodic crystal*, because the spatial order of these structures was described in terms of *quasiperiodic functions*[1]. In years after, a number of works reporting the existence of new quasicrystals characterized by the presence of different types of non-crystallographic symmetry axes appeared (Barber, 2009).

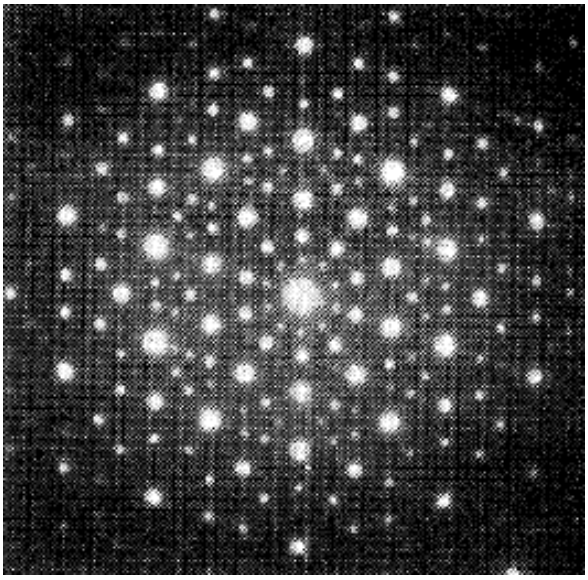

Figure 1.2: Diffraction pattern taken from a single grain of the icosahedral phase (Shechtman *et al.*, 1984).

Soon after, the notion of quasiperiodic order was extended from the atomic scale to the submicrometer scale. In 1985, Merlin and coworkers reported the first realization of a quasiperiodic superlattice, consisting of alternating layers of GaAs and AlAs forming a Fibonacci sequence in which the ratio of incommensurate periods is equal to the golden mean[2] (Merlin *et al.*, 1985). The sample, grown by molecular-beam epitaxy, composed of 377 bilayers had a thickness of $\sim 1.85\ \mu m$. The X-ray diffraction pattern showed a significant number of peaks superimposed to the main satellite reflection of the GaAs layers which occur in a geometric progression with the golden ratio as the common ratio[3], indicating the so called self-similarity of the lattice spectrum. This guarantees the existence of suitable resonant conditions at all scales (Maciá, 2006), implying the fragmented energy band structure of the sys-

[1] Quasicrystals are one of three types of aperiodic crystals (Janssen *et al.*, 2007).
[2] The golden mean or the golden ratio is an irrational number equal to $\left(1+\sqrt{5}\right)/2$.
[3] As a reminder, for a periodic superlattice the distance between successive peaks is constant.

tem. The subsequent research showed the particular electron transport properties of quasiperiodic heterostructures (Katsumoto *et al.*, 1993, Toet *et al.*, 1991, Yamaguchi *et al.*, 1990).

The idea of aperiodic order also initiated a new research direction in photonics.

The first example of a deterministic aperiodic system in optics was the 1D quasicrystal structure, consisting of optical layers following the Fibonacci sequence (cf. Fig.1.3), proposed by Kohmoto and coworkers in Kohmoto *et al.* (1987). The calculated transmission spectrum of the structure (Fig.1.4) showed the *multifractal* nature, what was the consequence of the existence of the so-called *critical* modes. Later on, the Fibonacci multilayer system became intensively studied concerning its reflectivity (Schwartz, 1988), photonic dispersion relation (Hattori *et al.*, 1994), scaling (multifractal) (Fujiwara *et al.*, 1989) and localization (Capaz *et al.*, 1990, Gellermann *et al.*, 1994, Maciá and Dominguez-Adame, 1996) properties. Besides, the Thue-Morse lattice was investigated in the same manner, theoretically (Liu, 1997), as well as experimentally (Dal Negro *et al.*, 2004).

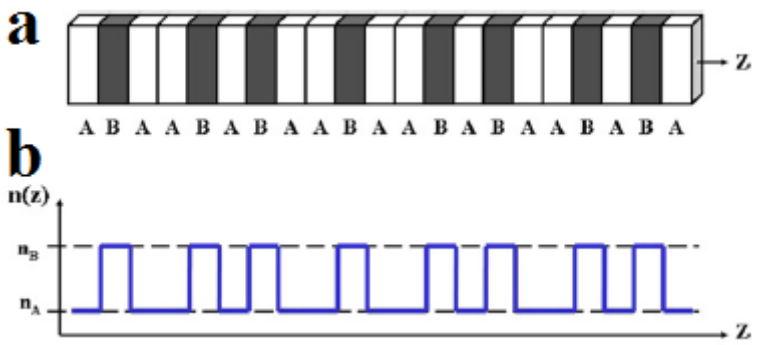

Figure 1.3: Fibonacci dielectric multilayer (Maciá, 2012). a) Fibonacci dielectric multilayer grown along the z direction. b) Refractive index profile $n(z)$ for an electromagnetic wave propagating through the structure.

The concept was extended in two dimensions. The first theoretical studies, e.g. of the Fibonacci system (Fu *et al.*, 1991, Lifshitz, 2002) or 12−fold symmetric system (Chan *et al.*, 1998), were followed by the experimental ones, e.g of Penrose-tiled (Kaliteevski *et al.*, 2000) or the 12−fold symmetric (Zoorob *et al.*, 2000) photonic quasicrystals. The realization of 3D photonic quasicrystal (Fig.1.5) has been achieved as well (Ledermann *et al.*, 2006).

The photonic quasicrystals were also considered in the terms of the *transverse transport properties*. In that sense, the first experiment, treated linear and nonlinear light propagation in decagonal symmetry (Freedman *et al.*, 2006). Nonetheless,

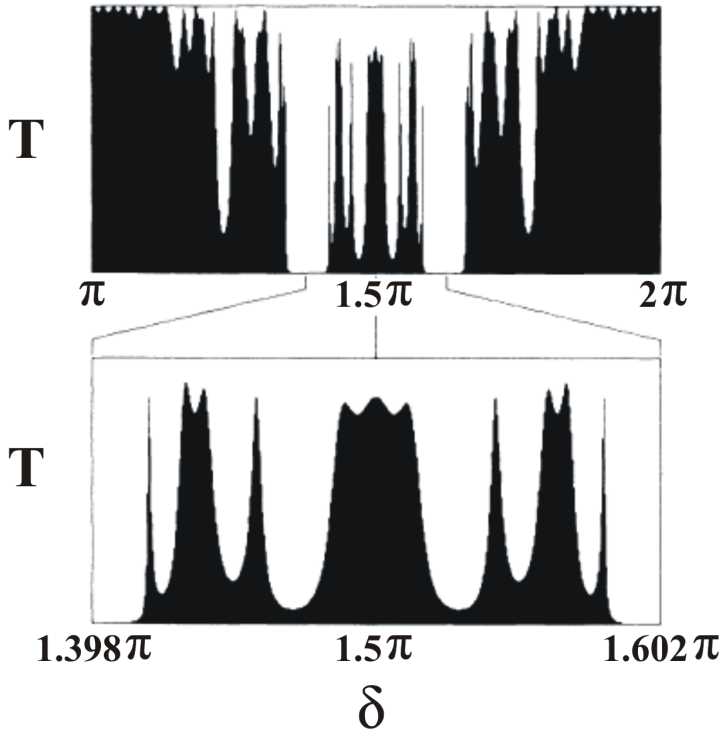

Figure 1.4: The transmission spectrum of a Fibonacci multilayer (Kohmoto *et al.*, 1987). The transmission coefficient T versus the optical phase length of a layer δ for a Fibonacci multilayer consisting of 55 layers of two materials with refractive indices 2 and 3.

in 2011 Levi and coworkers reported, while studying Penrose lattice, a seemingly counterintuitive property of disorder-enhanced transport in photonic quasicrystals (Levi *et al.*, 2011). They showed that a disorder introduced in the quasiperiodic lattice can increase the transverse transport, which contrasts directly with the characteristic suppression of transport by disorder. Considering 1D crystals, Lahini and coworkers reported the signature of a localization phase transition for light quasiperiodic Aubry-André photonic lattice (Lahini *et al.*, 2009), while Verbin and coworkers reported an interesting phenomenon of topological pumping in Fibonacci lattice (Verbin *et al.*, 2015).

The peculiar properties of deterministic aperiodic structures impose the question of their application. Their reflection spectra make them serious candidates in optical microcavities (Maciá, 1998) and multidirectional reflection devices (Barriuso *et al.*, 2005). The first observed coherent lasing action due to the optical feedback from quasiperiodicity was reported by Notomi and coworkers in 2004 (Notomi *et al.*, 2004). An optically pumped active medium, an SiO_2 substrate with holes arranged in Penrose manner covered by a DCM (a laser dye) doped Alq_3 (an

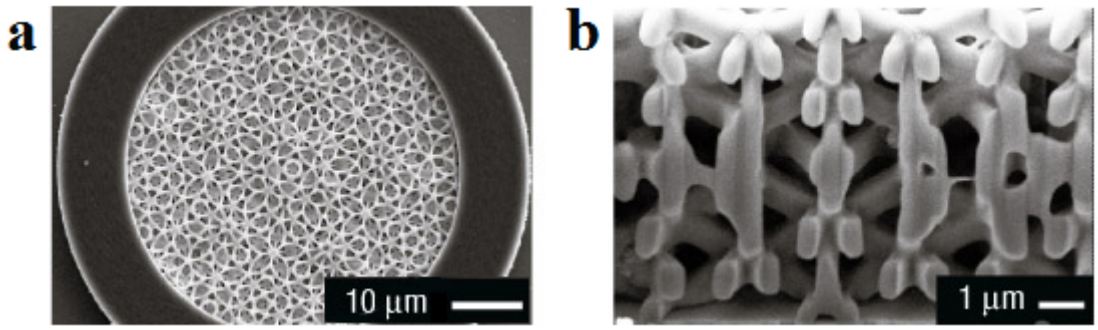

Figure 1.5: Electron micrographs of fabricated 3D icosahedral silicon quasicrystal structure. a) A top view, b) A side view of cut structure (Ledermann *et al.*, 2006).

organic gain medium) layer, generated a variety of 10-fold-symmetric lasing spot patterns. Mahler *et al.* demonstrated lasing in 1D photonic crystal by current injection (Mahler *et al.*, 2010). It was a terahertz quantum cascade laser based on a Fibonacci distributed feedback sequence, which allowed features beyond those possible with traditional periodic resonators, such as directional output independent of the emission frequency and multicolour operation.

The wealth of their Fourier's spectrum suggests potential advantages in nonlinear optics applications. Using the 1D Fibonacci optical superlattice the second harmonic generation is achieved the conversion efficiency of which is comparable with those of a periodic superlattice, but on multiple wavelength (Zhu, Zhu, Qin, Wang, Ge and Ming, 1997). In the same configuration a third harmonic generation efficiency turned out to be eight times higher then that realized in the periodic superlattice (Zhu, Zhu and Ming, 1997). Fibonacci photonic quasicrystals showed the ability of simultaneously phase matching several nonlinear optical interactions within a single sample in one (Fradkin-Kashi *et al.*, 2002) and two (Lifshitz *et al.*, 2005) dimensions. Significant light-emission enhancement effects at multiple wavelengths were experimentally observed in a 1D multilayer SiN_x/SiO_2 Thue-Morse structure, yielding a total emission enhancement of almost a factor of 6 in comparison to homogeneous light-emitting SiN_x samples (Dal Negro *et al.*, 2005).

One of the aspects of a medium arrangement impact on a light flow is the previously mentioned *transverse transport*. It refers to a coherent light beam evolution propagating along an array of coupled waveguides. In this configuration the refractive index is uniform along the propagation direction and modulated in the transverse plane.

The beam propagation in the system of this type can be modeled by paraxial

Helmholtz equation. Because of a formal analogy between paraxial Helmholtz equation and the Schrödinger equation, the evolution of a light beam in space resembles a behavior of a wave packet of a quantum particle in time (Segev *et al.*, 2013). This is why this analogy has been used to confirm theoretical predictions of solid-state physics in the optical set-ups. Apropos, Bloch oscillations (Morandotti *et al.*, 1999, Pertsch *et al.*, 1999), Zener tunneling (Trompeter *et al.*, 2006) and Rabi oscillations (Shandarova *et al.*, 2009) were experimentally observed. Besides, the light propagation through modulated (Garanovich *et al.*, 2012) or nonlinear (Christodoulides *et al.*, 2003) waveguide arrays have been imposing themselves as the appealing research topics.

The previously mentioned research about transverse light transport were essentially investigations of possibilities to control (and eventually totally suppress) diffraction by a specific position arrangement of waveguides. Another, in some sense, a complementary issue, is the impact of waveguide arrays on initially nondiffracting beams.

The term *nondiffracting beam* denotes a monochromatic optical field whose transverse intensity profile remains unchanged in free-space propagation (Bouchal, 2003). It is introduced in 1987 by Durnin and coworkers, when they realized experimentally the first beam of such characteristics (Durnin *et al.*, 1987). Today, this beam is known as Bessel beam, because its transverse intensity profile can be described by the zeroth-order Bessel function of the first kind. Later on, several classes of nondiffracting beams have been found, one of which are named Airy beams because the transverse electric field profile of the beam follows Airy function (Fig.1.6).

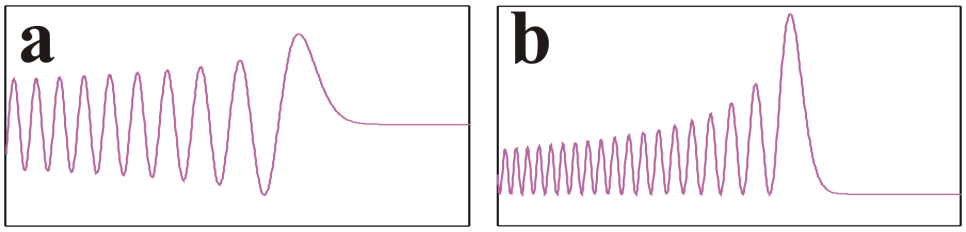

Figure 1.6: Transverse electric field and light intensity distribution of 1D Airy beam. a) Airy function - electric field distribution, b) Squared Airy function - light intensity distribution.

It is important to note that in real situations the nondiffracting beams cannot be realized because they carry an infinite energy. In experiments, only approximations known as *pseudo-nondiffracting* beams can be obtained (Bouchal, 2003)[1].

[1]The nondiffracting and pseudo-nondiffracting beams are sometimes denoted as *ideal* and *real*

The first experimental realization of Airy beams was reported in 2007 by Siviloglou and coworkers, where their ability to remain diffraction-free over long distances while they tend to freely accelerate (parabolic trajectory) during propagation was demonstrated (Siviloglou *et al.*, 2007). The parabolic longitudinal bending and transverse intensity profile are shown in Fig.1.7. Furthermore, Airy beams possess self-healing properties, preserving their parameters in different scattering and turbulent media (Broky *et al.*, 2008).

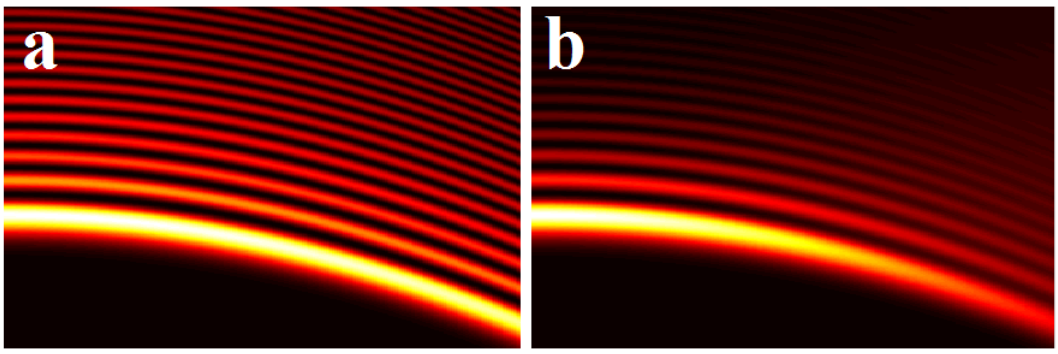

Figure 1.7: 1D Airy beam - longitudinal intensity profile. a) *Ideal* Airy beam. b) *Real* Airy beam.

These beams were shown to be useful for the generation of curved plasma channels in air (Polynkin *et al.*, 2009), for optical micro-manipulation of small particles (Baumgartl *et al.*, 2008) and for femtosecond laser micromachining of curved profiles in diamond and silicon (Mathis *et al.*, 2012).

This thesis summarizes the results of an experimental and numerical study of light propagation in arrays of coupled waveguides (photonic lattices). The research subjects are deterministic aperiodic photonic lattices arranged according to the Fibonacci sequence (Boguslawski *et al.*, 2016, Lučić *et al.*, 2015), as well as regular lattices with defects (Lučić *et al.*, 2013). Regarding the Fibonacci lattices, the goal is to determine the impact of this specific arrangement on transverse light transport, i.e. whether and to what extent these structures suppress diffraction and lead to localization. Concerning the regular lattice with and without defect, the intention is to determine its impact on a parabolic path and the transverse profile of the 1D Airy beam.

Here, the study of deterministic aperiodic photonic lattices refers to analysis of waveguide arrays whose values of geometrical or material parameters follow the Fi-

nondifracting beams, respectively.

bonacci sequence. The attention is paid to 1D and 2D arrays of identical waveguides arranged in such a way that the distances of adjacent waveguides obey the Fibonacci sequence, or to arrays of equidistant waveguides whose refractive index contrast is modulated by the Fibonacci sequence. The effective waist of the beam propagating in these lattices has been compared to the same parameter in regular lattices in order to find out if they suppress diffraction and in what degree, or if they can lead to localization.

Additionally, propagation of Airy beams has been investigated in a regular lattice and a regular with a negative (one waveguide left out) and a positive (one waveguide with doubled refractive index contrast) defect. The transverse acceleration and beam shape after the propagation through these three lattices has been compared to the same parameters of Airy beam propagating in homogenous medium.

The research presented in this thesis is based on several assumptions: (1) Fibonacci photonic lattices suppress diffraction and can lead to transverse localization, (2) presence of disorder in the Fibonacci lattice inhibits diffraction suppression, and (3) the regular lattice can affect the parabolic path of Airy beam, termed transverse acceleration.

In order to test these assumptions, various experimental techniques were necessary: for a generation of desired photonic structures in photorefractive materials, for shaping the exciting light beams, and finally imaging techniques for an investigation of transverse transport properties of the structures. Results obtained in experiments were confirmed in numerical simulations realized in a home-made software based on the Finite-Difference Beam Propagation Method.

It has been shown that the Fibonacci lattice does suppress diffraction, with the fact that the effect is more pronounced in a 1D compared to a 2D lattice. Besides, it turns out that a weak disorder superimposed to the Fibonacci lattice slightly inhibits this effect. Additionally, a regular lattice can suppress the transverse acceleration.

The potential possibility of a transverse light transport control qualifies these structures as candidates for optical signals routing in photonic integrated circuits, as well as high-quality image transport systems.

The thesis is organized as follows. After preliminary consideration presented in Chapter 1, Chapter 2 gives fundamental facts about the ordering of matter, as well as the general characteristics of a wave propagation in structures of different ordering. Chapter 3 covers basic theory of light propagation in photonic lattices, periodic and disordered ones. In Chapter 4, the numerical method for the simulations of light

propagation in photonic lattices is described. Chapter 5 presents the experimental techniques for lattice generation in photorefractive media and latter diagnostics. Chapter 6 contains experimental and numerical results, while Chapter 7 reviews the main results and concludes with some suggestions for future research directions.

Chapter 2

General properties of deterministic aperiodic structures

2.1 About periodicity, aperiodicity and disorder

Spatial periodicity has been considered as a synonym for the term *structural order*. The essence of periodicity is based on a motif or building block which is indefinitely repeated. Any vector function of position vector $\mathbf{r}$[1] satisfying the condition $f(\mathbf{r}) = f(\mathbf{r} + \mathbf{R}_0)$ is periodic in space with period $\mathbf{R}_0$, since its value is preserved under the set of translations generated by vector $\mathbf{R}_0$. Accordingly, it is said that periodic structures display a specific kind of long-range order characterized by translational invariance symmetry along certain spatial directions.

Opposite to previous, if there is no correlation between building blocks of a structure, or there is only a short-range correlation, it is denoted as *disordered* (or *amorphous*) one.

The third kind of structures, which present an intermediate domain between fully periodic and fully disordered media exhibit, just as periodic ones, long-range order in space, but the lack of translation symmetry. This leads to the notion of *aperiodic order* or *order without periodicity*. These structures should be clearly distinguished from amorphous structures, because the latter exhibit short-range correlation only (Maciá, 2012), i.e. there is no rule in spatial ordering. The term of aperiodic order implies that there is deterministic rule defining the structure. According to previous, these structures are labeled as *deterministic aperiodic* ones.

The deterministic rule is usually specified in terms of the so-called *substitution*

[1]The convention throughout this thesis is that boldface letters refer to vectors.

Sequence	Set	Substitution rule
Fibonacci	$\{A, B\}$	$A \to AB, B \to A$
Thue-Morse	$\{A, B\}$	$A \to AB, B \to BA$
Period-doubling	$\{A, B\}$	$A \to AB, B \to AA$
Cantor	$\{A, B\}$	$A \to ABA, B \to BBB$
Rudin-Shapiro	$\{A, B, C, D\}$	$A \to AC, B \to DC, C \to AB, A \to DB$

Table 2.1: Examples of the substitution rules determining the sequences considered in the study of aperiodic lattices (Maciá, 2012).

sequences. A substitution sequence is formally defined by its action on a set which consists of a certain elements (e.g. letters). It is a simple mathematical prescription, rooted in symbolic dynamics and Lindenmayer inflation rules (Dal Negro *et al.*, 2008). In actual structure, each set element corresponds to a different type of building block.

Some of sequences frequently discussed in the analysis of aperiodic lattices are shown in Table 2.1. As an example, Fibonacci lattice is formed by applying the substitution rule $A \to AB, B \to A$. A successive application of the rule generates the strings A, AB, ABA, $ABAAB$, $ABAABABA$, $ABAABABAABAAB$, and so on. In this way generated strings have also been in accordance with the Fibonacci recursion, wherein each sequence S_j has been obtained by combining the two previous ones as $S_j = S_{j-1}S_{j-2}$. The number of elements in a sequence of order n is given by *the Fibonacci number* F_n, which has been obtained from the recurrence relation $F_j = F_{j-1} + F_{j-2}$, $j \geq 2$ and $F_1 = F_0 \equiv 0$.

All aperiodic systems derived from the application of a substitution rule posses characteristic of *self-similarity* (Maciá, 2012), what means that that each portion can be considered as a reduced-scale image of the whole (Mandelbrot, 1967).

There are three types of aperiodic crystals: incommensurately modulated phases, composites and quasicrystals (Janssen *et al.*, 2007, Maciá, 2006). Theses types are not mutually exclusive.

Another way to define aperiodic structure is by using *quasiperiodic functions*, which belong to the class of *almost periodic functions*[1] (Maciá, 2006). A simple 1D example of quasiperiodic function is

[1] Almost periodic functions are functions that can be approximated by Fourier series containing a countable infinity of pairwise incommensurate frequencies. When the set of frequencies required can be generated from a finit-dimensional basis, the resulting functionis referred as a quasiperiodic one (Maciá, 2006).

$$f(x) = \cos(x) + \cos(\alpha x) \tag{2.1}$$

where α is an irrational number. The previous function for $\alpha = \sqrt{2}$ is presented in Fig.2.1.

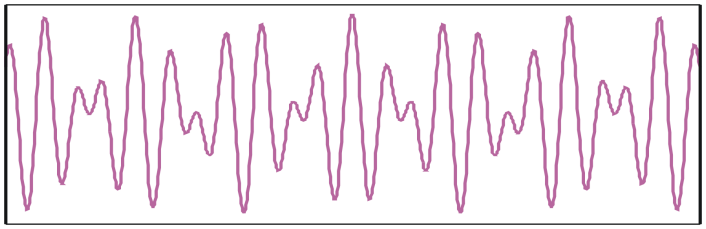

Figure 2.1: Quasiperiodic function $f(x) = \cos(x) + \cos(\alpha x)$

It is widely known, that these functions are images of periodic functions on the space of higher dimension (Blinov, 2015). For example, the 1D quasiperiodic function defined in Eq.2.1 can be obtained as 1D projection of 2D periodic function

$$f(x, y) = \cos(x) + \cos(y), \tag{2.2}$$

supposing that $y = \alpha x$. This feature is the basis of the so-called cut-and-project method, which is extensively used in the study of quasiperiodic crystals (Maciá, 2006). It assumes mathematical rules that treats a quasicrystal as periodic structure embeded in higher dimension space (hiperspace).

The concept of great importance in exposing the lattice structure is *the reciprocal space*. A corresponding notion of *the reciprocal lattice* plays a fundamental role in most analytic studies of periodic structures (Aschroft and Mermin, 1976), which actually represents the Fourier transform of a lattice (Duan and Guojun, 2005), or *lattice spectrum*. Accordingly, the understanding of the Fourier spectrum is of a crucial importance. This imposes diffraction as the primary technique for examining the lattices structure.

Namely, the diffraction pattern formed in a far field (the Fraunhofer regime) resembles the amplitude of the lattice spectrum. In this way, diffraction of matter waves (electrons, neutrons) by an atomic lattice, or electromagnetic waves by a dielectric superlattice, provide the most important experimental information for a further lattice structure analysis. Two examples of 2D lattices and corresponding diffraction patterns are shown in Fig.2.2

An interpretation of a lattice spectrum can be done by using a term of *mathemat-*

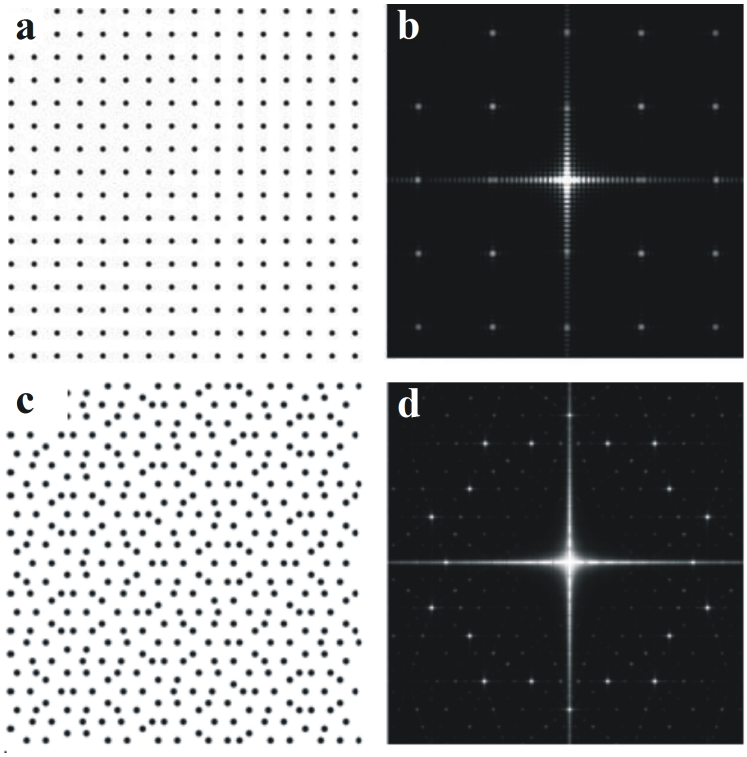

Figure 2.2: Lattices and corresponding diffraction patterns. a) A square lattice, b) Diffraction pattern of the square lattice, c) A Penrose lattice, d) Diffraction pattern of the Penrose lattice (Dal Negro and Boriskina, 2012).

ical measure and corresponding *Lebesgue's decomposition theorem.* It states that the spectrum of any arbitrary physical system can be uniquely decomposed in the terms of just three kinds of spectral measures (and mixtures of them), namely, *pure-point* (μ_P), *absolutely continuous* (μ_{AC}) and *singularly continuous* (μ_{SC}) spectra, in the form (Maciá, 2006)

$$\mu = \mu_P \cup \mu_{AC} \cup \mu_{SC}. \tag{2.3}$$

In that sense, periodic (and multi-periodic) lattices posses a pure-point lattice spectrum, meaning that corresponding diffraction patterns are characterized by well defined and sharp (δ-like) peaks (Bragg peaks) positioned at rational multiples of primitive reciprocal vectors. Unlike periodic, the disordered (amorphous) structures posses an absolutely continuous (diffuse) lattice spectrum. Aperiodic structures on the other hand, because of theirs large diversity, can posses all of three previously mentioned types of a lattice spectrum.

In Fig.2.3 are presented lattice spectra of three different 1D aperiodic lattices (Dal Negro *et al.*, 2008): pure-point spectrum of Fibonacci lattice, singularly continuous spectrum of Thue-Morse lattice and absolutely continuous spectrum of Rudin-

Shapiro lattice.

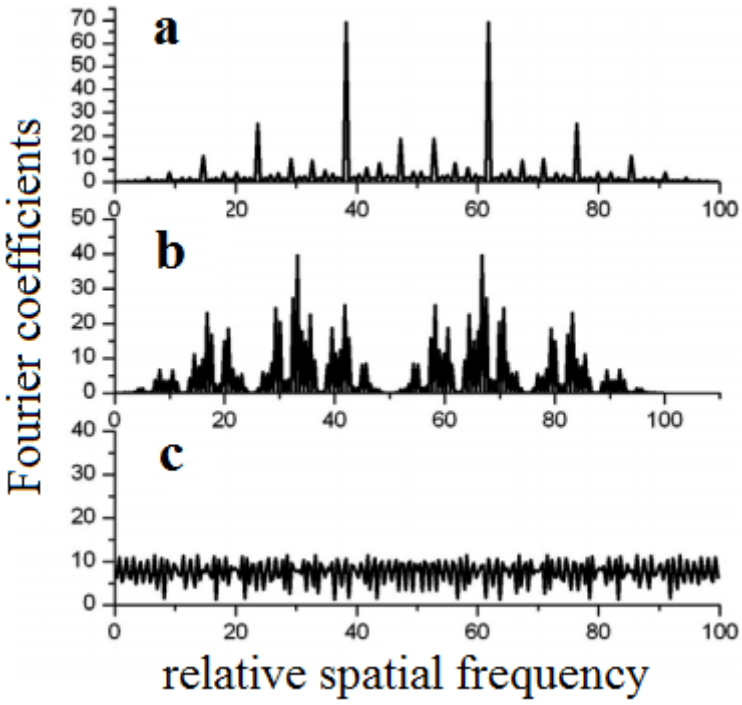

Figure 2.3: A lattice spectrum of three different deterministic aperiodic 1D structures (Dal Negro *et al.*, 2008). a) Fibonacci lattice - pure-point spectrum, b) Thue-Morse lattice - singularly continuous spectrum, c) Rudin-Shapiro lattice - absolutely continuous spectrum

The increasing number of deterministic aperiodic ordered structure types led to a redefining of the term of *crystal* by the International Crystallographic Union. In April 1991, the Commission on Aperiodic Crystals established it as follows: "In the following by *crystal* we mean any solid having an essentially discrete diffraction diagram, and by *aperiodic crystal* we mean any crystal in which three-dimensional lattice periodicity can be considered to be absent."(*Report of the Executive Committee for 1991*, 1992). In this way, the essential attribute of crystallinity is transferred from real space to reciprocal space. Besides, the generic attribute of solid state matter is presence of mathematically well defined, long range-atomic order, not periodicity.

2.2 Wave propagation in periodic, aperiodic and disordered structures

A wave propagation in periodic structures has been one of the basic problems in physics. Since Sir Isaac Newton deduced the formula for the speed of sound using a 1D lattice model (an array of balls interconnected by springs), the solution of the wave equation in a periodic structure has become a key modus for an understanding of behavior of many physical systems (Duan and Guojun, 2005). Although there are several different types of waves (electrons, lattice waves, electromagnetic waves), or different physical phenomena described by wave equation, there is significant formal (mathematical) similarity between them.

One of the main concepts in the treatment of waves in periodic structures is a *Bloch wave* (*Bloch state*, *Bloch function*). It is developed in 1928 by Felix Bloch. His intention was to explain electronic transport in metals, semiconductors and insulators based on a fact that electrons propagate in a periodic potential caused by the (regular) atomic arrangement of atoms in a crystal lattice (Duan and Guojun, 2005, Kittel, 1987). The state of the electron is described by the Schrödinger equation, that can be written in stationary form as:

$$\left[-\frac{\hbar^2}{2m}\nabla^2 + V(\mathbf{r})\right]\psi(\mathbf{r}) = E\psi(\mathbf{r}). \tag{2.4}$$

The first term on the left-hand side is the kinetic energy and the second is the potential, which is (in case of the crystal lattice) a periodic function, i.e.:

$$V(\mathbf{r}+\mathbf{l}) = V(\mathbf{r}), \tag{2.5}$$

where $\mathbf{l}$ is any lattice vector. In this case the solution of Eq.(2.4) is of the form

$$\psi_{\mathbf{k}}(\mathbf{r}) = u_{\mathbf{k}}(\mathbf{r})e^{i\mathbf{kr}}. \tag{2.6}$$

$u_{\mathbf{k}}$ is periodic function with the periodicity of the potential $V(\mathbf{r})$, i.e. $u_{\mathbf{k}}(\mathbf{r}+\mathbf{l}) = u_{\mathbf{k}}(\mathbf{r})$, and $\mathbf{k}$ is the reciprocal lattice vector. This statement is the famous *Bloch theorem*. A wave function of the form of Eq.(2.6) is a *Bloch wave*. The Bloch theorem can be written in a somewhat different form, giving an equation:

$$\psi_{\mathbf{k}}(\mathbf{r}+\mathbf{l}) = \psi_{\mathbf{k}}(\mathbf{r})e^{i\mathbf{kr}}. \tag{2.7}$$

According to a previous equation, the physical meaning of the Bloch theorem is that wave functions at positions $\mathbf{r}+\mathbf{l}$ and $\mathbf{r}$ are the same, except for a phase factor $e^{i\mathbf{kr}}$.

Another analytical tool for treatment of the periodic structures is a *reciprocal lattice* of a lattice. It represents Fourier transform of the original lattice. A primitive cell of the reciprocal lattice is a *Brillouin zone*.

The electrons (waves) that propagate in a lattice are not perfectly free. Because of their wave nature, most of electrons, with wavelengths largely different from the lattice constant, don't "feel" a presence of the lattice (in the first approximation). But if electron wavelength takes values comparable with the lattice constant, its interaction with the lattice becomes very strong. In other words, electrons with wave vectors ending near the edge of a Brillouin zone diffract intensively. Those which have wave vectors at the edge of a Brillouin zone form a standing waves. It leads to an energy splitting in two values, one slightly lower and the other slightly higher than free electron value for corresponding wave vector. Hence, an *energy gap* is formed. As a consequence, electrons of certain energies are forbidden to propagate in certain directions. If energy gap covers all possible propagation directions it is called a *complete* band gap.

The most common way for summarizing characteristics of a wave propagation through a medium is a dispersion relation. It relates a wave frequency (or energy) to its wave vector (wavelength). For electrons it can be obtained by solving the Eq.2.4 for different values of $\mathbf{k}$. Dispersion relations for free electron and electron in a periodic potential are presented in Fig.2.4a and c, respectively. Discontinuities in the dispersion relation curve shown in Fig.2.4c represent band gaps.

Previously mentioned ideas about interaction of electrons and crystal lattice can be applied to electromagnetic waves and macroscopic dielectric media, that leads to the notion of a *photonic crystal*. It is structure consisting of two or more dielectric materials arranged in a periodic order[1]. Also, it is supposed a low absorptivity of the materials. The behavior of the electromagnetic waves (photons) in these structures is to a large degree analogue to the behavior of the electronic waves (electrons) in the atomic lattice.

The propagation of the electromagnetic waves in the macroscopic media is governed by Maxwell equations. These can be expressed in terms of $\mathbf{E}$ and $\mathbf{H}$, which are electric and magnetic field vector respectively. Both $\mathbf{E}$ and $\mathbf{H}$ are time and

[1]Different metalo-dielectric structures are also falling into a category of photonic crystals, but they won't be scrutinized here. The attention is paid to the pure dielectric structures.

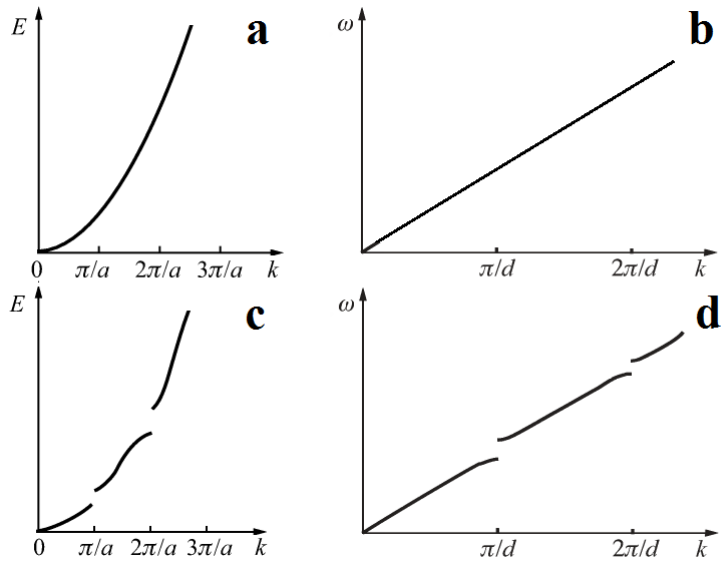

Figure 2.4: Dispersion relation of a) a free electron, b) a light wave in homogenous medium, c) an electron in a periodic lattice, d) a light wave in periodically modulated medium

position dependent functions. Because of a linearity of the Maxwell equations, they can be expanded into a set of harmonic modes. Further, if medium is linear, modes can be written as a product of spatial and time factor, $\mathbf{E}(\mathbf{r},t) = \mathbf{E}(\mathbf{r})e^{-i\omega t}$ and $\mathbf{H}(\mathbf{r},t) = \mathbf{H}(\mathbf{r})e^{-i\omega t}$, where ω is angular frequency. Substituting these in the Maxvell equations, and under a few (very reasonable) presumptions - the field strengths are small, material is isotropic, there is no material dispersion and the medium is transparent - one gets

$$\frac{1}{\epsilon\left(\mathbf{r}\right)}\nabla\times\left(\nabla\times\mathbf{E}\left(\mathbf{r}\right)\right)=\left(\frac{\omega}{c}\right)^{2}\mathbf{E}\left(\mathbf{r}\right), \tag{2.8a}$$

$$\nabla\times\left(\frac{1}{\epsilon\left(\mathbf{r}\right)}\nabla\times\mathbf{H}\left(\mathbf{r}\right)\right)=\left(\frac{\omega}{c}\right)^{2}\mathbf{H}\left(\mathbf{r}\right), \tag{2.8b}$$

with $\nabla\cdot\mathbf{H}(\mathbf{r})=0$ and $\nabla\cdot[\epsilon(\mathbf{r})\mathbf{E}(\mathbf{r})]=0$, where $\epsilon(\mathbf{r})$ is relative permittivity. In a similar way as in a case of electron, solving one of the propagation equations Eq.2.8 for different frequencies gives the band diagram, Fig2.4b and d. The eigenstates of a system described by a periodic potential are extended, having the same nominal amplitude at all positions in space.

The term *disordered structure* refers to a structure described with potential function of random distribution. The wave behavior in this kind of system turns out to be *localized* within finite region.

Whether the wave will be localized or not, it depends on the degree of disorder and the system dimensionality. Concerning this, the concept a *mobility edge* was introduced by Nevill Mott in the early 1960s. It is the critical energy at which the wavefunctions change their character from being extended to being localized (Lee and Ramakrishnan, 1985).

The coherent waves in 1D and 2D unbounded disordered systems are always localized, as it is shown in Abrahams *et al.* (1979). On the other hand, in 3D systems there is a threshold value of disorder (Sperling *et al.*, 2013) required for existence of localized eigenstate.

In disordered system waves undergo multiple scattering among the randomly distributed scatterers. There are three important characteristic lengths required for the investigation of a wave propagation through such a system[1] - wavelenght λ (or wavevector intensity k), transport mean free path l^* and the size of the sample L (cf. Fig.2.5) (Duan and Guojun, 2005). The ratios of these lengths determine a regime of the wave propagation.

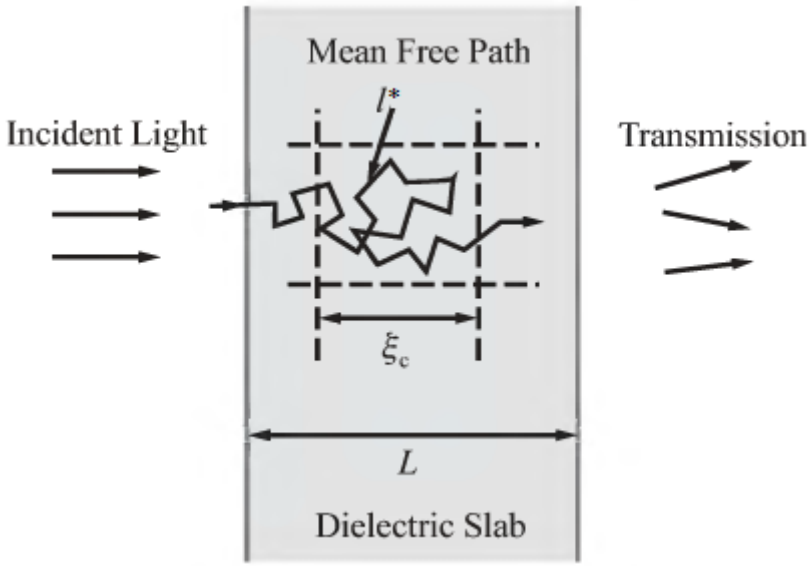

Figure 2.5: Light waves transport through disordered medium (Duan and Guojun, 2005).

If $l^* > L$ the medium behaves as it were homogeneous, i.e. beside the incident wave there are only reflected and transmitted waves, so this is the propagating case.

If $\lambda < l^* < L$ the wave loses memory of its initial direction caused by multiple scattering. This is a regime of *weak localization*, where localized eigenstate

[1]Non-dissipative medium

appear, but there are still a great many extended (but not periodic) eigenstates. The propagation of waves in these media can in general be described by a normal diffusion process. In this case transmission through a sample decreases linearly with its length (Wiersma *et al.*, 1997). Furthermore, in this regime appears coherent effect of *enhanced backscattering*. It is a precursor for strong localization.

If $l^* < \lambda < L$ the system is strongly disordered, satisfying the Ioffe-Regel criterion, $l^* \leq \lambda$. This is a regime of *strong localization*. Here, the oscillating field can not even perform one oscillation before the wave is scattered again. The eigenstate of strongly disordered systems may be described by exponentially decaying function in space, $\exp(-|\mathbf{r} - \mathbf{r}_0|/\xi_c)$, where $\mathbf{r}_0$ is a certain central position and ξ_c is the localization length (cf. Fig.2.6). This phenomena is known as Anderson localization. In the localized state, the transmission coefficient decreases exponentially instead of linearly with the thickness of a sample[1] (Wiersma *et al.*, 1997).

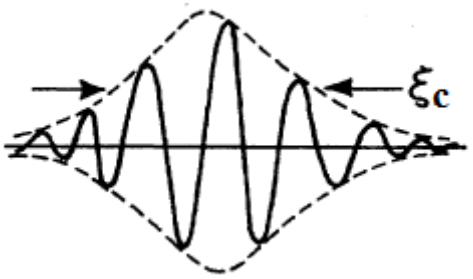

Figure 2.6: Localized state.(Lee and Ramakrishnan, 1985)

When sufficient disorder is introduced into a system, the bandgaps in dispersion curve disappear. Further, in the real systems, energy of localized mode, injected into that mode's region of space, cannot diffuse away, but remains trapped until it is dissipated (Dalichaouch *et al.*, 1991).

A wave behavior in deterministic aperiodic structures, because of their multiformity and complexity, is somewhat more difficult to analyze. A lack of translation symmetry leads to ineffectiveness of Bloch's theory and imply that eigenstates may not be extended. On the other hand, long-range order suggests that eigenstates won't be localized, at least not in the same way as those in disordered structures.

To explain a wave propagation in these structures, the notion of *critical* eigenstate (or *critical* wave function) is introduced. It exhibit strong spatial fluctuations showing distinctive self-similar features (Maciá and Dominguez-Adame, 1996), as

[1] In the experiments involving light waves the main problem is distinction between the effects of absorption and localization (Sperling *et al.*, 2013).

one can see in Fig.2.7. These eigenstates may, or may not be normalizable (thus, localized), depending on the critical exponent associated with a given state (Levi *et al.*, 2011).

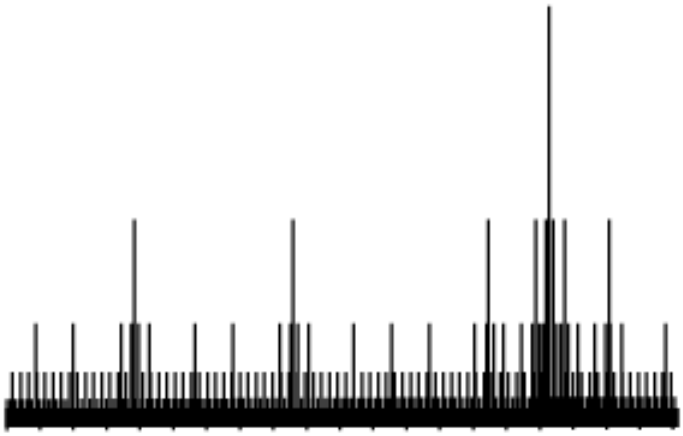

Figure 2.7: Critical wave function of one-dimensional Fibonacci lattice (Duan and Guojun, 2005).

Dispersion relations of deterministic aperiodic structures don't have band gaps, which are characteristics of periodic structures. In the dispersion relation of deterministic aperiodic structures there are regions where the density of eigenstates is considerably lower. These are named *pseudogaps*. Besides, higher density of eigenstates is generally associated with broader eigenfunctions, which support higher transport (Levi *et al.*, 2011).

In accordance with the foregoing, wave functions can be classified into three categories: extended, localized and critical ones (Duan and Guojun, 2005). If L is the size of the sample and d is the spatial dimension, an extended state is defined as

$$\int_{|\mathbf{r}|<L} |\psi(\mathbf{r})|^2 \, d\mathbf{r} \sim L^d, \tag{2.9}$$

which means that a wavefunction has asymptotical uniform amplitude. A localized state is characterized by a square integrable wavefunction, i.e.,

$$\int_{|\mathbf{r}|<\infty} |\psi(\mathbf{r})|^2 \, d\mathbf{r} \sim L^0. \tag{2.10}$$

A typical example of a critical state is a power-low function $\psi(\mathbf{r}) \sim |\mathbf{r}|^{-\nu}$, where $\nu \leq d/2$, so

$$\int_{|\mathbf{r}|<L} |\psi(\mathbf{r})|^2 \, d\mathbf{r} \sim L^{-2\nu+d}. \tag{2.11}$$

Chapter 3

Diffraction in waveguide arrays

In this chapter, the basic theory of light propagation in periodic evanescently coupled waveguide arrays is considered. Here, the term *coupled* means that optical waveguides are placed next to each other in such a way that their individual modes overlap (Christodoulides *et al.*, 2003), allowing the exchange of the light energy between adjacent waveguides. This overlapping strongly affects the light propagation in such a system.

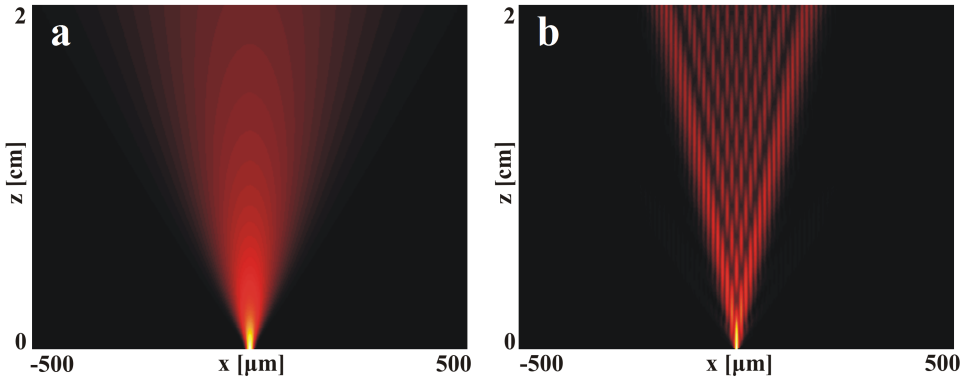

Figure 3.1: Diffraction in continuous and periodic medium. a) Normal diffraction - Gaussian beam diffraction in continuous medium, b) Discrete diffraction - Gaussian beam diffraction in periodic waveguide array

As the light beam propagates along the waveguides, in the case when only one waveguide is excited, it spreads into two main lobes with several secondary peaks between them. Here most of the optical energy is carried out along two major lobes far from the center. This particular diffraction pattern became known as discrete diffraction (Garanovich *et al.*, 2012). This is in contrast with diffraction process in continuous medium, where most of the energy is concentrated in central region of the beam, as shown in Fig.3.1.

A suitable tool for the explication of the light propagation behavior is the diffraction relation. The diffraction relation connects longitudinal and transverse wavevector components for a fixed optical frequency. In the coordinate system where x and y are the transverse directions and z is the propagation direction, the diffraction relation reads as

$$\beta = k_z = \sqrt{k_0^2 - k_x^2 - k_y^2} \tag{3.1}$$

where k_0 is the total wavevector, k_x and k_y are the transverse wavevectors, and β (or k_z) is the longitudinal wavevector. From this relation the direction and broadening of the light beam can be determined. In the paraxial approximation ($k_x \ll k_0$), assuming 1D[1] continuous medium, previous equation reads as

$$\beta = k_0 - \frac{k_x^2}{2k_0}. \tag{3.2}$$

Every finite beam is a superposition of plane waves each of which has a different value of transverse wavevector k_x. When a beam profile centered at k_x in the Fourier space propagates over a distance z, it is shifted in the x direction by an amount $\Delta x = \frac{\partial \beta}{\partial k_x} z$, meaning the propagation direction is $\alpha = \arctan(\frac{\partial \beta}{\partial k_x})$. The beam broadening is determined by parameter $D = \frac{\partial^2 \beta}{\partial k_x^2}$, termed diffraction (Eisenberg *et al.*, 2000).

Considering Eq.3.2, in continuous medium $D = -\frac{1}{k_0}$, so it's always negative, which indicates that the beam always spreads during a propagation. This is called normal diffraction.

In the case of photonic lattices, the beam propagation is to a large degree different. There are two complementary approaches to the study of photonic lattices: coupled-mode theory and Floquet-Bloch theory.(Garanovich *et al.*, 2012)

3.1 The coupled-mode theory

Coupled-mode description, also known as the tight-binding approximation, considers lattice as a set of individual waveguides that are coupled together. Light propagation in waveguide array is primarily characterized by coupling due to the overlap between the fundamental modes of (only) the nearest-neighboring waveguides. In this case, light propagation in 1D array can be described by a set of discrete equa-

[1]Here the adjective one-dimensional refers to one transverse dimension.

tions(Trompeter *et al.*, 2003)

$$(i\frac{\partial}{\partial z} + \beta_0)\psi_n + C(\lambda)[\psi_{n+1} - \psi_{n-1}] = 0, \tag{3.3}$$

where β_0 is the propagation constant of the waveguide, $\psi_n(z)$ is the mode amplitude, z is the propagation distance along the waveguides, n is the waveguide number and $C(\lambda)$ is the coupling constant between adjacent waveguides, which depends on the field overlap between the neighboring waveguides. All waveguides are identical, having the same propagation constant. Besides, periodical positioning of the waveguides makes all coupling coefficients mutually equal. If one assumes that only one waveguide, e.g. $n = 0$, is excited at the input, i.e. $\psi_{n\neq 0}(z = 0) = 0$, then the solution for the electrical field in the n-th waveguide is given as (Eisenberg *et al.*, 1998)

$$\psi_n(z) = i^n \psi_0(z = 0) J_n(2Cz) e^{i\beta_0 z}. \tag{3.4}$$

Here J_n is the Bessel function of the order n. For arbitrary initial conditions, the diffraction pattern can be calculated as a linear superposition of the functions defined in Eq.3.4.

Eigensolutions of Eq.3.3 are plane waves (Bloch-modes) of the form

$$\psi_n(z) = \psi_0 \exp(ik_x d + i\beta z), \tag{3.5}$$

where k_x and β are transverse and longitudinal component of the two-dimensional wavevector k_0 respectively, and d is the distance between the centers of the adjacent waveguides. Substitution of previous expresion into Eq.3.3 gives the relation

$$\beta_z = \beta_0 + 2C \cos k_x d, \tag{3.6}$$

which is previously mentioned diffraction relation, connecting transverse and longitudinal dynamics. This relation is periodic, as opposed to Eq.3.2 for the homogenous medium.

The angle of propagation is defined by its tangens as (Szameit and Nolte, 2010)

$$\frac{\partial \beta}{\partial k_x} = -2dC \sin k_x d \tag{3.7}$$

which is periodic function of transverse wavevector, meaning the coupled waveguide array exhibits anomalous refraction. The propagation angle oscillates as transverse

wavevector is increased, so refraction is restricted to a cone, irrespective of initial tilt of the input beam. If the excitation is tilted in such a way that the phase difference between adjacent waveguides is of integer multiplies of π, the propagation field returns to initial waveguide (Pertsch *et al.*, 2002), that is represented in Fig.3.2 for the case of $tilt = 2.2°$.

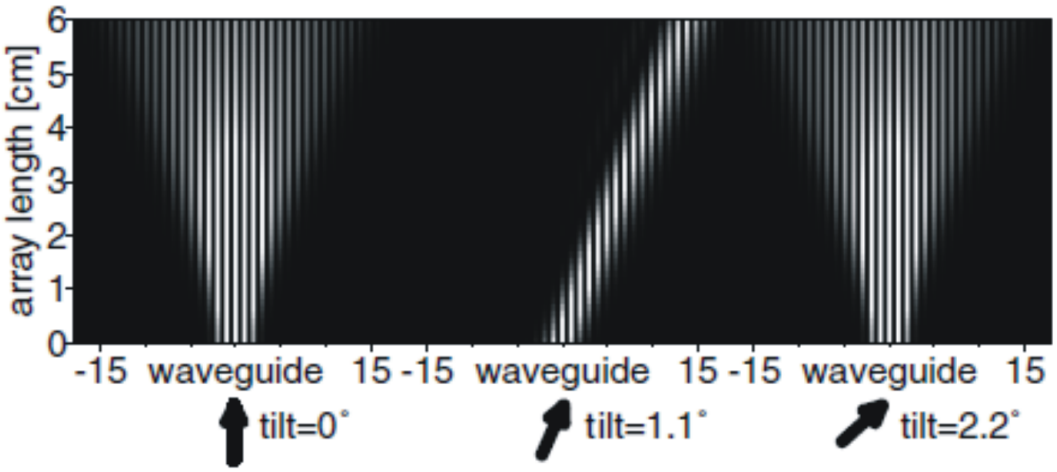

Figure 3.2: Anomalous refraction and diffraction in one-dimensional periodic lattice. Broad Gaussian beam excitation (overlapping several waveguides), for three different input incident angles (Pertsch *et al.*, 2002)

Diffraction strength, determined by the diffraction coefficient, gives the relative spread of adjacent rays. The diffraction coefficient is determined by second derivative of the diffraction relation:

$$\frac{\partial^2 \beta}{\partial {k_x}^2} = -2d^2 C \cos k_x d. \tag{3.8}$$

For negative value of diffraction coefficient the beam acquires a convex wavefront during propagation, so it undergoes normal diffraction. On the other hand, for positive value of diffraction coefficient the beam acquires concave wavefront, undergoing anomalous diffraction. At specific transverse wave components, satisfying the condition $k_x d = \frac{\pi}{2}$, there is no diffraction of propagating beam (Garanovich *et al.*, 2012).

One should note, comparing the Fig.3.1 and Fig.3.2, that the lattice effects on light propagation depend strongly on the size of an excitation beam relative to the lattice period. While a broad Gaussian beam mostly preserve initial shape, a narrow beam leads to discrete diffraction pattern.

The lack of the coupled-mode theory is the fact that it describes only propagation within the first band (the ground state).

3.2 The Floquet-Bloch theory

A more general and accurate description of light propagation in photonic lattices can be obtained using Floquet-Bloch theory. It predicts that the propagation constant spectrum of the lattices eigenmodes is divided into bands, separated by gaps in which propagating modes do not exist (Mandelik *et al.*, 2003). Floquet-Bloch analysis provides formal description not only of the on-site fundamental modes, but also of the high order waveguide modes, and radiation modes that propagate between the waveguides (Garanovich *et al.*, 2012). It gives the full physical picture of the light behavior in the periodic lattice. The reason is the fact that the Floquet-Bloch waves are independent solutions of the wave equation and therefore self-sufficient, on the one hand, and, on the other, a possibility to explain light propagation inside a lattice through excitation, interference, refraction and reflection of the Floquet-Bloch waves (Russell, 1986).

The wave equation for one-dimensional photonic lattice in paraxial approximation can be written as (cf. (Lifante, 2003))

$$\frac{1}{2k_0}\frac{\partial^2 E}{\partial x^2} + k_0\frac{n(x)}{n_0}E = -i\frac{\partial E}{\partial z}, \tag{3.9}$$

where E is the electric field intensity, k_0 is the wavevector, n_0 is the refractive index of substrate and $n(x)$ is periodically modulated refractive index, following $n(x) = n(x+d)$. The solution of Eq.3.9 can be written as

$$E(x,z) = A(x)e^{i\beta z}. \tag{3.10}$$

According to the Bloch theorem, the amplitude term of previous equation, $A(x)$, can take the form of the Bloch wave,

$$A(x) = u(x)e^{ik_x x}. \tag{3.11}$$

Substituting Eq.3.10 and Eq.3.11 in Eq.3.9, one obtains

$$\frac{1}{2k_0}\frac{\partial^2 u(x)}{\partial x^2} + i\frac{k_x}{k_0}\frac{\partial u(x)}{\partial x} - \frac{k_x^2}{2k_0}u(x) + k_0\frac{n(x)}{n_0}u(x) = \beta u(x), \tag{3.12}$$

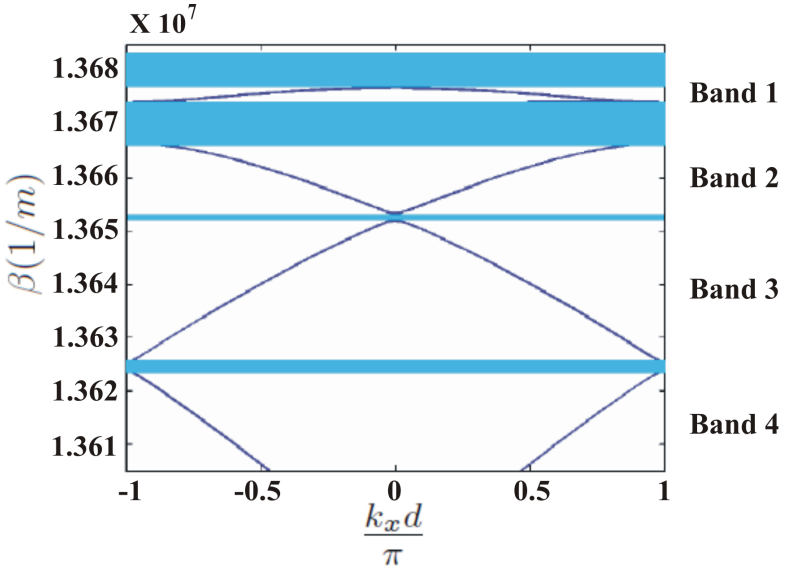

Figure 3.3: Reduced band-gap diagram of a typical waveguide array (Mandelik *et al.*, 2003).

which is the diffraction relation, connecting propagation constant β and transverse wavevector k_x. The calculated diffraction relation of a typical one-dimensional photonic lattice is shown in Fig.3.3. It is a band-gap diagram reduced to the first Brillouin zone. The blue regions represent the gaps. The normal to the diffraction curve determines the propagation direction of each mode. The diffraction curve of the first band is nearly sinusoidal. This result is also predicted by coupled-mode theory (Eq.3.6).

3.3 Diffraction in disordered waveguide arrays

Disorder in the lattice can be introduced by randomly changing some of its parameters, e.g. the width or refractive index of waveguides, thus changing the propagation constant associated with particular waveguide, or their positions, which affects the coupling between adjacent waveguides. These parameters are changed in a finite range around their mean values. If the initial propagation constant is randomized, the disorder is termed as *diagonal*(Lahini *et al.*, 2008), and if the coupling is randomized, the disorder is termed as *off-diagonal*(Martin *et al.*, 2011).

As discussed in Chapter 2, disorder leads to the localization of wavepacket. If disordered lattice is excited, what happens is a transverse localization of a light beam (the suppression of diffraction). The information about the evolution of the light beam can be extracted from averaged intensity profiles of light beams obtained

in different realizations of disorder (Segev *et al.*, 2013). The envelop of the averaged transverse intensity profile, according to Anderson's theory, is the exponential function. In waveguide lattices, this is strictly true in case of diagonal disorder. On the other hand, this is not strictly true for off-diagonal disorder[1] (Mafi, 2015).

In 2D systems, the confinement of the beam in a transverse plane is quantified by the inverse participation ratio (Schwartz *et al.*, 2007),

$$P(z) \equiv \frac{\int I^2(x,y,z)dxdy}{[\int I(x,y,z)dxdy]^2}, \tag{3.13}$$

where I is a light intensity, and an average effective width

$$\omega_{eff} = \langle P \rangle^{-1/2}. \tag{3.14}$$

In 1D case these parameters are

$$P(z) \equiv \frac{\int I^2(x,z)dx}{[\int I(x,z)dx]^2}, \tag{3.15}$$

and

$$\omega_{eff} = \langle P \rangle^{-1}. \tag{3.16}$$

Different random realization of the lattice leads to different rates of a beam expansion and a final beam localization width. Nevertheless, a stronger disorder results in a smaller eventual localization width on average. Also, stronger disorder leads to a smaller variation around the average beam width (Mafi, 2015).

As an illustration, in Fig.3.4 are shown numerical simulations of the impact of disorder on a beam diffraction in 1D lattice. The Gaussian beam of 5 μm in width[2] is injected into 71^{st} waveguide in a 151 waveguide array, 40 mm long. Width of one waveguide is 3 μm, refractive index of substrate is 1.46 and refractive index contrast of the waveguide is 1×10^{-3}. The lattice in a) is regular with period of 11 μm. The waveguides in lattices shown in b)-d) are randomly distributed around the initial positions (positions of waveguides in the regular lattice) according to uniform probability distribution function. The amplitude of distribution is 1 μm, 2 μm and 3 μm in b), c) and d) respectively, meaning the increasing degree of disorder. In e)-h) are shown averaged intensity profiles at 40 mm of the corresponding lattices.

[1]The diagonal disorder case meets the conditions assumed by Anderson in his original model.(Lahini *et al.*, 2008)

[2]full width at half maximum

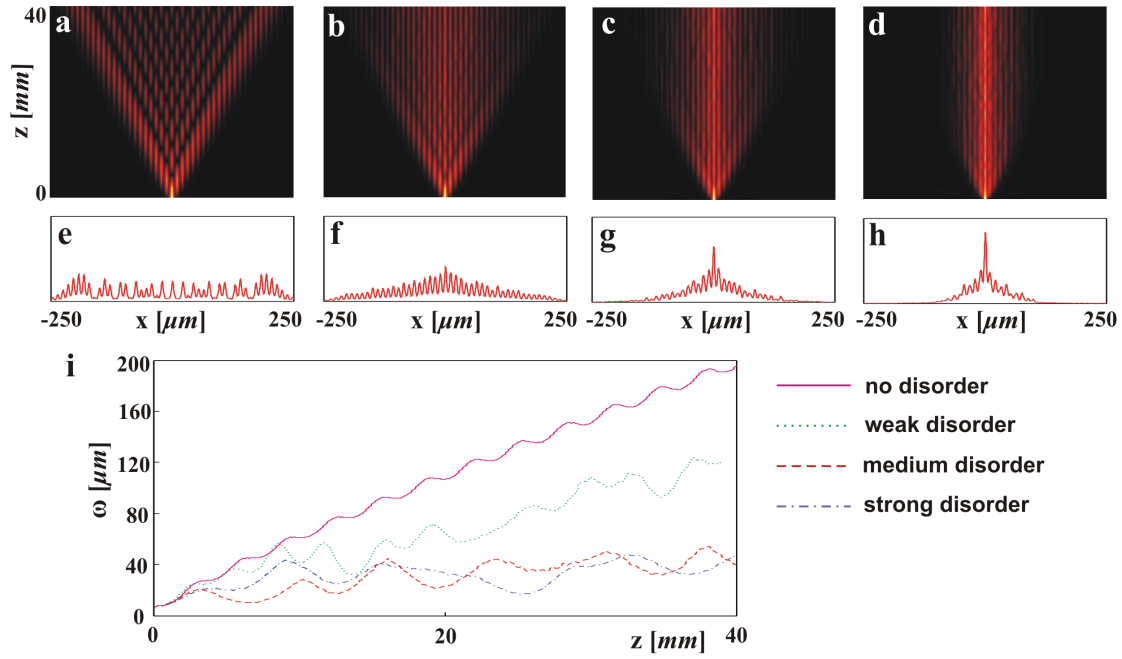

Figure 3.4: The beam profile evolution in regular and disordered lattice with off-diagonal disorder. a) regular, b)-d) disordered, e)-h) the beam profile at $40mm$, i) the comparison of the effective beam width expansion rate

One can see that as disorder is increased, the intensity profile is more localized, with exponential envelope function. In i) is shown the effective width versus propagation distance dependence. With increased degree of disorder, the expansion beam width rate is decreased.

Chapter 4

Numerical tools for treatment of light propagation in waveguide arrays

The most rigorous treatment of light waves behavior in an optical component is the solving of Maxvell's equations with appropriate boundary conditions. In many practical situations this approach is very difficult to implement. The main reason is a large difference of transverse and propagation dimensions, which makes the boundary-value approach highly demanding in terms of computer memory and CPU performance (Coldren *et al.*, 2012). On the other hand, plenty of optical structures allows to introduce paraxial approximation and only scalar wave treatment. These assumptions enabled a developing of the beam-propagation method (BPM), which provides reliable and computationally efficient optical structures diagnostics.

The method was originally introduced by Feit and Fleck in Feit and Fleck (1978). It is a numerical method extensively used in solving of the Helmholtz equation and nonlinear Schrödinger equation. It was initially based on fast Fourier transform (FFT) algorithm. Later on it has been extended to finite-difference based BPM schemes (FD-BPM), finite-element BPM (FE-BPM) and many others (Wartak, 2013). BPM is the most powerful technique to investigate linear and nonlinear lightwave propagation phenomena in different waveguide-based structures. BPM is also important for the analysis of ultrashort light pulse propagation in optical fibers (Okamoto, 2006).

There is a several reasons for wide acceptance of BPM (*BeamPROP 8.2*, 2010): relatively easily implementation of the basic technique, readily application to com-

plex geometries on the same way as to basic ones, automatically inclusion of the effects of both guided and radiating fields as well as mode coupling and conversion, flexibility and extensibility.

For implementation of the BPM it is necessary to know only the index of refraction distribution over the structure, and field distribution at the initial position. This means, the problem is reduced to an initial value problem, instead of a boundary value problem, which makes it computationally efficient.

The initially developed BPM had a few drawbacks (*BeamPROP 8.2*, 2010). Since it was based on scalar Helmholtz equation in paraxial approximation, as the first, it was limited to small angles around primary direction of propagation, and, as the second, it hadn't considered the polarization effects. The third, it couldn't account for backward reflections since the one-way wave equation on which it is based does not allow both positive and negative traveling waves.

The problem of small angles had been overcome using more accurate approximations to the Helmholtz equation. The exact scalar Helmholtz equation was replaced, instead of parabolic approximation, by one of a sequence of higher-order Padé approximants (Hadley, 1992*a*,*c*). There had also been several vectorial BPM-s developed, as reported in Huang and Xu (1993), Xu *et al.* (1994) and references therein. The problem of backward reflections had been overcome introducing bidirectional algorithm (Kaczmarski and Lagasse, 1988, Rao *et al.*, 1999).

4.1 Basic equation of BPM

The basis of BPM is the scalar three-dimensional Helmholtz equation[1]

$$\frac{\partial^2\psi}{\partial x^2} + \frac{\partial^2\psi}{\partial y^2} + \frac{\partial^2\psi}{\partial z^2} + k^2(x,y,z)\psi = 0, \tag{4.1}$$

where ψ is the spatial part of the electric field vector E, i.e. $E(x,y,z,t) = \psi(x,y,z)e^{-i\omega t}$, $k(x,y,z) = k_0 n(x,y,z)$, where $n(x,y,z)$ is spatial distribution of refractive index, and k_0 is the wave vector of the light in free space.

If the light beam propagates primarily along the positive z direction, and the refractive index changes slowly along this direction, the field $\psi(x,y,z)$ can be written as

$$\psi(x,y,z) = u(x,y,z)e^{i\bar{k}z}. \tag{4.2}$$

[1]The mathematical procedure carried out in this section can be found in many books on the subject of photonic devices modeling, e.g. Lifante (2003) or Okamoto (2006).

Here, $u(x, y, z)$ is complex field amplitude of slow variation, $e^{i\overline{k}z}$ denotes a fast oscillating wave moving in the positive z direction. $\overline{k}$ is a constant which represents the characteristic propagation wave vector and it is equal to $k_0 n_s$, where n_s is the reference refractive index, usually choosen to be equal to the refractive index of substrate or cladding.

Substitution of the previous expression in equation 4.1, leads to

$$\frac{\partial^2 u}{\partial z^2} + 2i\overline{k}\frac{\partial u}{\partial z} + \nabla_\perp^2 u + (k^2 - \overline{k}^2)u = 0, \tag{4.3}$$

where $\nabla_\perp^2 = \frac{\partial^2}{\partial x^2} + \frac{\partial^2}{\partial y^2}$.

The next step is the assumption that the amplitude of the wave is slowly varying function in the propagation direction - *slowly varying envelope approximation*. Mathematically it is formulated as

$$\left|\frac{\partial^2 u}{\partial z^2}\right| \ll \left|2\overline{k}\frac{\partial u}{\partial z}\right|. \tag{4.4}$$

This approximation is also known as the paraxial or Fresnel approximation, and it gives the so-called paraxial or Fresnel equation:

$$\frac{\partial u}{\partial z} = \frac{i}{2\overline{k}}(\nabla_\perp^2 u + (k^2 - \overline{k}^2)u), \tag{4.5}$$

which is the basic BPM equation. For a given input field $u(x, y, z = 0)$, the equation determines its evolution in the space $z > 0$.

There are two basic numerical techniques used to solve the Fresnel equation (Lifante, 2003). In the first, a beam propagation is modeled as a plane wave spectrum in the spatial frequency domain. This method is called fast Fourier transform BPM (FFT-BPM), because the fast Fourier transform is used to connect spatial and spectral domains. The second way is solving directly in spatial domain using finite-difference scheme. It is called finite-difference BPM (FD-BPM). FD-BPM allows the simulation of strong guiding structures, and also of structures that vary in the propagation direction. It turned out that FD-BPM is more efficient and stable compared to FFT-BPM (Chung and Dagli, 1990). In the next section the numerical implementation of FD-BPM method is introduced.

4.2 Numerical implementation of FD-BPM

The finite-difference method is the mathematical method for an approximative numerical solving of partial differential equations. It is based on the substitution of the derivatives of a function by finite differences of the function in adjacent discrete samples. Thereby, a differential equation becomes difference equation, which has a form of an algebraic equation. The solution of this equation is a set of numerical values corresponding to particular discrete element of space domain in which the function is considered.

The first step in the finite-difference procedure is to discretize the area of interest in an appropriate way, as it is shown in Fig.4.1. It means, to select optimal computational window in the transverse plane ((x, y)-plane), as well as convenient grid size in the z-direction. The optimal computational window means, on the one hand, that its dimensions should be large enough to cover desired field distribution all along the propagation path, and, on the other, that the size of the grid is small enough to provide all necessary details of the field distribution.

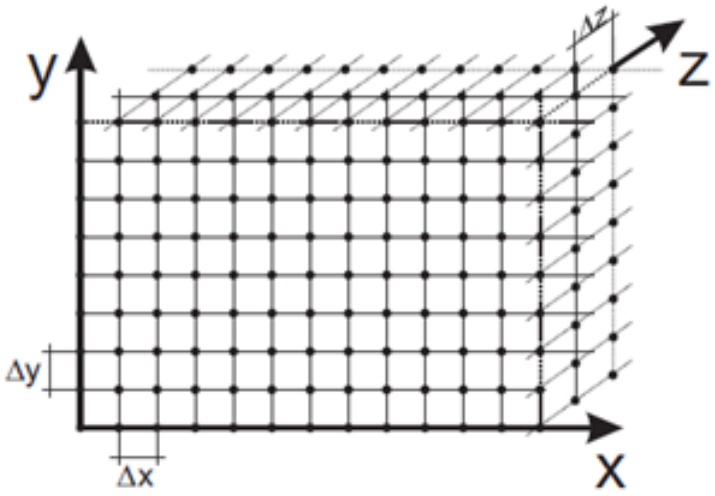

Figure 4.1: Discretization of a space in finite-difference method.

When performing discretization of the z-axis, it is necessary to take into account the Courant-Friedrichs-Lewy stability criterion (Press *et al.*, 2007). It is a criterion for convergence in a numerical solving of certain partial differential equations using finite-difference method. In case represented here, it can be expressed as

$$C = \frac{\Delta z}{\Delta x} + \frac{\Delta z}{\Delta x} \leq C_{max}, \tag{4.6}$$

where Δx, Δy and Δz are the length intervals in x, y and z, respectively, and C is called the Courant number. The maximum value of the Courant number,C_{max}, depends on a modus of solving difference equation, and it is in the range of one to several.

An important issue in BPM application is a problem of boundary conditions. As the computational window is finite, the optical field is going to have non-zero values at boundaries, causing that derivatives at specified positions have wrong values. This leads, in the first possible scenario, to the reflections of the field at the limits of the computational window, causing the light comes back to the region of interest. The second scenario is a disappearance of light through a boundary, but its appearance from the opposite boundary. What will happen depends of applied method (Lifante, 2003). As a consequence, unwanted interferences are introduced, and erroneous optical field distributions are obtained. This is why the boundary conditions are necessary to be adequately chosen. There are several different ways to define boundary conditions. Two most frequent are Absorbing Boundary Conditions (ABC) and Transparent Boundary Conditions (TBC).

ABC are realized by introducing an artificial complex refractive index distribution around the computational window to generate a boundary that adequately absorb incoming field but with a sufficiently smooth profile that doesn't add spurious reflections (Vassallo and Collino, 1996). In general, if absorbing region is adequately tailored, this procedure is accurate. The lack of this method are first, the fact that absorbing region should be modified for every particular problem, that is a difficult and time-consuming process, and second, increasing of both memory requirements and CPU time. The advanced version of ABC technique is developed by Berenger, known as Perfectly Matched Layers (PML) (Berenger, 1994). In this technique, there is no risk of reflections, but there is still problem of the additional computational resources.

TBC technique simulates nonexistent boundaries. Here, radiation is allowed to freely escape the computational domain without appreciable reflection, whereas radiation flux back into the domain is prevented (Hadley, 1992*b*). The important assumption of this technique is that at the boundary,the electric field has a form of $E = E_0 e^{ik_x x}$, where E_0 and k_x are complex constants. In this situation, as long as the real part of k_x is positive, radiative energy can only flow out of the computational domain. There is practically no extra computational resources requirements and the method is generally highly successful. The lack of the method is the fact that it

cannot be applied in the case of highly diverging beams.

FD-BPM can be implemented using implicit or explicit finite-difference method (Coldren *et al.*, 2012).

The Matlab® script developed for numerical analysis of structures studied in this thesis use an implicit finite-difference method based on Crank-Nicolson algorithm[1]. The Crank-Nicolson algorithm provides an unconditional stability, meaning that fields will not diverge or diminish without any physical reason, regardless of the grid size (Coldren *et al.*, 2012). The ABC technique is used, because it is easy to implement and provides sufficiently reliable results.

[1]Detailed explanation of the method is shown in A.

Chapter 5

Experimental methods for photonic structures generation and characterization

5.1 Photorefractivity

The photorefractive effect is a phenomenon in which the local index of refraction of a medium is changed by the illumination of light of a nonuniform intensity (Yeh, 1993). It was discovered in Bell Laboratories by Ashkin et al. in 1966 (Ashkin *et al.*, 1966). The effect was first described as *optical damage*. It manifested as a distortion of the wave front of laser beam passing through $LiNbO_3$ crystal, what was a consequence of the refractive index inhomogeneity induced by the beam itself.

A theoretical explanation of the photorefractive effect, known as *band transport model*, was introduced by Kukhtarev and coworkers in 1979 (Kukhtarev *et al.*, 1979). The model describes creation of an internal electric field by photo-excited space-charge in the material. If the material behaves as the *linear electro-optical* one, the field brings an intensity dependent modulation of the refractive index.

There are several distinctive characteristics of the photorefractive effect (Günter and Huignard, 2006). First, it is critically dependent on intentional doping, material impurities or imperfections. Second, it is highly sensitive effect, meaning it is observable at low light intensities (down to mW/cm^2). Further, it is relatively slow effect, depending on light intensity, carrier mobility and external field intensity. In some photorefractive materials the refractive index patterns are highly persistent in the dark. Also, the patterns are erasable by homogenous illumination or high

temperature.

In the illuminated regions mobile charge carriers, e.g. electrons, are photo-excited to the conduction band from donor atoms. The free electrons move towards non-illuminated regions by diffusion, drift or the photovoltaic effect (Jensen, 1999). *Diffusion* is movement of particles from regions of high to regions of low concentration, while *drift* is the motion of charged particles in an electric field. The *photovoltaic effect* is an optically induced unidirectional current based on asymmetry in the crystal structure. In the non-illuminated regions electrons recombine with acceptor ions leaving behind a fixed nonuniform charge distribution, that creates a strong local spatially varying electric field. The field is mapped into a refractive index modulation by the linear electro-optic effect.

The final goal of the band transport model is to determine resulting space-charge electrical field as a function of an initial light intensity distribution. In this model governing equation of charge-carriers dynamics can be written as (Boyd, 2008):

$$\frac{\partial N_D^+}{\partial t} = (sI + \beta)\left(N_D^0 - N_D^+\right) - \gamma n_e N_D^+, \tag{5.1}$$

which is the rate equation of immobile donors,

$$\frac{\partial n_e}{\partial t} = \frac{\partial N_D^+}{\partial t} + \frac{1}{e}\nabla \mathbf{j}, \tag{5.2}$$

the continuity equation of free electrons,

$$\mathbf{j} = n_e e \mu \mathbf{E} + eD\nabla n_e + \mathbf{j}_{pv}, \tag{5.3}$$

the equation that describes the current density caused by charge transport mechanism, and

$$\epsilon_{dc}\nabla \mathbf{E} = -e\left(n_e + N_A - N_D^+\right), \tag{5.4}$$

Gauss' low in the differential form. Here, N_D and N_A are the concentrations of donors and acceptors respectively, N_D^+ is the concentration of ionized donors, s is the ionization cross section of a donor, β is the thermal generation rate for electrons, γ is the recombination coefficient, e is the elementary charge, $\mathbf{j}$ is the current density, n_e is the concentration of electrons in the conduction band, μ is the electron mobility, D is diffusion constant, $\mathbf{j}_{pv}$ is the photovoltaic contribution to the current density, ϵ_{dc} is the static dielectric constant of the crystal.

The previous four equations constitute the simplest band transport model among a whole range of band transport models - *the one-center model* (Buse, 1997). It discusses a transport that includes only electrons dispensed and trapped by a single donor ion. In many materials the charge transport process is more complicated, since it involves electrons and holes at the same time, provided and trapped by several donors or acceptors.

The photorefractive effect is essentially dependent on *the linear electro-optic effect*. The electro-optic effect is the change in refractive index of a material induced by the presence of a static (or low-frequency) electric field (Boyd, 2008). If the refractive index depends linearly on the magnitude of the applied electric field, the effect is called *linear* or *Pockels effect*. It is a second-order nonlinear effect, meaning that it can be described by a second-order nonlinear susceptibility[1]. Since all photorefractive materials are also electro-optic, the presence of an electric field in these media will induce a refractive index change via the Pockels effect (Yeh, 1993). The refractive index changes are usually described by changes in the impermeability tensor, the inverse of the relative dielectric tensor, as

$$\Delta\eta \equiv \Delta\epsilon^{-1} = \Delta\left(\frac{1}{n^2}\right) = \mathbf{r}\cdot\mathbf{E}, \tag{5.5}$$

where η is the impermeability tensor, ϵ is the relative dielectric tensor, $\mathbf{r}$ is the linear electro-optic tensor, and $\mathbf{E}$ is the applied electric field vector.

The applications of photorefractive effect include volume hologram recording (Peltier and Micheron, 1977), beam coupling (Yeh, 1989), phase conjugation of the optical waves (Feinberg, 1982), image amplification (Brignon *et al.*, 1995), real-time holographic interferometry (Cedilnik *et al.*, 2000), etc.

The photorefractive properties are found in several classes of electro-optic materials, including ferroelectric crystals such as $LiNbO_3$, $Sr_xBa_{1-x}Nb_2O_3$, $BaTiO_3$, $KNbO_3$, sillinite crystals such as $Bi_{12}SiO_{20}$, $Bi_{12}GeO_{20}$ and $Bi_{12}TiO_{20}$, semiconductors such as GaAs, InP and CdS, and polymers (Jensen, 1999). The materials used in experiments presented in this thesis are iron doped lithium-niobate (Fe:LNB) and cerium doped strontium-barium-niobate (Cr:SBN).

[1]This is the quadratic term in the expansion of the material polarization in terms of an applied DC electrical field.

5.1.1 Properties of lithium-niobate and strontium-barium-niobate

Lithium-niobate is one of the most versatile nonlinear crystals with a wide range of applications, including electro-optic (Pockels cells) and acusto-optic modulators, Q-switching devices, second harmonic generation, optical parametric oscillation, phase matching, integrated optical waveguides generation, etc.. Besides, lithium-niobate is widely used photorefractive material, because of his high electro-optic coefficient and possibility of getting high photorefractive sensitivity by appropriate doping. In this purpose transition metals are used, particularly iron (Shah *et al.*, 1976).

The iron ions occur in lithium-niobate in two different valence states, Fe^{2+} and Fe^{3+} (Peithmann *et al.*, 1999). The iron is doped in form of Fe_2O_3, and its optimum concentration for photorefractive applications is $0.06wt\%$[1]. Electrons are optically excited from Fe^{2+} to the conduction band, they are moved by diffusion, drift and the bulk photovoltaic effect and they are trapped elsewhere by Fe^{3+} ions.

Iron doped lithium-niobate is of great interest in the fields of holographic data storage and narrow-band wavelength filters for optical telecommunications (Nee *et al.*, 2000).

Strontium-barium-niobate ($Sr_xBa_{1-x}Nb_2O_6$, $0.25 \leq x \leq 0.75$ or SBN) is another frequently used photorefractive material. This is because of its particularly large electro-optic, thermo-optic, pyro-electric and piezo-electric coefficients, and excellent optical quality (Günter and Huignard, 2006). The most widely used compositions of SBN are those with $x = 0.6$ and $x = 0.75$.

Another attractive feature of SBN is the large number of vacant lattice sites that can be occupied by dopants to provide a high density of photorefractive charge carriers (Vazquez *et al.*, 1991). Because of this, doping of SBN by appropriate materials (in a case of SBN it is cerium, chromium or rhodium) the photorefractive response can be improved (increased charge density and photorefractive structure formation rate) (Ewbank *et al.*, 1987).

Besides being useful in applications such as two-wave mixing (Sayano *et al.*, 1989) and self-pumped phase conjugation (Wood *et al.*, 1987), it is the most widely used material in research on photorefractive solitons (Segev *et al.*, 1992).

[1] weight percent

5.2 Generation and characterization of waveguide arrays

5.2.1 1D arrays

For the generation of the 1D Fibonacci waveguide array the Fe:LNB is used. The mass fraction of Fe_2O_3 is 0.05 %. Dimensions of the crystal are 3 $mm \times 0.5$ $mm \times$ 10 mm, with the optical axis along the z direction (10 mm). Waveguides are fabricated using an in-house developed laser writing system comprising CW laser at 473 nm (Oxius - SLIM-473), a precise two-axis positioning platform (Ludl Electronic Products Ltd. - BioPoint 2 Precision Stage System), two stepper motors (Standa Ltd - 8MR150), mirrors for directing the laser beam, and a microscope objective (50X Mitutoyo Plan Apo Infinity-Corrected Long WD Objective).

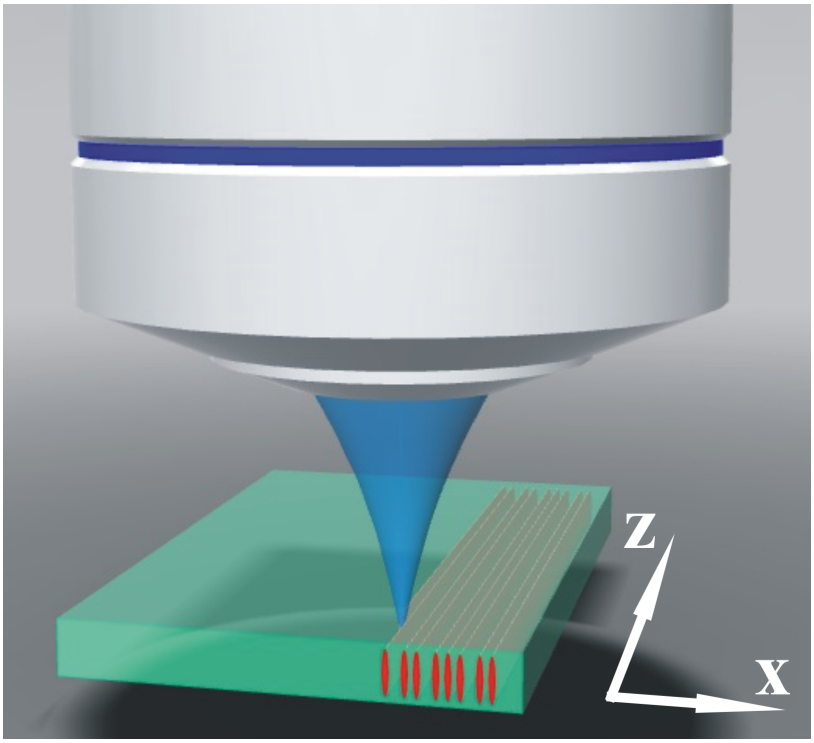

Figure 5.1: Illustration of 1D waveguide array writing process.

The principle of waveguides writing is shown in Fig.5.1. The platform can move the crystal in the x-z plane. The laser beam propagates along the y axis and it is focused by the microscope objective slightly below the upper surface of the crystal. In this way, the laser makes a controllable local change of the refractive index. By moving the sample along the z direction, a uniform modification of the refractive

index profile is achieved. A detailed explanation of the writing system one can find in Zarkov *et al.* (2012). The width of the waveguide obtained in this way is approximately 5 μm with a maximum refractive index contrast of $\Delta n \sim 1 \times 10^{-4}$, estimated from numerical simulations.

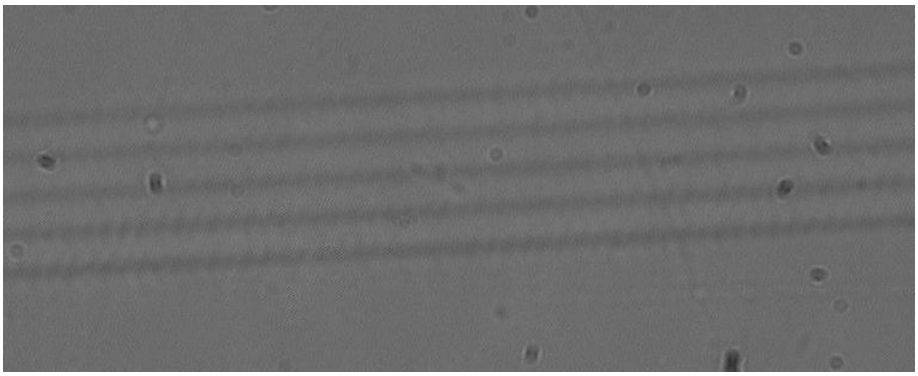

Figure 5.2: Array of the waveguides seen under microscope.

A scheme of the experimental setup for the structure diagnostics is shown in Fig.5.3. The He:Ne laser is used for an excitation beam generation, because the absorption coefficient of Fe:LNB is relatively low at 633 nm (Shah *et al.*, 1976).

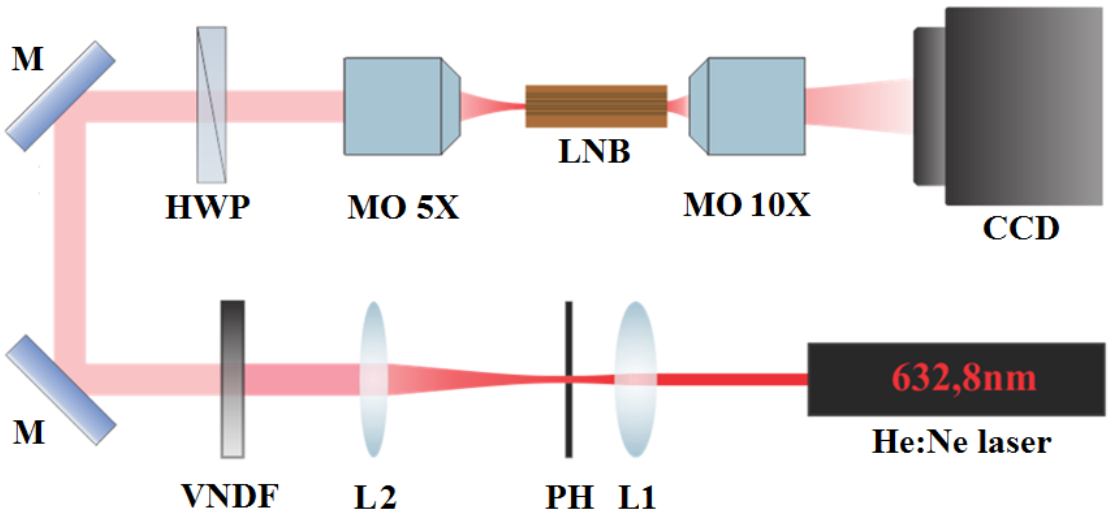

Figure 5.3: Scheme of experimental setup for one-dimensional waveguide array diagnostics. L - lens, PH - pinhole, M - mirror, MO - microscope objective, VNDF - variable neutral density filter, HWP - half-wave plate, CCD - camera, LNB - Fe:LNB crystal with inscribed waveguides, He:Ne laser is vertically polarized.

The diameter of the emerging beam is enlarged by a beam expander, consisting of the lenses L1 and L2, with focal lenghts of 30 mm and 100 mm, respectively. A pinhole of 20 μm placed between the lenses in the position where their focal

points overlap filters the transverse modes higher than TEM00. The beam power is reduced by variable neutral density filter (VNDF) from approximately 1 mW to 20 μW. The light is initially polarized linearly in the vertical direction, so that the mirrors don't affect the polarization direction. The half-wave plate (HWP) can be used afterwards to change the direction of polarization, if necessary.

An excitation beam is focused on the front face of the crystal and propagates along the z direction. The beam waist is 10.5 μm and the power is roughly 10 μW. The crystal is situated in a holder which can be moved continuously in the x direction. In this way, the beam can be launched into appropriate position in the waveguide array.

The intensity pattern appearing at the exit face of the crystal is recorded by means of an imaging system which consists of a microscope objective (Newport M-10X), and CCD camera (Canon EOS 60D). An image formed in this way is shown in Fig.5.4a. The final result of the measurement is the light intensity distribution over the middle horizontal line (yellow line in the figure), as it is shown in Fig.5.4b. No image processing is carried out.

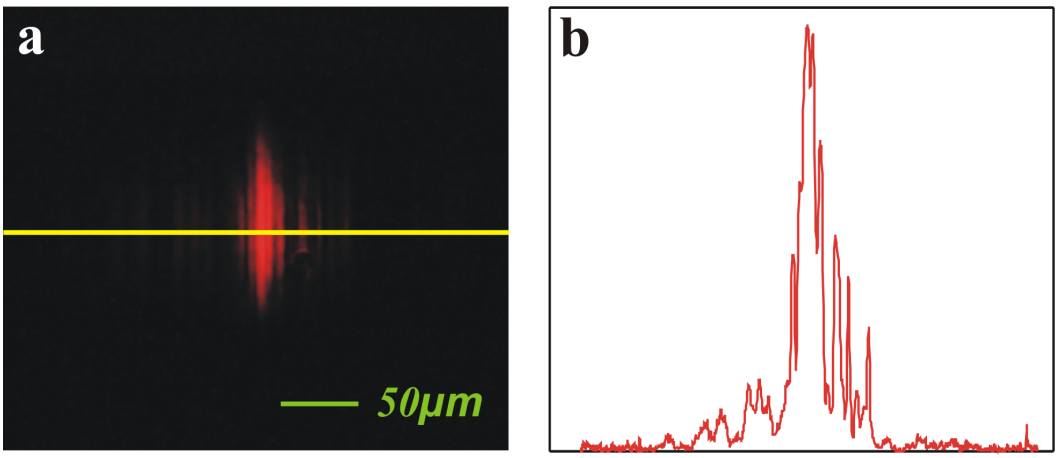

Figure 5.4: The light intensity distribution acquisition. a) The intensity distribution of light at the back side of the crystal, and b) the intensity distribution of light along a cross-section denoted by the yellow line in a).

The scheme of experimental setup for excitation of a lattice generated in LNB by 1D Airy beam is represented in Fig.5.5.

The Nd:YAG lase with doubled frequency (532 nm) is used as a light source. After appropriate preparation, the same as those shown in Fig.5.4 (using L1, PH and L2), the broad Gaussian beam is sent to the spatial light modulator (SLM - HoloEye LC 2002). It is transmissive LCD (600 $\times$ 800 pixels, 32 μm pixel pitch)

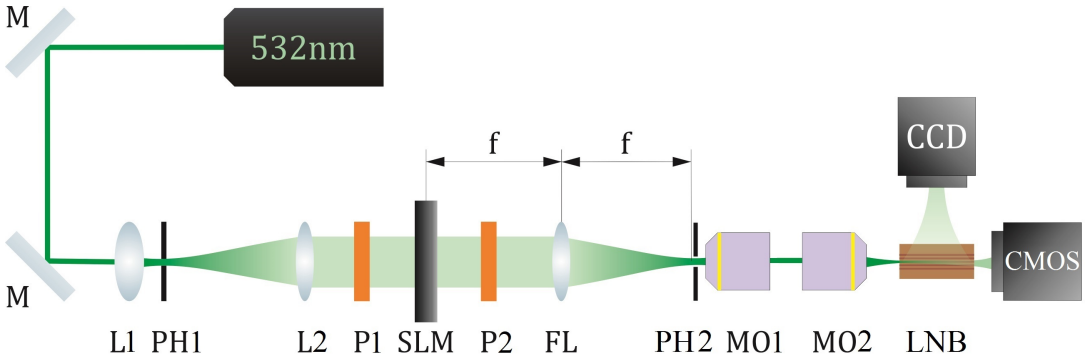

Figure 5.5: Scheme of experimental setup for 1D waveguide array excitation by Airy beam. L - lens, PH - pinhole, M - mirror, MO - microscope objective, SLM - spatial light modulator, FL - Fourier lens, CCD - camera, CMOS - camera, LNB - Fe:$LiNbO_3$ crystal with inscribed waveguides

which modulates the light passes through. The modulation can be amplitude or phase, depending on polarization of incoming light (defined by polarizer P1). This means that each pixel can attenuate the intensity or change the phase of light in the controlled manner[1]. The gray scale of the picture displayed at the SLM is mapped into modulation intensity. In this experiment the phase modulation is utilized because, in this case, it provided Airy beam of better quality (without distortion of beam profile). To generate 1D Airy beam, the phase distribution represented in Fig.5.6a (a cubic function) was displayed at the SLM. Since the light polarization state passing through the SLM become slightly elliptic, the polarizer P2 let one particular linearly polarized component. In this way a deterioration of the generated beam profile was avoided.

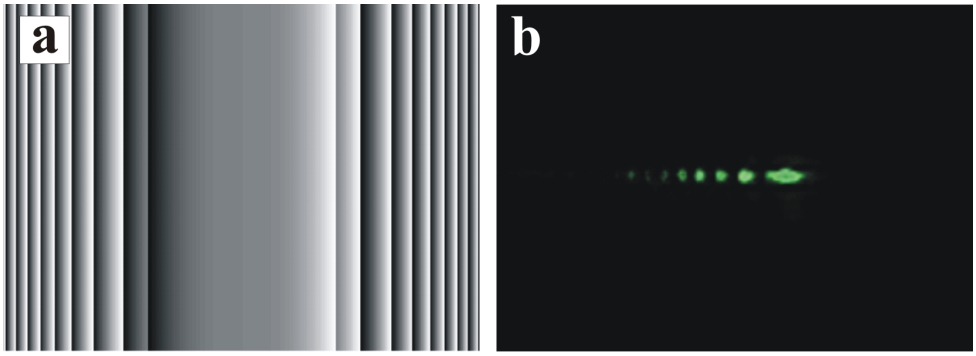

Figure 5.6: 1D Airy beam generation. a) Phase distribution (a cubic function) displayed at the SLM. b) 1D Airy beam generated by the setup shown in Fig.5.5.

The 1D Airy beam is formed in image plane of the Fourier lens (FL). Since the

[1]The SLM modulation range strongly depends on wavelength. The wavelength of 532 *nm* provides nearly optimal functioning (maximum modulation range).

SLM generates multitude of Airy beams[1], the spatial Fourier filter (FF) was placed in the focal plane of the FL in order to pass only one of them. The beam is then focused by imaging system made of two microscope objectives (MO) at the crystal front face.

The intensity pattern appearing at the exit face of the crystal was recorded with a CMOS camera (BCi_4 CMOS camera, C-Cam Technologies). Simultaneously, the light intensity distribution along the crystal was provided recording a scattered light with a CCD camera (Canon EOS 60D) mounted above the crystal. Since its intensity was very low, the exposition of two minutes was applied.

5.2.2 2D arrays

For the generation of the two-dimensional Fibonacci waveguide array the Ce:SBN is used. The mass fraction of CeO_2 is 0.2 %, providing a good photorefractive response and a low absorption. Dimensions of the crystal are $5\ mm \times 5\ mm \times 20\ mm$. The c-axis (extraordinary axis) is lined along the x direction, as shown in Fig.5.7b. The copper electrodes for crystal voltage biasing along extraordinary axis are placed on its $y-z$ sides. In this configuration a z-axis directed light beam, if the crystal is voltage biased (usually $1-2\ kV/cm$), makes a refractive index change proportional to the beam intensity by means of the photorefractive effect.

The reason for using SBN in this experiment is its large electro-optic anisotropy, i.e. significant difference between relevant electro-optic coefficients (Efremidis *et al.*, 2002). Namely, the refractive index along the ordinary axis is $n_o(@\ 514.5\ nm) = 2.36$ and along the extraordinary one is $n_e(@\ 514.5\ nm) = 2.33$, and the relevant electro-optic coefficients of this crystal are $r_{33} = 235\ pm/V$ and $r_{13} = 47\ pm/V$ (Ewbank *et al.*, 1987). If propagated in z-direction an y-polarized wave will see a refractive index

$$n_o'^{\,2} = n_o^2 - n_o^4 r_{13} E_{sc}, \tag{5.6}$$

while an x-polarized wave will see a refractive index

$$n_e'^{\,2} = n_e^2 - n_e^4 r_{33} E_{sc}, \tag{5.7}$$

where $E_{sc}\vec{e}_x$ is the space-charge field generated by the external bias (Efremidis *et al.*, 2002).

[1]SLM display behaves as 2D diffraction lattice.

When a light beam propagates in the z-direction and external voltage is applied, the photorefractive effect occurs, which means generation of free charge carriers, their redistribution by external electric field and at the end relaxation, forming the space-charge field and eventually a refractive index change. If the beam is ordinary polarized, the refractive index changes according to Eq.5.6. Since the corresponding electro-optic coefficient is relatively small, the generated space-charge field changes the refractive index in very small amount, which in practice can be neglected. It means that the medium is optically homogeneous for ordinary polarized light, despite the presence of space-charge field. This is the reason why the ordinary polarized beams are used for a lattice generation.

Now, if the crystal is excited by extraordinary polarized light beam, a situation is pretty much different. The refractive index distribution is defined by Eq.5.7, meaning that it follows previously generated space-charge field distribution. Since the corresponding electro-optic coefficient has the large value, the propagating beam is strongly affected by photo-induced refractive index profile. This is why the extraordinary polarized beams are used as probing beam. It should be emphasized that the bias voltage has to be switched off to prevent deterioration of the induced structure.

The ordinary polarized beam used for the induction of a photonic lattice, so-called a lattice beam, has to be transversely modulated, but of longitudinally translation invariant intensity distribution. All beams satisfying this condition posses the sharp δ-like angular spectrum represented by a circle at the Fourier plane (Bouchal, 2003). It means that the lattice beams can be obtained by coherent superposition of the plane waves axes lie on a conical surface. These kind of beams are in literature often denoted as *the nondiffracting beams*.

First lattices realized by this technique were those of the simplest geometries, such as diamond, square or hexagonal ones (Desyatnikov *et al.*, 2005, 2006, Fleischer *et al.*, 2003), corresponding with discrete polygonal Fourier spectrum. Since an arbitrary azimuthal modulation of the Fourier spectrum is allowed, there exist an infinite number of nondiffracting beams, meaning that more complex lattices can be induced. In that sense, the photonic Bessel, Mathieu and Weber lattices were realized (Rose *et al.*, 2012).

Further improvement of this technique is an implementation of an incremental recording technique for multiplexed hologram storage (Taketomi *et al.*, 1991). Here, lattice waves of different periodicity are incoherently superimposed, leading to multiperiodic lattices (Rose *et al.*, 2008). Based on this idea a large variety of complex

photonic lattices were realized (Boguslawski *et al.*, 2012*a*,*b*).

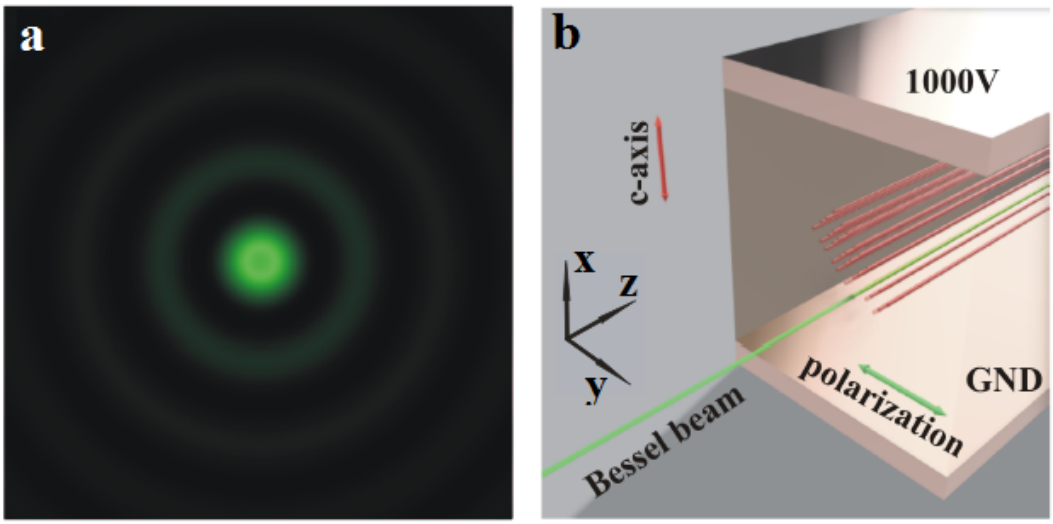

Figure 5.7: 2D waveguide array writing. a) Intensity profile of a zero order Bessel beam, b) Multiplexing of the Bessel beams.

Despite the flexibility provided by the previously mentioned technique, it cannot be used in this form for 2D Fibonacci lattice generation. The reason is a complete absence of periodicity in the lattice. That's why the modified technique, proposed by Diebel and coworkers in (Diebel *et al.*, 2014), is used. It is based on multiplexing of nondiffracting Bessel beams (Durnin *et al.*, 1987). The idea is to photo-induce each lattice site by a zero order Bessel beam (Fig.5.7a). The principle of the technique is shown in Fig.5.7b.

The scheme of the experimental setup for 2D photonic structures generation is illustrated in Fig.5.8.

A beam at wavelength of 532 *nm*, generated by frequency doubled continuous wave Nd:YAG laser, after appropriate expansion illuminates the first spatial light modulator (Holoeye Pluto). It acts as a phase spatial light modulator (PSLM) which means that it writes in a spatial phase distribution onto the illuminating beam. It is positioned in real space related to the image plane defined by an optical imaging system consisting of two lenses positioned in the front of SBN crystal. The second spatial light modulator (Holoeye LC-R 2500), acts as an amplitude spatial light modulator (ASLM), modifying the intensity distribution of the illuminating beam. ASLM is positioned in Fourier space related to the image plane, playing a role of a spectral low-pass filter. All these components generate inducing Bessel beam with predefined parameters, such as a structural size (width of a central disc)

and a transverse position.

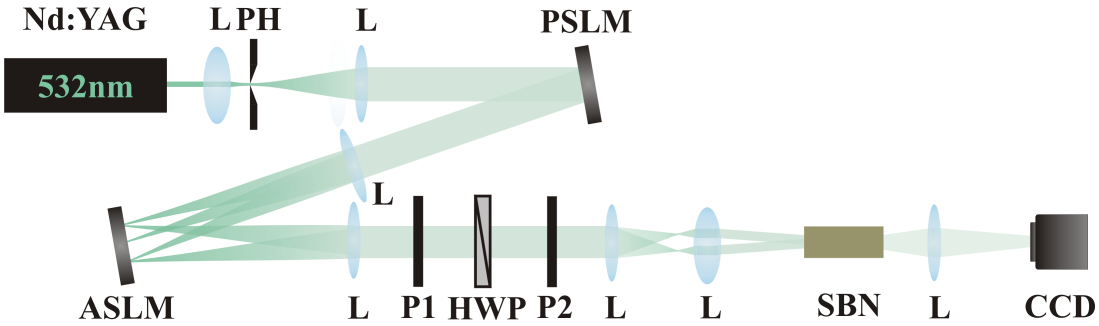

Figure 5.8: Scheme of the experimental setup for 2D waveguide array generation and diagnostics. L - lens, PH - pinhole, P - polarizer, PSLM - phase spatial light modulator, ASLM - amplitude spatial light modulator, HWP - half-wave plate, CCD - camera

The polarizers and the half-wave plate define polarization direction of a beam passing the crystal. The polarizer P1 provides vertical (x-direction) linear polarization. The polarizer P2 is mounted on a rotational holder which sets its polarizing axis in one of two required positions - vertical or horizontal. The half-wave plate, also mounted on a (different) rotational holder, rotates the polarization vector of the incident linearly polarized light. Changing the polarization direction of the beam incident on polarizer P2, one can modulate the intensity of linearly polarized beam appearing after the polarizer. In the lattice induction process, meaning the successive generation of the identical Bessel beams at different transverse positions, the polarization axis of the polarizer P2 is horizontally directed.

The desired lattice is generated by setting the central intensity maximum of the writing Bessel beam to predefined lattice site positions. A consecutive illumination of the crystal by the Bessel beam leads to an incoherent superposition of all writing light fields. The incoherent superposition is a crucial idea of this induction approach, because coherent superposition, simultaneous generation of the all required beams, would cause modulation of the field intensity in the z-direction. The illumination time per one beam is $0.5s$, and 10 cycles was performed. A central disc diameter of the writing Bessel beam is 13 μm. The biasing voltage is 1 kV.

The induced lattice is excited by a Gaussian beam, Fig.5.9. The probe beam is generated by setting the appropriate phase and amplitude distributions on the spatial light modulators. The diameter of the beam is 14 μm.

The intensity distributions of probing beams are recorded by a CCD camera imaging system.

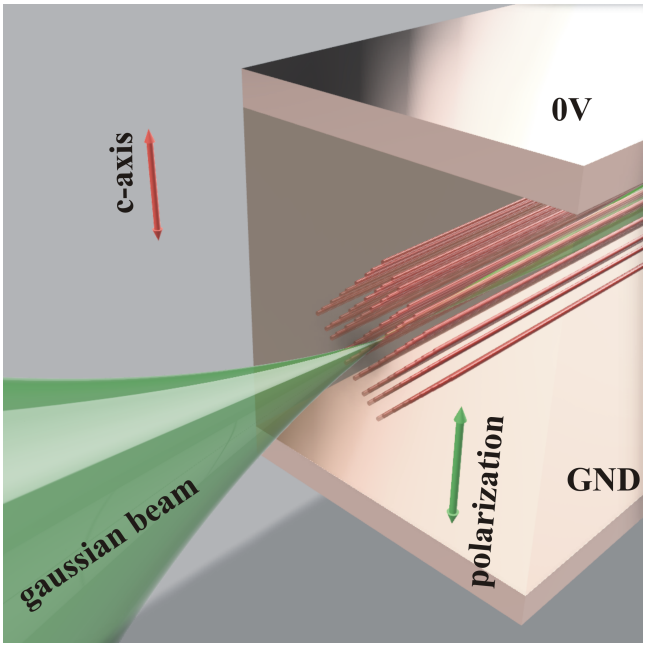

Figure 5.9: The excitation of the 2D Fibonacci lattice by Gaussian beam - a single site excitation.

A LED is placed above the crystal (not shown in Fig.5.8) in order to erase the inscribed lattice when diagnostics is complete.

Chapter 6

Results and discussion

6.1 Light propagation in position modulated 1D Fibonacci lattice

In this section there would be considered the beam propagation in 1D Fibonacci waveguide array fabricated in Fe:LNB crystal, launched at different incident positions. In Fig.6.1 it is shown the refractive index profile of the realized structure. In numerical simulations it is modeled as $n(x) = n_s + \Delta n \sum_{i=1}^{N} e^{-(x-x_i)^2/2\sigma^2}$. Here, n_s is a bulk material refractive index, Δn is an optically induced refractive index contrast, x_i denotes central position of i^{th} waveguide and σ defines a waveguide width. The two elements of the Fibonacci word, A and B, to the distances between the central positions of waveguides (x_i), a and b are mapped (cf. Fig.6.1). It means that an array of N waveguides is arranged in such a way that a series of successive differences $(x_i - x_{i-1})$, $i = 2 :$ N, follow a part Fibonacci word. In this experiment, it is experimentally realized a waveguide array that represents the following Fibonacci word: ABAABABAABAABABAABA (the first 20 elements).

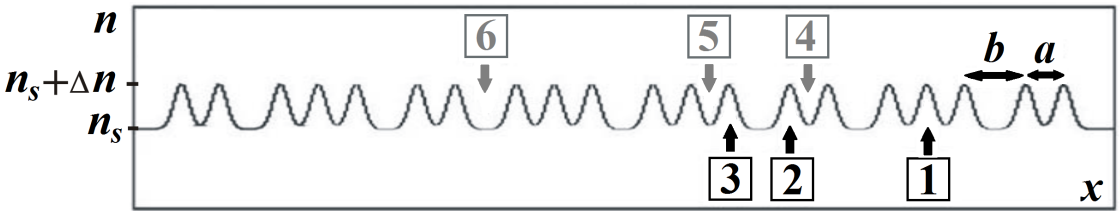

Figure 6.1: The refractive index profile of 1D Fibonacci waveguides array

Three incident positions inside waveguides marked by numbers 1, 2, and 3 in

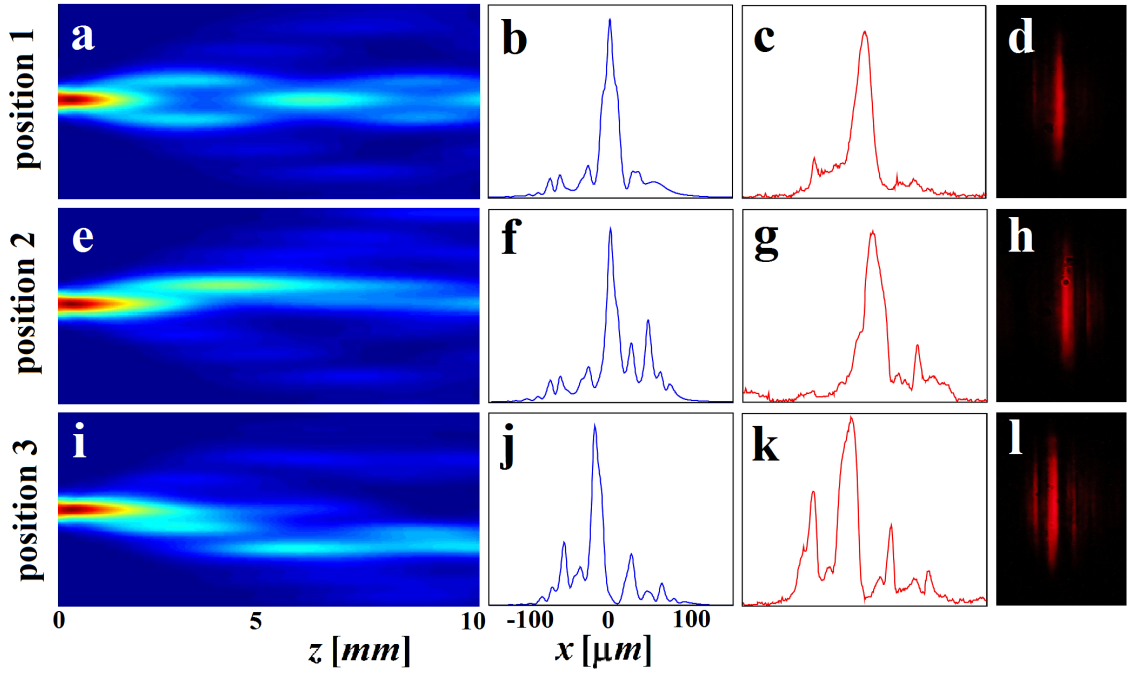

Figure 6.2: Light propagation through Fibonacci waveguide arrays. Incident positions of the excitation beam are inside certain waveguides, marked with numbers 1, 2 and 3 in Fig.6.1. In the first column (a, e, i) the numerically calculated light intensity distributions along waveguide array are shown. The second column (b, f, j) presents calculated intensity distributions at the exit face of the structure, while the third column (c, g, k) presents corresponding experimental results, provided from the snapshots of the exit face of the crystal (fourth column - d, h, l). Physical parameters: the crystal length $L = 10\ mm$, refractive index contrast $\Delta n = 1 \times 10^{-4}$, and Gaussian beam width 10 μm.

Fig.6.1 are chosen. Corresponding light intensity distributions are presented in the first, second, and third row in Fig.6.2. The first column presents numerically calculated intensity distribution along the propagation distance, with output profiles in the second column. The experimental results for the same incident positions are presented as intensity distributions at the exit face of the crystal (the forth column) with corresponding profiles in the third column. One can see a very good agreement with numerically obtained profiles.

Next, the beam propagating characteristics for incident positions between waveguides, marked by numbers 4, 5, and 6 in Fig.6.1, are investigated. The Fig. 6.3 represents the summary of the the numerical and experimental results for these cases. The layout of this figure is the same as in Fig.6.2: incident positions 4, 5, and 6 correspond to the results in the first, second, and third row in Fig.6.3, respectively. Beam diffraction for incident positions between waveguides is more pronounced than for incident positions inside waveguides (cf. Fig.6.2).

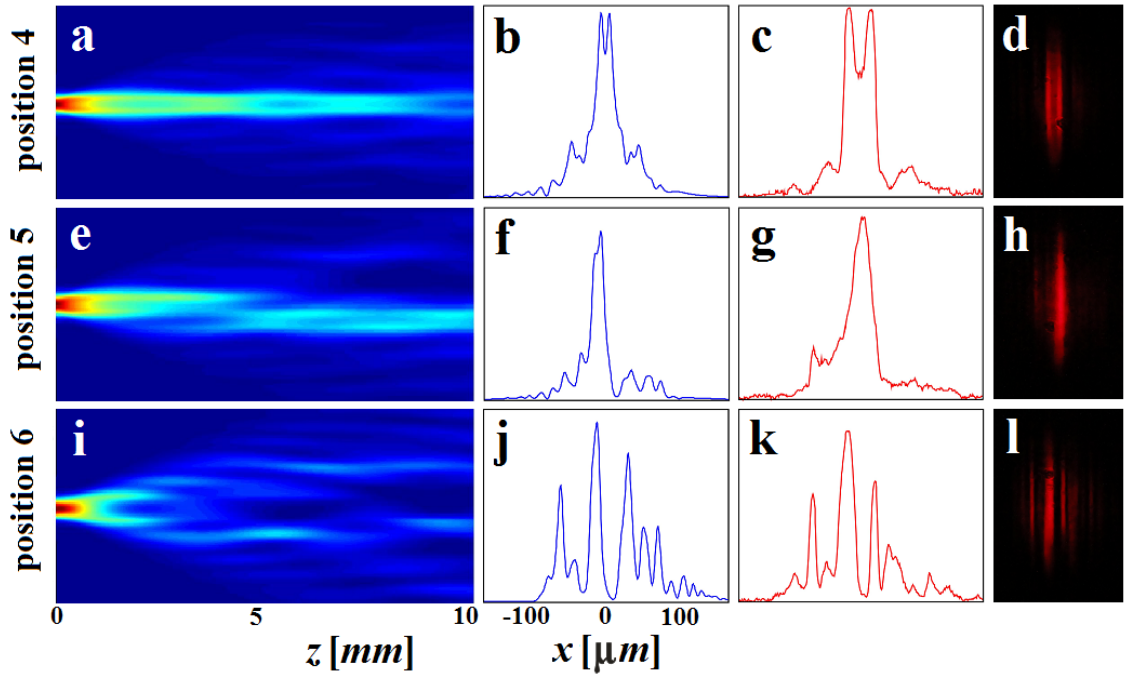

Figure 6.3: Light propagation through Fibonacci waveguide arrays. Incident positions of the excitation beam are at the positions between waveguides, marked with numbers 4, 5 and 6 in Fig.6.1. In the first column (a, e, i) the numerically calculated light intensity distributions along waveguide array are shown. The second column (b, f, j) presents calculated intensity distributions at the exit face of the structure, while the third column (c, g, k) presents corresponding experimental results, provided from the snapshots of the exit face of the crystal (fourth column - d, h, l). Physical parameters: the crystal length $L = 10\ mm$, refractive index contrast $\Delta n = 1 \times 10^{-4}$, and Gaussian beam width 10 μm.

Next, the beam propagation in Fibonacci waveguide arrays considering longer propagation distances ($L = 100\ mm$) is studied. In this case, only simulations are conducted. It is used the effective beam width as a measure of the beam expansion. Here an averaging (arithmetic mean) of the effective beam widths of more then a hundred different beams, each of which is obtained by the excitation of one of the consecutive waveguides, is performed. The reason is a removing of the effects of the local environment, i.e. the influence of the neighboring waveguides. The averaged effective beam width is calculated along the propagation distance, and compared for the Fibonacci waveguide array and three different periodic waveguide arrays. Separations a and b in the Fibonacci waveguide array are used as periods $d = 16.18\ \mu m$ and 10 μm for the two periodic waveguide arrays. The third periodic array is produced in such a way that the same number of waveguides as in the quasi-periodic array is arranged in periodic manner in the same space (in our geometry, its lattice period is $d = 12.38\ \mu m$), aimed as the most appropriate for comparison

with Fibonacci waveguide array.

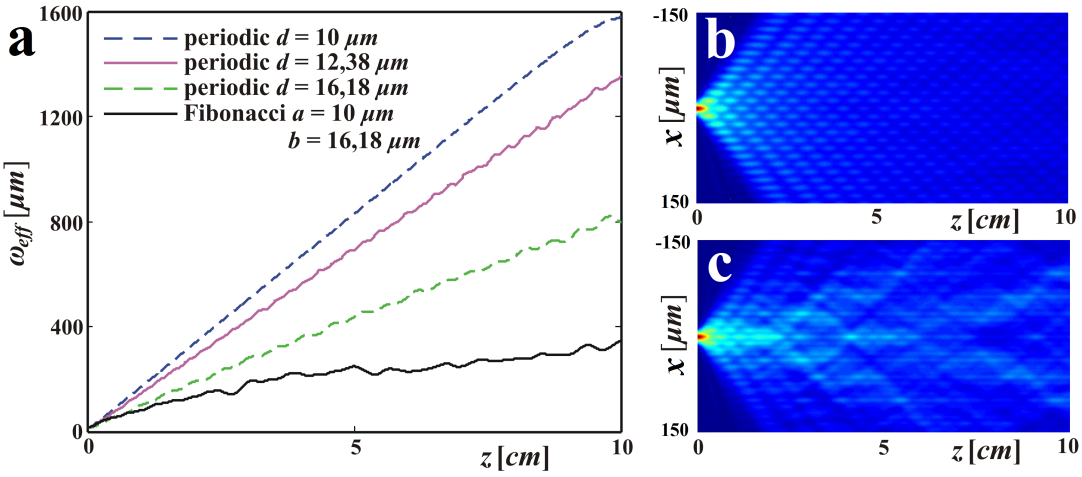

Figure 6.4: Comparison between beam diffraction in periodic and quasi-periodic waveguide arrays. (a) Averaged effective beam widths versus the propagation distance, for refractive index contrast $\Delta n = 1 \times 10^{-4}$. (b) Field intensity of the beam in longitudinal direction (z) during the propagation for periodic lattice with $d = 12.38\ \mu m$. (c) Averaged field intensity distribution for Fibonacci lattice. Crystal length is $L = 100\ mm$.

Fig.6.4a presents the averaged effective beam width along the propagation distance for Fibonacci lattice, and the effective beam width for several other periodic lattices with the same value of refractive index contrast of $\Delta n = 1 \times 10^{-4}$. The beam propagation in periodic lattice with $d = 10\ \mu m$ shows the strongest discrete diffraction (with linear increase of effective beam width), followed by periodic lattices with $d = 12.38\ \mu m$ and $d = 16.18\ \mu m$, respectively. This represents an expected result, because shorter lattice constant implies stronger coupling, leading to faster transverse energy transport. The most important result, considering Fig.6.4a, is the fact that the effective width expansion rate of the beam propagating in the Fibonacci lattice is notably lower then those propagating in all of three regular lattices (except in first 1.5 cm, where effective beam with in regular lattice with $d = 16.18\ \mu m$ is a bit lower because of the weaker coupling between adjacent waveguides in this lattice). Comparing the beam evolution in Fibonacci and corresponding regular ($d = 12.38\ \mu m$) lattice[1], one can see that the width in Fibonacci lattice is more than three times less then the width in the regular one. Besides, the effective beam width curve corresponding to Fibonacci lattice has slightly concave shape, unlike the one corresponding to regular lattice which is linear.

[1] the same number of waveguides at the same space

The reason is a particular arrangement of the Fibonacci lattice. Namely, the aperiodicity of waveguide positions, or, equivalently, coupling constants[1], tends to support localized eigenstates, while, the self-similarity can lead to extended eigenstates. A synergy of these two concurrent trends leads to formation of critical eigenstates. This explains the significantly lower effective beam width in Fibonacci lattice comparing to the regular one in one hand, and its undoubted increase, on the other.

Fig.6.4b presents a field distribution along the propagation distance, for a periodic lattice with $d = 12.38\ \mu m$, simulated for 10 cm of propagation. The averaged field distribution for more than hundred of different incident positions in a Fibonacci lattice is presented in Fig.6.4c.

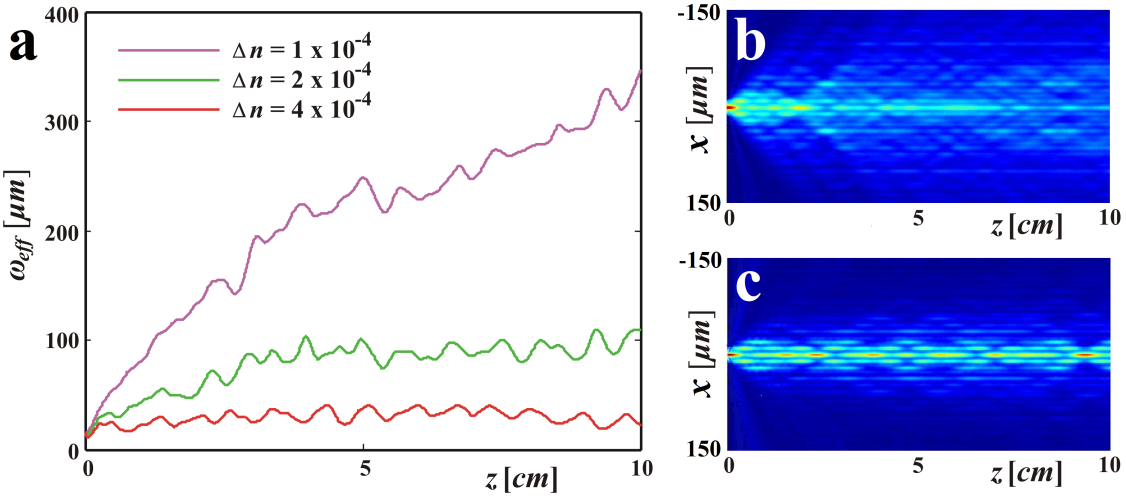

Figure 6.5: Light propagation in Fibonacci lattice for a higher refractive index contrast. (a) Comparison between propagation in waveguide arrays with different refractive index contrast: averaged effective beam widths versus the propagation distance. Averaged field intensit distributions for (b) $\Delta n = 2 \times 10^{-4}$ and (c) $\Delta n = 4 \times 10^{-4}$.

At the end, the influence of various refractive index contrasts (Δn) on the beam propagation through Fibonacci waveguide arrays is investigated. Again, the averaged effective width along the propagation distance for each value of Δn is calculated. The increase of refractive index contrast makes diffraction suppression more pronounced (Fig.6.5a): the broadening of the beam becomes almost completely suppressed for longer propagation distances. The averaged intensity distribution, for more than hundred of different incident positions, is presented for $\Delta n = 2 \times 10^{-4}$ in Fig.6.5b, and $\Delta n = 4 \times 10^{-4}$ in Fig.6.5c. These should be compared with the

[1] off-diagonal disorder

corresponding distribution in Fig.6.4c for $\Delta n = 1 \times 10^{-4}$. If a refractive index contrast is increased, the light energy become more localized in the vicinity of excited waveguide.

6.2 Light propagation in position modulated 2D Fibonacci lattice

This section deals with the results of a light propagation through position modulated 2D Fibonacci lattice.

The lattice is realized as the 9×9 matrix of identical waveguides with mutual distances of $a = 37.5\ \mu m$ and $b = 23.2\ \mu m$ (cf. Fig.6.6) by using technique presented in Section 5.2.2. The ratio of these two values, a/b, approximately equals a value of the Golden ratio, that is $(1 + \sqrt{5})/2$. They also lead to an effective waveguide distance of 32 μm. The effective distance is used as lattice constant of a square lattice consisting of the same number of waveguides in the same volume as the Fibonacci lattice. The SBN crystal is 20 mm long, while the initial refractive index, n_s, equals 2.33. Typical refractive index contrast in the vicinity of a lattice site, Δn, extracted from comparison of numerical and experimental results, is 3×10^{-5}.

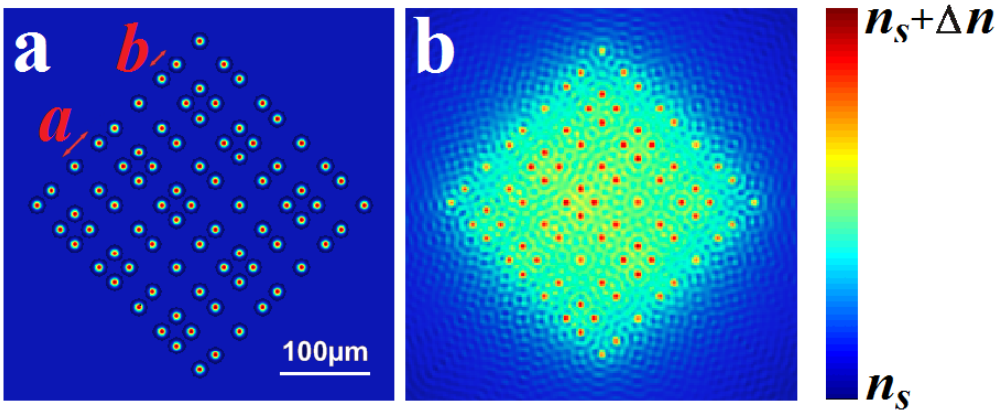

Figure 6.6: 2D Fibonacci lattice. a) The "ideal" lattice (a Gaussian refractive index profile of a single waveguide), b) The lattice obtained by incoherent superposition of zeroth order Bessel beams.

The lattice is excited at different input positions, on and between waveguides, in order to investigate the influence of diverse local conditions on the beam evolution. An excitation is a Gaussian beam of 14 μm beam waist. The beam power is several μW so the linear regime is considered. For numerical modeling of the beam evolution the paraxial wave equation is solved using a split-step method.

In Fig.6.7 transverse light distributions after 20 *mm* propagation length for three different input positions are presented. Top row images present output light distributions experimentally observed at the exit face of the crystal. Bottom row represents the corresponding distributions obtained by simulations. There is a very good agreement between experimentally and numerically obtained results.

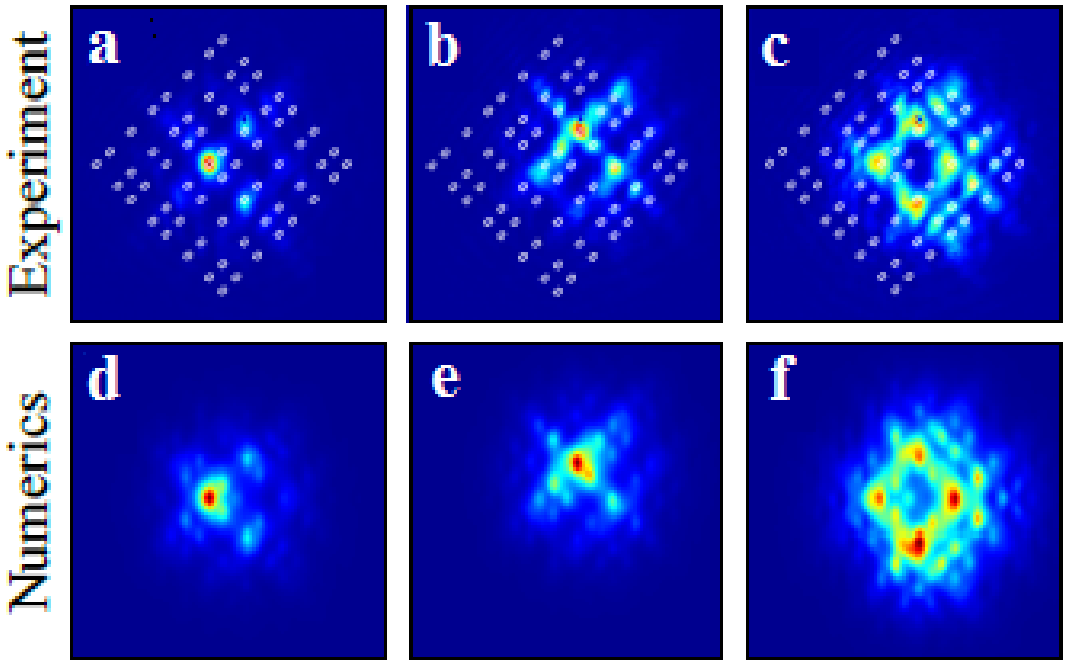

Figure 6.7: Light propagation through 2D Fibonacci lattice for three different input positions. Light intensity distributions at the exit face of the crystal. a-c Experimental results, d-f Numerical results.

In order to verify a potential of the Fibonacci lattice to suppress (or maybe completely stop) diffraction, the propagation of the probing Gaussian beam in this lattice is compared with the propagation in a (regular) square lattice.

The square lattice is induced in the same way as the aperiodic one, using the Bessel beam multiplexing technique. This is because of preservation of a comparability of the two lattices (Fibonacci and regular)[1]. A calculated refractive index profile is shown in Fig.6.8a. The central waveguide is excited by a Gaussian beam of 14 μm beam waist. The intensity distribution at the output face of the crystal is shown in Fig.6.8b, which is a typical discrete diffraction pattern expected in a square lattice (cf. (Pertsch *et al.*, 2004)). This matching implies that waveguide-like

[1]A standard procedure of a square lattice generation in SBN crystal is using the interference pattern of four coherent plane waves (Efremidis *et al.*, 2002)

structures appearing between preferred positions (the lattice sites) during the Bessel beam induction technique process do not significantly affect exciting beam evolution. Consequently, one can expect that the Fibonacci lattice induced by Bessel beams affects a propagating light in a very similar way as "ideal" one (cf. Fig6.6).

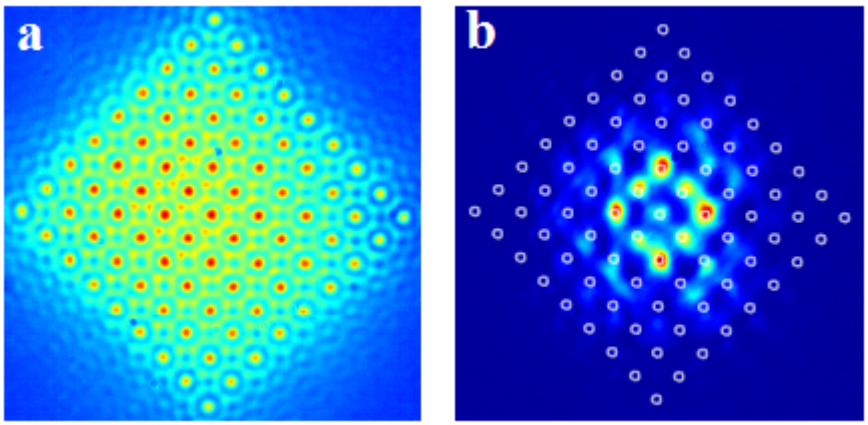

Figure 6.8: The square lattice induced by the Bessel beam multiplexing technique. a) Refractive index profile, b) experimental image of the light distribution at the crystal output face - one site excitation.

For a quantitative comparison of the transverse probe beam dynamics, it is used the effective beam width (cf. Section 3.3). To obtain a more comprehensive insight, the parameter was calculated for a crystals of 80 mm in length. An averaged effective beam width of the Fibonacci lattice is calculated as the arithmetic mean of beam widths for 50 different randomly chosen input on-site positions. Instead of being calculated for each of the 50 beams excited in one large Fibonacci lattice, the effective width has been calculated for the beams generated by excitation of the middle lattice sites of 50 different 30×30 Fibonacci lattices. In this way, a much more time efficient calculations had been achieved. The 30×30 matrices of waveguides was considered in order to avoid an influence of the surfaces, because in the lattice of this size, the excited beams do not reach the bordering waveguides for the considered length. According to the first neighbors arrangement (mutual position of the excited and each of eight adjacent waveguides), one can distinguish three different input positions, shown in the Fig.6.9.

The results are summarized in Fig.6.10. The dotted black line presents effective beam width in regular lattice,while the red line presents averaged effective beam width for 50 different input positions. Two gray lines denote extreme widths in Fibonacci lattice.

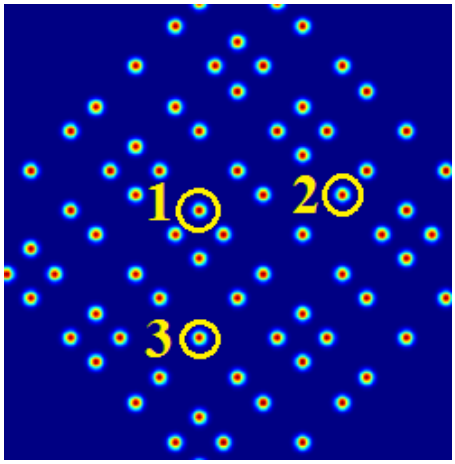

Figure 6.9: Exciting beam input positions according to the first neighbors arrangement

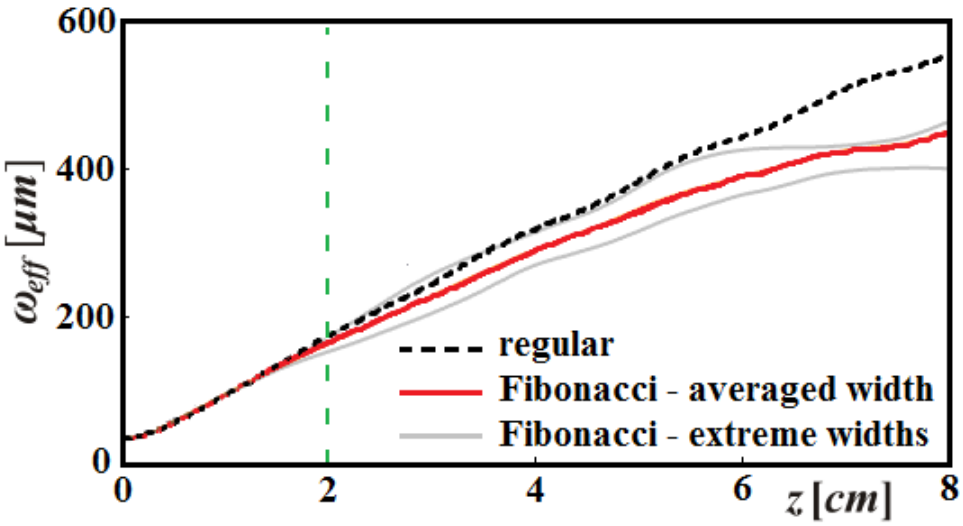

Figure 6.10: The comparison of the effective beam width - 2D Fibonacci lattice vs. square lattice

The results point out the reduced beam width expansion rate in the aperiodic lattice compared to the periodic one. In first 10 mm the widths are nearly equal due to the fact that the most of light energy is located in the excited waveguide. After 10 mm light starts to couple to adjacent waveguides with respect to the excited one. General uniqueness of propagation conditions (arrangement of waveguides) for every particular excitation beam, leads to propagation mode diversity, and consequently to different effective beam width. Despite this diversity, all analyzed modes have lower value compared to the regular lattice mode. There are few exceptions which exceed the regular lattice width close to $z = 30$ mm (cf. Fig.6.10). These are modes obtained by excitation of lattice sites with initial conditions denoted by number 3

in Fig.6.9. This is because the light is distributed between few waveguides, so the aperiodic order doesn't come to the fore. When the propagation distance becomes higher than 60 mm, the impact of aperiodic order starts to affect the propagation strongly, so widths of all modes become significantly lower than the reference one.

6.3 Light propagation in refractive index modulated 1D Fibonacci lattice

In this section 1D Fibonacci lattice of equidistant waveguides with modulated refractive index contrast (diagonal disorder) is considered numerically. It is compared to a random lattice relating their localization properties.

The refractive index profiles of these two lattices are shown in Fig.6.11. The Fibonacci lattice consists of waveguides with two different values of refractive index contrasts, Δn, higher and lower one, corresponding to symbols A and B in Fibonacci word, respectively (cf. Chapter 2). The refractive index contrast of waveguides in the random lattice follows uniform distribution. Both of the lattices have the same mean value of waveguides' refractive index contrasts, Δn_0 (dashed red line in Fig.6.11).

The lattices consisting of $N = 151$ waveguides positioned equidistantly, with the period of 11 μm. The width of a waveguide is 4 μm. Refractive index of the medium, n_s, equals 1.46[1], while the mean value of waveguides' refractive index contrasts equals 0.001. The lattices are 10 cm long.

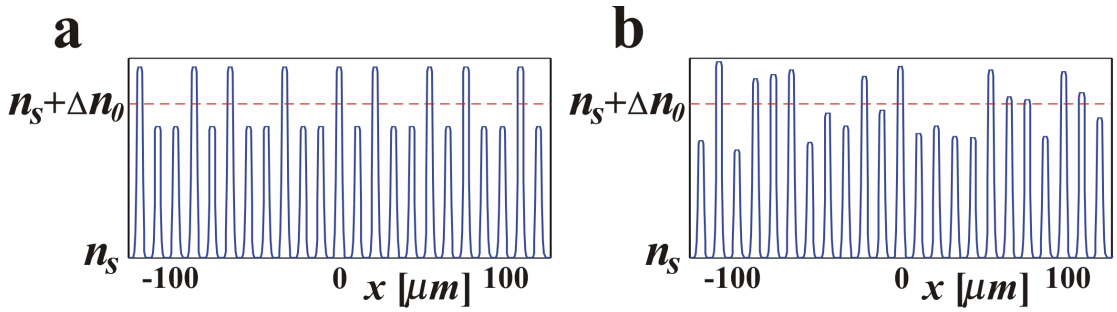

Figure 6.11: The refractive index profile of diagonal disordered Fibonacci and random lattice. a) Fibonacci lattice, b) random lattice.

As a measure of "aperiodicity level" in a lattice it is used the relative standard deviation of refractive index contrast, $\sigma_{rel} = \frac{1}{\Delta n_0}\sqrt{\frac{1}{N}\sum_{i=1}^{N}(\Delta n_i - \Delta n_0)^2}$, where Δn_i denotes refractive index contrast of a single waveguide.

[1]Approximate value of fused silica refractive index @633 nm

As a structure excitation it is used Gaussian beam of 5 μm in waist at wavelength of 632.8 nm. The effective beam width is calculated for several values of σ_{rel}: $5, 10, 20, 30$ and 40 percents[1], in Fibonacci, as well as in random lattices. It is performed an averaging over 128 different incident beam positions. Fig.6.12 summarizes these results.

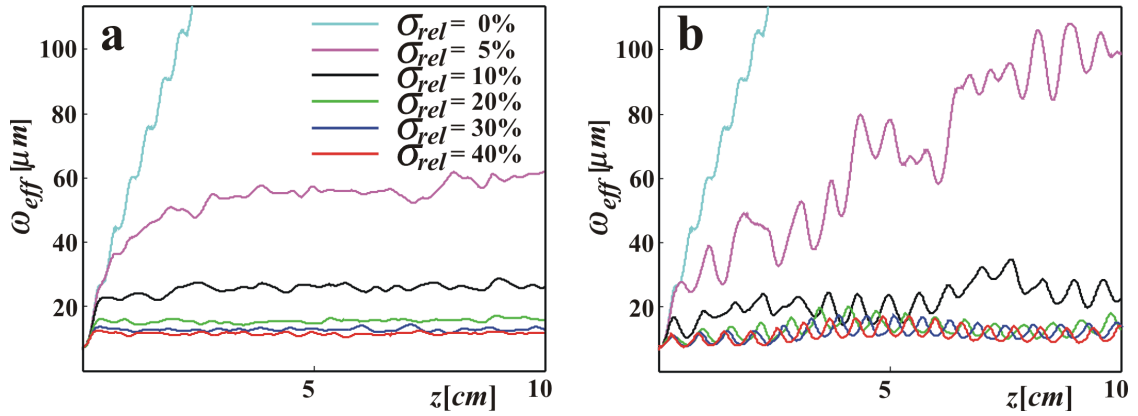

Figure 6.12: Effective beam width in 1D Fibonacci and random lattice for different levels of aperiodicity. a) Fibonacci lattice, b) Random lattice

In Fig.6.12a the effective beam width in random lattice is presented. $\sigma_{rel} = 0\%$ denotes a regular (periodic) lattice, in which the effective beam width increases linearly (it is round 400 μm at 10 cm), here acting as a reference for estimation of diffraction suppression. It is obvious that the random 1D lattice necessary leads to transverse localization (all curves go to saturation), and as σ_{rel} increases, eventual effective beam width decreases, as it is presented in Chapter 2.

In the Fibonacci lattice one can recognize a similar behavior - as aperiodicity increases, the effective beam width decreases, as it is presented in Fig.6.12b. But, unlike disordered lattice which is characterized only by localized eigenstates, the Fibonacci lattice posses self-similar properties, thus supporting extended eigenstates. Interference of aperiodicity and self-similarity leads to formation of critical eigenstates. When $\sigma_{rel} = 5\%$ these two properties are balanced in a sense, so in one hand the transverse spreading of the beam is considerably slower than in regular lattice, but on the other, the effective beam width curve doesn't approach saturation. In other cases aperiodicity dominantly affects transverse transport properties, so all curves achieve a kind of saturation, up to an irregular oscillatory behavior.

Next, an impact of disorder superimposed to the Fibonacci lattice on the transverse transport properties is considered. In Fig.6.13 the effective beam width in

[1]In Fig.6.11 the lattices with $\sigma_{rel} = 20\%$ are shown.

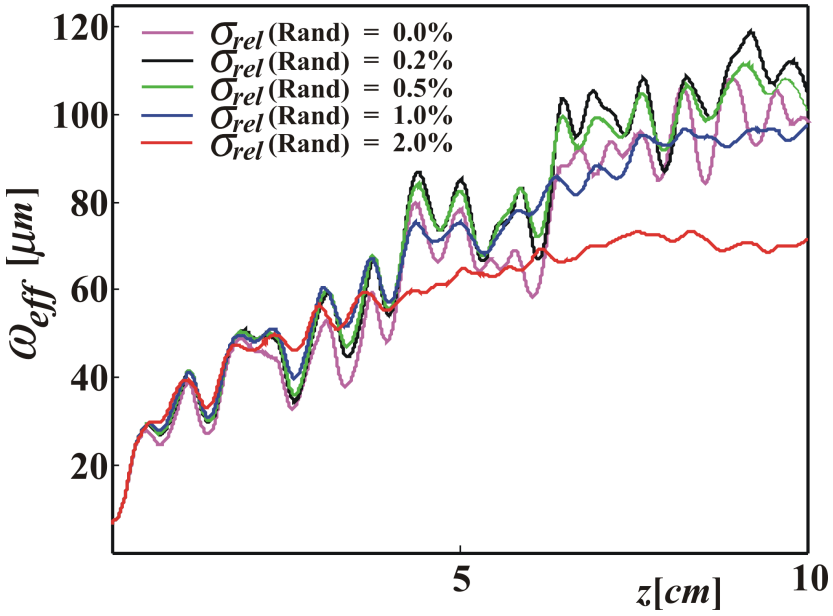

Figure 6.13: Effective beam width in 1D Fibonacci lattice for different levels of superimposed disorder - $\sigma_{rel}(Fibonacci) = 5\%$

quasiperiodic lattice with $\sigma_{rel}(Fibonacci) = 5\%$ for different degree of disorder, $\sigma_{rel}(Rand)$, is shown.

The effective beam width in the lattices with small degree of disorder, $\sigma_{rel}(Rand) = 0.2$ and $\sigma_{rel}(Rand) = 0.5$, exceeds the same parameter in the pure quasicrystal lattice. This is, as suggested in Levi *et al.* (2011), the result of coupling of the highly localized states near the pseudogap (cf. Section 2.2) to one another, leading to the states which are broader and less localized. With further increasing of disorder degree, $\sigma_{rel}(Rand) = 1.0$ and $\sigma_{rel}(Rand) = 2.0$, the effective beam width falls bellow the initial value ($\sigma_{rel}(Rand) = 0$). All this is due to the fact that the disorder makes broader eigenstates (which support transverse transport) more localized, in a similar way as in the case of a regular lattice.

6.4 Airy beam propagation in 1D regular lattice with defect

Here, the impact of 1D photonic lattices to self-banding and non-diffraction properties of 1D Airy beam was examined. Three different lattices were considered: the regular (equidistantly ordered identical waveguides), the regular with positive defect (one of the waveguides has doubled refractive index contrast) and the regular with negative defect (one waveguide left out) one. The corresponding refractive index

profiles are presented in Fig.6.14, where $d = 20\ \mu m$ is a period of lattices, and Δn is refractive index contrast. At the same Figure, the intensity distribution of exciting Airy beam relative to the previously mentioned lattices are shown. A width of the main lobe in Airy beam is 10 μm. The beam propagation was investigated experimentally (cf. Section 5.2.1) and numerically.

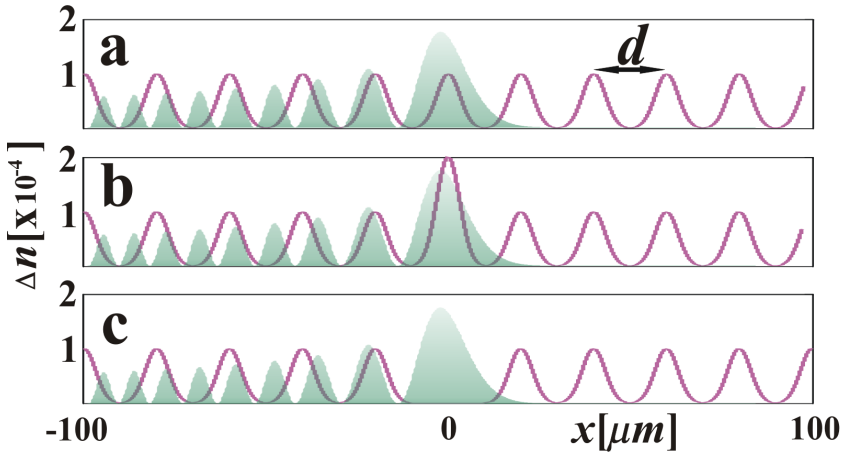

Figure 6.14: Airy beam propagation - refractive index profiles. a) Regular lattice, b) Regular lattice with positive defect and c) Regular lattice with negative defect

First, to compare appropriate effects we test the Airy beam propagation in the crystal without waveguides, i.e. in homogeneous medium. There is a typical Airy beam bending with a transverse displacement at the output, with no diffraction evident in the main lobe, observed both experimentally, Fig.6.15a and b, and numerically Fig.6.15c, after 10 mm of propagation.

Next, keeping all conditions unchanged, the Airy beam is launched in the regular lattice, with the main lobe positioned in one waveguide (an incident waveguide), as it is shown in Fig.6.14a. In Fig.6.15e it is possible to notice that the beam shape is to a large degree preserved, keeping nearly non-diffraction properties. Coupling of main Airy beam lobe to a lattice site gives completely opposite result to coupling of a Gaussian beam (cf. Fig.3.1b). Besides, one can see that the bending of the main lobe of the Airy beam is slightly weaker, Fig.6.15d-f, in comparison with the uniform case, Fig.6.15a-c. This implies that by changing refractive index contrast of the regular lattice, one can shift to a certain extent the output position of the Airy beam downward, giving the possibility to control an optical energy delivering position.

It is also studied the influence of defects on the Airy beam propagation, and its potential for active control and manipulation of the beam acceleration. The results,

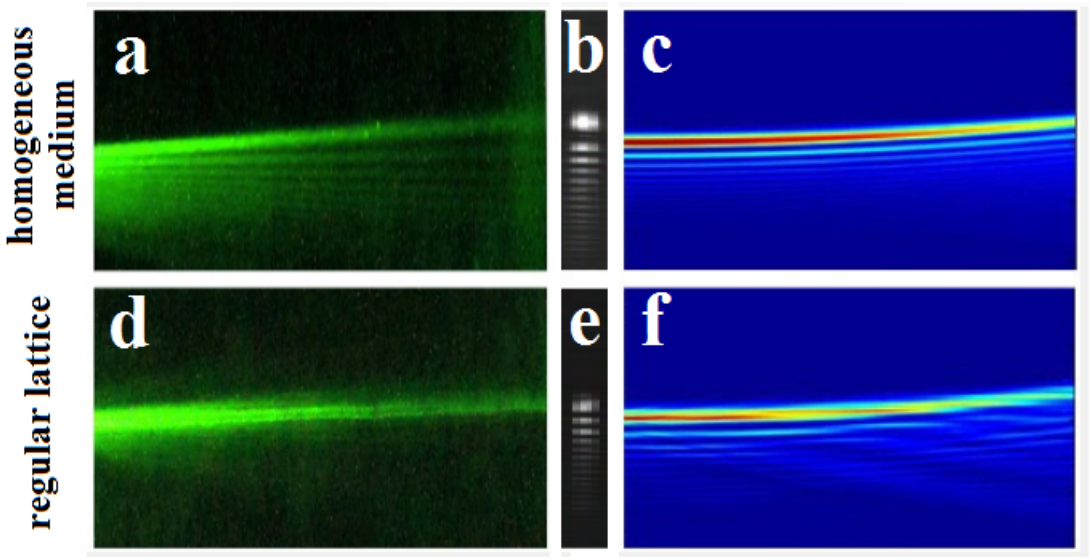

Figure 6.15: Airy beam propagation in uniform medium and in the regular lattice. Top row - homogeneous medium, bottom row - the regular lattice. a, d - experiment, longitudinal intensity profiles, b, e - experiment, corresponding back face intensity profiles, c, f - numerics, longitudinal intensity profiles

obtained with the same Airy beam as before, but using two different types of lattices - one with negative and one with positive defect (cf. Fig.6.14) are presented. In both cases the main lobe of the Airy beam excites the defect guide. In the case of negative defects a strong beam repulsion is observed, Figs.6.16a-c. The Airy

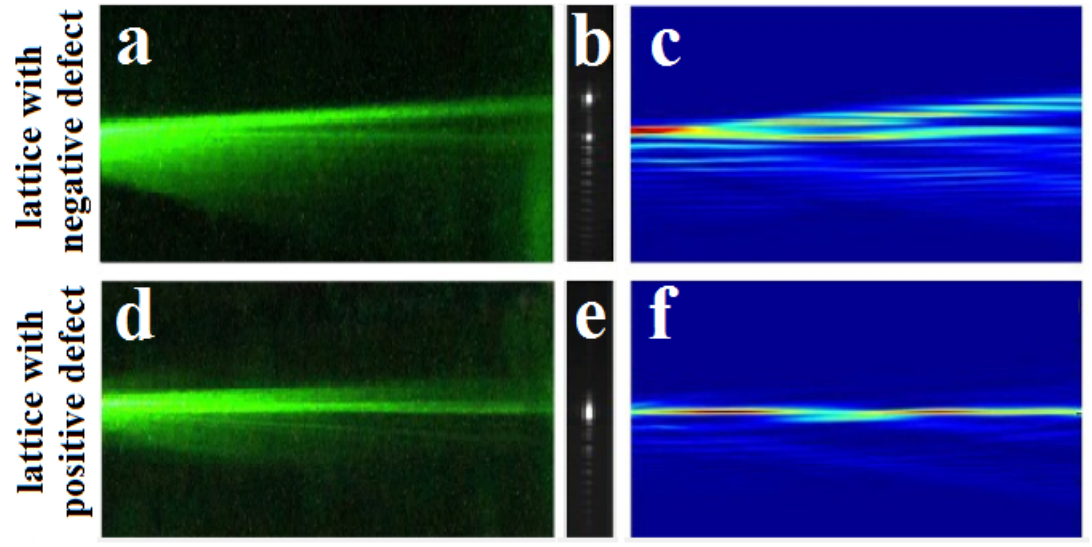

Figure 6.16: Airy beam propagation in the lattice with negative and positive defect. Top row - the lattice with negative defect, bottom row - the lattice with positive defect. a, d - experiment, longitudinal intensity profiles, b, e - experiment, corresponding back face intensity profiles, c, f - numerics, longitudinal intensity profiles

beam propagation is drastically changed in the presence of a positive defect so the formation of simple localized waves is possible with appropriate positive defects Fig.6.16d-f.

Chapter 7

Conclusions and outlook

The study presented in this thesis is set out to explore the behavior of light propagating in the 1D and 2D Fibonacci lattices, i.e. the effect of this specific order on diffraction of exciting light beam. The main questions are: does this structure suppress diffraction compared to regular lattice, can it create localization, how the dimensionality affects these issues, and does the disorder superimposed to the Fibonacci lattice inhibit suppression of diffraction?

The second topic of interest here is the impact of a 1D regular lattice on the non-diffracting Airy beam, raising questions: does the regular lattice disrupt non-diffractive property and parabolic trajectory of the beam, and how the presence of a lattice defect affects the trajectory? These issues were explored both, experimentally and numerically.

In the experiment, the 1D lattices, the Fibonacci and the regular one (with/without a defect), were generated in Fe:LNB crystal by a direct laser writing technique. The 2D Fibonacci lattice was optically induced by incoherent superposition of Bessel beams in Cr:SBN. In order to perform numerical simulations, a software based on the Beam Propagation Method has been developed. For both crystals, the light intensity profiles at the exit facet were recorded on a CCD sensor and compared with numerical results. The comparisons showed a very good agreement between the predictions and experimental results. Results obtained from simulations have been used to explain light beam evolution in a more detailed manner.

It has been shown that the 1D spatially modulated Fibonacci lattice does suppress diffraction considerably compared to the corresponding regular lattice. For a relatively small refractive index contrast the effective beam width increases during the propagation implying that true localized states (those that are characteristic of

disordered systems) cannot be achieved. The increase of a refractive index contrast leads to a strong diffraction suppression so the states become almost completely localized.

the 2D spatially modulated Fibonacci lattice, similar to the 1D one, does suppress diffraction compared to corresponding regular lattice, but in this case the suppression is not as intense as in 1D case.

A 1D refractive index contrast modulated Fibonacci lattice affects diffraction in a similar way to a position modulated one. If the modulation of refractive index contrast is relatively small, diffraction is suppressed to a large degree, but the effective beam width increases during the propagation, so it do not come to localization. But if refractive index contrast modulation is high enough, the effective beam width curve reaches saturation. Even more, the effective width of achieved localized states in Fibonacci lattice is similar to effective width of localized states in corresponding disordered lattice. In addition, it is shown that slightly disordered Fibonacci lattice with relatively small refractive index contrast modulation inhibits diffraction suppression.

Considering the propagation of the Airy beam through the regular 1D lattice, it has been shown that its transverse beam profile is slightly disrupted and the transverse acceleration is reduced, but the energy stays localized. The presence of defect strongly affects the propagation.

The experiments presented in this thesis have certain deficiency. Despite the flexibility that photorefractive materials provide (multiple writing and erasing of the structures), commercially available samples were not long enough so the localized states could not be demonstrated experimentally. Additionally, a refractive index profile cannot be easily engineered or controlled within these materials. The issues could be overcome by the use of inexpensive silica glass of arbitrary dimensions, and femtosecond laser writing technique. In addition, glass samples could be excited with very strong light beams, which would then allow one to study aforementioned problems in nonlinear regime.

The research presented in the thesis can be extended to studies of other deterministic aperiodic photonic lattices, such as Thue-Morse, Rudin-Saphiro, etc. It could give us new fundamental understanding of wave transport properties in these specially designed structures. This would open new engineering possibilities in light flow control, and perhaps offer an additional flexibility in applications (optical signals routing, image transmission, etc.).

Appendix A

Difference equations of implicit FD-BPM based on Crank-Nicolson algorithm

When the domain is discretized (Fig.4.1), one can introduce the substitutions $x = p\Delta x$, $y = q\Delta y$ and $z = l\Delta z$, where $p = 1, \ldots, P$, $q = 1, \ldots, Q$ and $l = 1, \ldots, L$, and P,Q and L are the numbers of elements of the computational domain in x, y and z direction, respectively. Also, the slowly varying field value, $u(x, y, z)$ is written as $u^l_{p,q}$. Than, the left-hand side of equation 4.5 can be represented as

$$\frac{\partial u}{\partial z} = \frac{u^{l+1}_{p,q} - u^l_{p,q}}{\Delta z}. \tag{A.1}$$

The right-hand side of the equation 4.5 involves the second-order partial derivatives of x and y, and can be written as

$$\frac{\partial^2 u}{\partial x^2} = \frac{1}{2}\left\{\frac{u^{l+1}_{p+1,q} - 2u^{l+1}_{p,q} + u^{l+1}_{p-1,q}}{\Delta x^2} + \frac{u^l_{p+1,q} - 2u^l_{p,q} + u^l_{p-1,q}}{\Delta x^2}\right\} \tag{A.2a}$$

$$\frac{\partial^2 u}{\partial y^2} = \frac{1}{2}\left\{\frac{u^{l+1}_{p+1,q} - 2u^{l+1}_{p,q} + u^{l+1}_{p-1,q}}{\Delta y^2} + \frac{u^l_{p+1,q} - 2u^l_{p,q} + u^l_{p-1,q}}{\Delta y^2}\right\} \tag{A.2b}$$

where the average discretization at $z = l\Delta z$ and $z = (l+1)\Delta z$ is taken. This method of representation of the derivatives is called the Crank-Nicolson method. The rest part of the right-hand side of equation4.5 is represented as

$$(k^2 - \overline{k}^2) = k_0^2 \left\{ \frac{(n_{p,q}^{l+1})^2 + n_{p,q}^l)^2}{2} - n_r^2 \right\} \frac{u_{p,q}^{l+1} + u_{p,q}^l}{2}. \tag{A.3}$$

Substitution of previous for expressions in equation 4.5, dividing it with k_0^2 and introducing new variables $\Delta X = k_0^2 x$, $\Delta Y = k_0^2 y$ and $\Delta Z = k_0^2 z$, gives

$$\begin{aligned} &- \frac{u_{p-1,q}^{l+1}}{2\Delta X^2} + \left\{ -b u_{p,q-1}^{l+1} + a_{p,q} u_{p-1,q}^{l+1} - b u_{p,q+1}^{l+1} \right\} - \frac{u_{p+1,q}^{l+1}}{2\Delta X^2} = \\ &\qquad - \frac{u_{p-1,q}^{l}}{2\Delta X^2} + \left\{ -b u_{p,q-1}^{l} + a_{p,q} u_{p-1,q}^{l} - b u_{p,q+1}^{l} \right\} - \frac{u_{p+1,q}^{l}}{2\Delta X^2}, \end{aligned} \tag{A.4}$$

where

$$\begin{aligned} b &= \tfrac{1}{2\Delta Y^2}, \\ a_{p,q} &= \tfrac{2jn_r}{\Delta Z} + \tfrac{1}{\Delta X} + \tfrac{1}{\Delta Y} - \tfrac{1}{2} \left\{ \tfrac{(n_{p,q}^{l+1})^2 + (n_{p,q}^l)^2}{2} - n_r^2 \right\}, \\ c_{p,q} &= -a_{p,q} + \tfrac{4jn_r}{\Delta Z}. \end{aligned} \tag{A.5}$$

At each z step, one obtains $P \times Q$ coupled equations. What follows is solving of these equations in matrix form.

First, a vector involving the field values in y-direction for each x position, i.e. each p, is formed:

$$u_p^l = \begin{bmatrix} u_{p,1}^l \\ \vdots \\ u_{p,Q}^l. \end{bmatrix} \tag{A.6}$$

Next, a set of all Q equations A.4 for a given p can be written in a compact form of a matrix difference equation along x-direction as

$$- \mathbf{B} u_{p-1}^{l+1} + \mathbf{A}_p u_p^{l+1} - \mathbf{B} u_{p+1}^{l+1} = + \mathbf{B} u_{p-1}^{l} + \mathbf{C}_p u_p^{l} + \mathbf{B} u_{p+1}^{l}, \tag{A.7}$$

where

$$
\begin{aligned}
\mathbf{B} &= \tfrac{1}{2\Delta X^2}\mathbf{I}, \\
\mathbf{A}_p &= \begin{bmatrix}
a_{p,1} & -b & 0 & \cdots & 0 & 0 \\
-b & a_{p,2} & -b & \cdots & 0 & 0 \\
0 & -b & a_{p,3} & \ddots & 0 & 0 \\
\vdots & \vdots & \ddots & \ddots & -b & 0 \\
0 & 0 & 0 & -b & a_{p,Q-1} & -b \\
0 & 0 & 0 & 0 & -b & a_{p,Q}
\end{bmatrix}, \\
\mathbf{C}_p &= \begin{bmatrix}
c_{p,1} & b & 0 & \cdots & 0 & 0 \\
b & c_{p,2} & b & \cdots & 0 & 0 \\
0 & b & c_{p,3} & \ddots & 0 & 0 \\
\vdots & \vdots & \ddots & \ddots & b & 0 \\
0 & 0 & 0 & b & c_{p,Q-1} & b \\
0 & 0 & 0 & 0 & b & c_{p,Q}
\end{bmatrix},
\end{aligned}
\tag{A.8}
$$

and $\mathbf{I}$ is the $Q \times Q$ identity matrix. Now, all of P equations A.7 along x-direction are assembled in a matrix form:

$$
\mathbf{A}u^{l+1} = \mathbf{C}u^{l} \tag{A.9}
$$

where

$$\begin{aligned}
\mathbf{A}_p &= \begin{bmatrix} \mathbf{A}_1 & -\mathbf{B} & 0 & \cdots & 0 & 0 \\ -\mathbf{B} & \mathbf{A}_2 & -\mathbf{B} & \cdots & 0 & 0 \\ 0 & -\mathbf{B} & \mathbf{A}_3 & \ddots & 0 & 0 \\ \vdots & \vdots & \ddots & \ddots & -\mathbf{B} & 0 \\ 0 & 0 & 0 & -\mathbf{B} & \mathbf{A}_{P-1} & -\mathbf{B} \\ 0 & 0 & 0 & 0 & -\mathbf{B} & \mathbf{A}_P \end{bmatrix}, \\
\mathbf{C}_p &= \begin{bmatrix} \mathbf{C}_1 & \mathbf{B} & 0 & \cdots & 0 & 0 \\ \mathbf{B} & \mathbf{C}_2 & \mathbf{B} & \cdots & 0 & 0 \\ 0 & \mathbf{B} & \mathbf{C}_3 & \ddots & 0 & 0 \\ \vdots & \vdots & \ddots & \ddots & \mathbf{B} & 0 \\ 0 & 0 & 0 & \mathbf{B} & \mathbf{C}_{P-1} & \mathbf{B} \\ 0 & 0 & 0 & 0 & \mathbf{B} & \mathbf{C}_P \end{bmatrix}, \\
u^l &= \begin{bmatrix} u_1^l \\ \vdots \\ u_P^l \end{bmatrix}.
\end{aligned} \tag{A.10}$$

$\mathbf{A}$ and $\mathbf{C}$ are square matrices of the dimensions $PQ \times PQ$, and u^l is column-matrix of the length PQ, containing the field value at every pixel of a computational window at the position l in z-direction.

Previously introduced technique was designed for two-dimensional problems[1]. In many practical situations, the one-dimensional approach is sufficient for estimation of behavior of optical structures. In this situation, corresponding equations become

$$\begin{aligned}
b &= \tfrac{1}{2\Delta X^2}, \\
a_p &= \tfrac{2jn_r}{\Delta Z} + \tfrac{1}{\Delta X} - \tfrac{1}{2}(n_p - n_r), \\
c_p &= -a_p + \tfrac{4jn_r}{\Delta Z}
\end{aligned} \tag{A.11}$$

and

$$\mathbf{A}u^{l+1} = \mathbf{C}u^l \tag{A.12}$$

where

[1]Two transverse dimensions.

$$
\begin{aligned}
\mathbf{A} &= \begin{bmatrix}
a_1 & -b & 0 & \cdots & 0 & 0 \\
-b & a_2 & -b & \cdots & 0 & 0 \\
0 & -b & a_3 & \ddots & 0 & 0 \\
\vdots & \vdots & \ddots & \ddots & -b & 0 \\
0 & 0 & 0 & -b & a_{P-1} & -b \\
0 & 0 & 0 & 0 & -b & a_P
\end{bmatrix}, \\
\mathbf{C} &= \begin{bmatrix}
c_1 & b & 0 & \cdots & 0 & 0 \\
b & c_2 & b & \cdots & 0 & 0 \\
0 & b & c_3 & \ddots & 0 & 0 \\
\vdots & \vdots & \ddots & \ddots & b & 0 \\
0 & 0 & 0 & b & c_{P-1} & b \\
0 & 0 & 0 & 0 & b & c_P
\end{bmatrix}.
\end{aligned}
\tag{A.13}
$$

In this case $\mathbf{A}$ and $\mathbf{C}$ are square matrices of the dimensions $P \times P$, and u^l is column-matrix of the length P. This approach requires significantly less computer resources than two-dimensional one.

Bibliography

Abdullaev, S. S. and Abdullaev, F. K. (1980), On propagation of light in fiber bundles with random parameters, *Radiofizika* **23**, 766–767. 4

Abrahams, E., Anderson, P. W., Licciardello, D. C. and Ramakrishnan, T. V. (1979), Scaling theory of localization: absence of quantum diffusion in two dimensions, *Phys. Rev. Lett.* **42**, 673–676. 22

Anderson, P. W. (1958), Absence of diffusion in certain random lattices, *Phys. Rev.* **109**, 1492–1505. 3

Aschroft, N. W. and Mermin, N. D. (1976), *Solid State Physics*, Harcourt, Inc. 1, 16

Ashkin, A., Boyd, G. D., Dziedzic, J. M., Smith, R. G., Ballman, A. A., Levinstein, J. J. and Nassau, K. (1966), Optically-induced refractive index inhomogeneities in $LiNbO_3$ and $LiTaO_3$, *Appl. Phys. Lett.* **9**, 72–74. 39

Barber, E. M. (2009), *Aperiodic Structures in Condensed Matter: Fundamentals and Applications*, Taylor & Francis Group, LLC. 5, 6

Barriuso, A. G., Monzón, J. J., Sánchez-Soto, L. L. and Felipe, A. (2005), Comparing omnidirectional reflection from periodic and quasiperiodic one-dimensional photonic crystals, *Opt. Exp.* **13**, 3913–3920. 8

Baumgartl, J., Mazilu, M. and Dholakia, K. (2008), Optically mediated particle clearing using Airy wavepackets, *Nature Photon.* **2**, 675–678. 11

BeamPROP 8.2 (2010), `www.rsoftdesign.com`. 33, 34

Berenger, J.-P. (1994), A perfectly matched layer for the absorption of electromagnetic waves, *J. Comput. Phys.* **114**, 185–200. 37

Blinov, I. V. (2015), Periodic almost-Schrödinger equation for quasicrystals, *Sci. Rep.* **5**, 11492(5pp). 16

Bloch, F. (1928), Über die Quantenmechanik der Elektronenin Kristallgittern, *Z. Phys.* **52**, 555–600. 1

Boguslawski, M., Kleberer, A., Rose, P. and Denz, C. (2012*a*), Multiplexing complex two-dimensional photonic superlattices, *Opt. Exp.* **20**, 27331–27343. 49

Boguslawski, M., Kleberer, A., Rose, P. and Denz, C. (2012*b*), Photonic ratchet superlattices by optical multiplexing, *Opt. Lett.* **37**, 797–799. 49

Boguslawski, M., Lučić, N. M., Diebel, F., Timotijević, D. V., Denz, C. and Jović Savić, D. M. (2016), Light localization in optically induced deterministic aperiodic Fibonacci lattice, *arXiv:1501.04479v2* . 11

Bouchal, Z. (2003), Nondiffracting optical beams: physical properties, experiments, and applications, *Czech. J. Phys.* **53**, 537–578. 10, 48

Boyd, R. W. (2008), *Nonlinear optics*, Elsevier Inc. 40, 41

Bragg, W. H. and Bragg, W. L. (1913), The reflexion of X-rays by crystals, *Proc R. Soc. Lond. A* **88**, 428–438. 1

Brignon, A., Breugnot, S. and Huignard, J.-P. (1995), Very high-gain two-wave mixing in $BaTiO_3$ with a self-bent pump beam, *Opt. Lett.* **20**, 1689–1691. 41

Broky, J., Siviloglou, G. A., Dogariu, A. and Christodoulides, D. N. (2008), Self-healing properties of optical Airy beams, *Opt. Exp.* **16**, 12880–12891. 11

Buse, K. (1997), Light-induced charge transport processes in photorefractive crystals I: models and experimental methods, *Appl. Phys. B* **64**, 273–291. 41

Capaz, R. B., Koiller, B. and de Queiroz, S. L. A. (1990), Gap states and localization properties of one-dimensional Fibonacci quasicrystals, *Phys. Rev. B* **42**, 6402–6407. 7

Cedilnik, G., Esselbach, M., Kiessling, A. and Kowarschik, R. (2000), Real-time holographic interferometry with double two-wave mixing in photorefractive crystals, *Appl. Opt.* **39**, 2091–2100. 41

Chan, Y. S., Chan, C. T. and Liu, Z. Y. (1998), Photonic band gaps in two dimensional photonic quasicrystals, *Phys. Rev. Lett.* **80**, 956–959. 7

Christodoulides, D. N., Lederer, F. and Silberberg, Y. (2003), Discretizing light behaviour in linear and nonlinear waveguide lattices, *Nature* **424**, 817–823. 10, 25

Chung, Y. and Dagli, N. (1990), An assessment of finite difference beam propagation method, *IEEE J. Quantum Electron.* **26**, 1335–1339. 35

Coldren, L. A., Corzine, S. W. and Mašanović, M. L. (2012), *Diode Lasers and Photonic Integrated Circuits*, John Wiley & Sons. 33, 38

Dal Negro, L. and Boriskina, S. V. (2012), Deterministic aperiodic nanostructures for photonics and plasmonics applications, *Laser Photon. Rev.* **6**, 178–218. 5, 17

Dal Negro, L., Feng, N.-N. and Gopinath, A. (2008), Electromagnetic coupling and plasmon localization in deterministic aperiodic arrays, *J. Opt. A: Pure Appl. Opt.* **10**, 064013(10pp). 15, 17, 18

Dal Negro, L., Stolfi, M., Yi, Y., Michel, J., Dua, X., Kimerling, L. C., LeBlanc, J. and Haavisto, J. (2004), Photon band gap properties and omnidirectional reflectance in Si/SiO_2 Thue-Morse quasicrystals, *Appl. Phys. Lett.* **84**, 5186–5188. 7

Dal Negro, L., Yi, J. H., Nguyen, V., Yi, Y., Michel1, J. and Kimerling, L. C. (2005), Spectrally enhanced light emission from aperiodic photonic structures, *Appl. Phys. Lett.* **86**, 261905(3pp). 9

Dalichaouch, R., Armstrong, J. P., Schultz, S., Platzman, P. M. and McCall, S. L. (1991), Microwave localization by two-dimensional scattering, *Nature* **354**, 53–55. 4, 23

Desyatnikov, A. S., Neshev, D. N., Kivshar, Y. S., Sagemerten, N., Träger, D., Jägers, J., Denz, C. and Kartashov, Y. V. (2005), Nonlinear photonic lattices in anisotropic nonlocal self-focusing media, *Opt. Lett.* **30**, 869–871. 48

Desyatnikov, A. S., Sagemerten, N., Fischer, R., Terhalle, B., Träger, D., Neshev, D. N., Dreischuh, A., Denz, C., Krolikowski, W. and Kivshar, Y. S. (2006), Two-dimensional self-trapped nonlinear photonic lattices, *Opt. Exp.* **14**, 2851–2863. 48

Diebel, F., Rose, P., Boguslawski, M. and Denz, C. (2014), Optical induction scheme for assembling nondiffracting aperiodic Vogel spirals, *Appl. Phys. Lett.* **104**, 191101. 49

Duan, F. and Guojun, J. (2005), *Introduction to condensed matter physics*, Vol. 1, World Scientific Publishing Co. Pte. Ltd. 5, 16, 19, 22, 24

Durnin, J., Miceli, J. J. and Eberly, J. H. (1987), Diffraction-free beams, *Phys. Rev. Lett.* **58**, 1499–1501. 10, 49

Efremidis, N. K., Sears, S., Christodoulides, D. N., Fleischer, J. W. and Segev, M. (2002), Discrete solitons in photorefractive optically induced photonic lattices, *Phys. Rev. E* **66**, 046602(5pp). 47, 58

Eisenberg, H. S., Silberberg, Y., Morandoti, R. and Aitchison, J. S. (2000), Diffraction management, *Phys. Rev. Lett.* **85**, 1863–1866. 26

Eisenberg, H. S., Silberberg, Y., Morandoti, R., Boyd, A. R. and Aitchison, J. S. (1998), Discrete spatial optical solitons in waveguide arrays, *Phys. Rev. Lett.* **81**, 3383–3386. 27

Ewbank, M. D., Neurgaonkar, R. R., Cory, W. K. and Feinberg, J. (1987), Photorefractive properties of strontiumbarium niobate, *J. Appl. Phys.* **62**, 374–380. 42, 47

Feinberg, J. (1982), Self-pumped, continuous-wave phase conjugator using internal reflection, *Opt. Lett.* **7**, 486–488. 41

Feit, M. D. and Fleck, J. A. (1978), Light propagation in graded-index optical fibers, *Appl. Opt.* **17**, 3990–3998. 33

Fink, Y., Winn, J. N., Fan, S., Chen, C., Michel, J., Joannopoulos, J. D. and Thomas, E. L. (1998), A dielectric omnidirectional reflector, *Science* **282**, 1679–1682. 2

Fleischer, J. W., Segev, M., Efremidis, N. K. and Christodoulides, D. N. (2003), Obsevation of two-dimensional discrete solitons in optically induced nonlinear photonic lattices, *Nature* **422**, 147–150. 48

Fradkin-Kashi, K., Arie, A., Urenski, P. and Rosenman, G. (2002), Multiple nonlinear optical interactions with arbitrary wave vector differences, *Phys. Rev. Lett.* **88**, 023903(4pp). 9

Freedman, B., Bartal, G., Segev, M., Lifshitz, R., Christodoulides, D. N. and Fleischer, J. W. (2006), Wave and defect dynamics in nonlinear photonic quasicrystals, *Nature* **440**, 1166–1169. 7

Fu, X., Liu, Y., Cheng, B. and Zheng, D. (1991), Spectral structure of two-dimensional Fibonacci quasilattices, *Phys. Rev. B* **43**, 10808–10814. 7

Fujiwara, T., Kohmoto, M. and Tokihiro, T. (1989), Multifractal wave functions on a Fibonacci lattice, *Phys. Rev. B* **40**, 7413–7416. 7

Garanovich, I. L., Longhi, S., Sukhorukov, A. A. and Kivshar, Y. S. (2012), Light propagation and localization in modulated photonic lattices and waveguides, *Phys. Rep.* **518**, 1–79. 10, 25, 26, 28, 29

Gellermann, W., Kohmoto, M., Sutherland, B. and Taylor, P. C. (1994), Localization of light waves in Fibonacci dielectric multilayers, *Phys. Rev. Lett.* **72**, 633–636. 7

Günter, P. and Huignard, J.-P. (2006), *Photorefractive Materials and Their Applications 1*, Springer Science+Business Media, Inc. 39, 42

Hadley, G. R. (1992*a*), Multistep method for wide-angle beam propagation, *Opt. Lett.* **17**, 1743–1745. 34

Hadley, G. R. (1992*b*), Transparent boundary condition for the beam propagation method, *IEEE J. Quant. Electron.* **28**, 363–370. 37

Hadley, G. R. (1992*c*), Wide-angle beam propagation using Padé approximant operators, *Opt. Lett.* **17**, 1426–1428. 34

Hattori, T., Tsurumachi, N., Kawato, S. and Nakatsuka, H. (1994), Photonic dispersion relation in a one-dimensional qnasicrystal, *Phys. Rev. B* **50**, 4220–4223. 7

He, S. and Maynard, J. D. (1986), Detailed measurements of inelastic scattering in Anderson localization, *Phys. Rev. Lett.* **57**, 3171–3174. 3, 4

Hu, H., Strybulevych, A., Page, J. H., Skipetrov, S. E. and van Tiggelen, B. A. (2008), Localization of ultrasound in three-dimensional elastic network, *Nature Phys.* **4**, 945–948. 3

Huang, W. and Xu, C. (1993), Simulation of three-dimensional optical waveguides by a full-vector beam propagation method, *IEEE J. Quant. Electron.* **29**, 2639–2649. 34

Janssen, T., Chapuis, G. and de Boissieu, M. (2007), *Aperiodic Crystals: From Modulated Phases to Quasicrystals*, Oxford University Press. 6, 15

Jensen, S. J. (1999), *Spatial Structures and Temporal Dynamics in Photorefractive Nonlinear Systems*, PhD thesis, Risø National Laboratory, Roskilde, Denmark. 40, 41

Joannopoulos, J. D., Johnson, S. G., Winn, J. N. and Meade, R. D. (2008), *Photonic crystals: molding the flow of light*, Princeton University Press. 2

John, S. (1984), Electromagnetic absorption in a disordered medium near a photon mobility edge, *Phys. Rev. Lett.* **53**, 2169–2172. 4

John, S. (1987), Strong localization of photons in certain disordered dielectric superlattices, *Phys. Rev. Lett.* **58**, 2486–489. 4

Kaczmarski, P. and Lagasse, P. E. (1988), Bidirectional beam propagation method, *Electron. Lett.* **24**, 675–676. 34

Kaliteevski, M. A., Brand, S., Abram, R. A., Krauss, T. F., Rue, R. D. and Millar, P. (2000), Two-dimensional Penrose-tiled photonic quasicrystals: from diffraction pattern to band structure, *Nanotechnology* **11**, 274280. 7

Karbasi, S., Frazier, R. J., Koch, K. W., Hawkins, T., Ballato, J. and Mafi1, A. (2014), Image transport through a disordered optical fibre mediated by transverse Anderson localization, *Nat. Commun.* **5**, 3362(9pp). 4

Katsumoto, S., Sano, N. and Kobayashi, S. (1993), Electron propagation through a Fibonacci lattice, *Solid State Commun.* **85**, 223–226. 7

Kittel, C. (1987), *Quantum theory of solids*, John Wiley & Sons, Inc. 19

Kohmoto, M., Sutherland, B. and Iguchi, K. (1987), Localization in optics: quasiperiodic media, *Phys. Rev. Lett.* **58**, 2436–2438. 7, 8

Kukhtarev, N., Markov, V., Odulov, S., Soskin, M. and Vinetskii, V. (1979), Holographic storage in electrooptic crystals. I. Steady state, *Ferroelectrics* **22**, 949–960. 39

Lagendijk, A., van Tiggelen, B. and Wiersma, D. S. (2009), Fifty years of Anderson localization, *Phys. Today* **62**, 24–29. 3

Lahini, Y., Avidan, A., Pozzi, F., Sorel, M., Morandotti, R., Christodoulides, D. N. and Silberberg, Y. (2008), Anderson localization and nonlinearity in one-dimensional disordered lattices, *Phys. Rev. Lett.* **100**, 013906(4pp). 4, 30, 31

Lahini, Y., Pugatch, R., Pozzi, F., Sorel, M., Morandotti, R., Davidson, N. and Silberberg, Y. (2009), Observation of a localization transition in quasiperiodic photonic lattices, *Phys. Rev. Lett.* **103**, 013901(4pp). 8

Ledermann, A., Cademartiri, L., Hermatschweiler, M., Toninelli, C., Ozin, G. A., Wiersma, D. S., Wegener, M. and von Freymann, G. (2006), Three-dimensional silicon inverse photonic quasicrystals for infrared wavelengths, *Nat. Mater.* **5**, 942–945. 7, 9

Lee, K.-H., Baek, J.-H., Hwang, I.-K., Lee, Y.-H., Lee, G.-H., Ser, J.-H., Kim, H.-D., and Shin, H.-E. (2004), Square-lattice photonic-crystal vertical-cavity surface-emitting lasers, *Opt. Exp.* **12**, 4136–4143. 2

Lee, P. A. and Ramakrishnan, T. V. (1985), Disordered electronic systems, *Rev. Mod. Phys.* **57**, 287–337. 3, 22, 23

Levi, L., Rechtsman, M., Freedman, B., Schwartz, T., Manela, O. and Segev, M. (2011), Disorder-enhanced transport in photonic quasicrystals, *Science* **332**, 1541–1544. 8, 24, 63

Levine, D. and Steinhardt, P. J. (1984), Quasicrystals: a new class of ordered structures, *Phys. Rev. Lett.* **53**, 2477–2480. 6

Lifante, G. (2003), *Integrated photonics: fundamentals*, John Wiley & Sons Ltd. 34, 35, 37

Lifshitz, R. (2002), The square Fibonacci tiling, *J. Alloy. Compd.* **342**, 186–190. 7

Lifshitz, R., Arie, A. and Bahabad, A. (2005), Photonic quasicrystals for nonlinear optical frequency conversion, *Phys. Rev. Lett.* **95**, 133901(4pp). 9

Liu, N. (1997), Propagation of light waves in Thue-Morse dielectric multilayers, *Phys. Rev. B* **55**, 3542–3547. 7

Lord Rayleigh (1887), On the maintenance of vibrations by forces of double frequency, and on the propagation of waves through a medium endowed with a periodic structure, *Philos. Mag.* **24**, 145–159. 2

Lord Rayleigh (1917), On the reflection of light from a regularly stratified medium, *Proc. R. Soc. of London* **93**, 565–577. 2

Lučić, N. M., Bokić, B. M., Grujić, D. Ž., Pantelić, D. V., Jelenković, B. M., A. Piper, D. M. J., and Timotijević, D. V. (2013), Defect-guided Airy beams in optically induced waveguide arrays, *Phys. Rev. A* **88**, 063815(4pp). 11

Lučić, N. M., Jović Savić, D. M., Piper, A., Grujić, D. Ž., Vasiljević, J. M., Pantelić, D. V., Jelenković, B. M. and Timotijević, D. V. (2015), Light propagation in quasiperiodic Fibonacci waveguide arrays, *J. Opt. Soc. Am. B* **32**, 1510–1513. 11

Maciá, E. (1998), Optical engineering with Fibonacci dielectric multilayers, *Appl. Phys. Lett.* **73**, 3330–3332. 8

Maciá, E. (2006), The role of aperiodic order in science and technology, *Rep. Prog. Phys.* **69**, 397–441. 5, 6, 15, 16, 17

Maciá, E. (2012), Exploiting aperiodic designs in nanophotonic devices, *Rep. Prog. Phys.* **75**, 036502(42pp). 7, 14, 15

Maciá, E. and Dominguez-Adame, F. (1996), Physical nature of critical wave functions in Fibonacci systems, *Phys. Rev. Lett.* **76**, 2957–2960. 7, 23

Mafi, A. (2015), Transverse Anderson localization of light: a tutorial, *Adv. Opt. Photonics* **7**, 459–515. 4, 31

Mahler, L., Tredicucci, A., Beltram, F., Walther, C., Faist, J., Beere, H. E., Ritchie, D. A. and Wiersma, D. S. (2010), Quasi-periodic distributed feedback laser, *Nature Photon.* **4**, 165–169. 9

Mandelbrot, B. (1967), How long is the coast of Britain? Statistical self-similarity and fractional dimension, *Science* **156**, 636–638. 15

Mandelik, D., Eisenberg, H. S., Silberberg, Y., Morandoti, R. and Aitchison, J. S. (2003), Band-gap structure of waveguide arrays and excitation of Floquet-Bloch solitons, *Phys. Rev. Lett.* **90**, 053902(4pp). 29, 30

Martin, L., Giuseppe, G. D., Perez-Leija, A., Keil, R., Dreisow, F., Heinrich, M., Szameit, S. N. A., Abouraddy, A. F., Christodoulides, D. N. and Saleh, B. E. A. (2011), Anderson localization in optical waveguide arrays with off-diagonal coupling disorder, *Opt. Exp.* **19**, 13636–13646. 30

Mathis, A., Courvoisier, F., Froehly, L., Furfaro, L., Jacquot, M., Lacourt, P. A. and Dudley, J. M. (2012), Micromachining along a curve: femtosecond laser micromachining of curved profiles in diamond and silicon using accelerating beams, *Appl. Phys. Lett.* **101**, 071110(3pp). 11

Merlin, R., Bajema, K., Clarke, R., Juang, F. Y. and Bhattacharya, P. K. (1985), Quasiperiodic GaAs-AlAs heterostructures, *Phys. Rev. Lett.* **55**, 1768–1770. 6

Morandotti, R., Peschel, U., Aitchison, J. S., Eisenberg, H. S. and Silberberg, Y. (1999), Experimental observation of linear and nonlinear optical Bloch oscillations, *Phys. Rev. Lett.* **83**, 4756–4759. 10

Nee, I., Müller, M., Buse, K. and Krätzig, E. (2000), Role of iron in lithium-niobate crystals for the dark-storage time of holograms, *J. Appl. Phys.* **88**, 4282–4286. 42

Notomi, M., Suzuki, H., Tamamura, T. and Edagawa, K. (2004), Lasing action due to the two-dimensional quasiperiodicity of photonic quasicrystals with a Penrose lattice, *Phys. Rev. Lett.* **92**, 123906(4pp). 8

Okamoto, K. (2006), *Fundamentals of Optical Waveguides*, Elsevier Inc. 33, 34

Peithmann, K., Wiebrock, A. and Buse, K. (1999), Photorefractive properties of highly-doped lithium niobate crystals in the visible and near-infrared, *Appl. Phys. B* **68**, 777–784. 42

Peltier, M. and Micheron, F. (1977), Volume hologram recording and charge transfer process in $Bi_{12}SiO_{20}$ and $Bi_{12}GeO_{20}$, *J. Appl. Phys* **48**, 3683. 41

Pertsch, T., Dannberg, P., Elflein, W., Bräuer, A. and Lederer, F. (1999), Optical Bloch oscillations in temperature tuned waveguide arrays, *Phys. Rev. Lett.* **83**, 4752–4755. 10

Pertsch, T., Peschel, U., Lederer, F., Burghoff, J., Will, M., Nolte, S. and Tünnermann, A. (2004), Discrete diffraction in two-dimensional arrays of coupled waveguides in silica, *Opt. Lett.* **29**, 468–470. 58

Pertsch, T., Zentgraf, T., Peschel, U., Bräuer, A., and Lederer, F. (2002), Anomalous refraction and diffraction in discrete optical systems, *Phys. Rev. Lett.* **88**, 093901(4pp). 28

Polynkin, P., Kolesik, M., Moloney, J. V., Siviloglou, G. A. and Christodoulides, D. N. (2009), Curved plasma channel generation using ultraintense Airy beams, *Science* **324**, 229–232. 11

Press, W. H., Teukolsky, S. A., Vetterling, W. T. and Flannery, B. P. (2007), *Numerical Recipes: The Art of Scientific Computing*, Cambridge University Press. 36

Raedt, H. D., Lagendijk, A. and de Vries, P. (1989), Transverse localization of light, *Phys. Rev. Lett.* **62**, 47–50. 4

Rao, H., Scarmozzino, R. and R.M. Osgood, J. (1999), A bidirectional beam propagation method for multiple dielectric interfaces, *IEEE Photon. Technol. Lett.* **11**, 830–832. 34

Report of the Executive Committee for 1991 (1992), *Acta Cryst. A* **48**, 922. 18

Rose, P., Boguslawski, M. and Denz, C. (2012), Nonlinear lattice structures based on families of complex nondiffracting beams, *New J. Phys.* **14**, 033018(11pp). 48

Rose, P., Terhalle, B., Imbrock, J. and Denz, C. (2008), Optically induced photonic superlattices by holographic multiplexing, *J. Phys. D: Appl. Phys.* **41**, 224004(4pp). 48

Russell, P. (2003), Photonic crystal fibers, *Science* **299**, 358–362. 2

Russell, P. S. J. (1986), Optics of Floquet-Bloch waves in dielectric gratings, *Appl. Phys. B* **39**, 231–246. 29

Sayano, K., Yariv, A. and Neurgaonkar, R. R. (1989), Photorefractive gain and response time of Cr-doped strontium barium niobate, *Appl. Phys. Lett.* **55**, 328–330. 42

Schrödinger, E. (1945), *What is life? The physical aspects of the living cell*, Cambridge University Press. 5

Schwartz, C. (1988), Reflection properties of pseudorandom multilayers, *Appl. Opt.* **27**, 1232–1234. 7

Schwartz, T., Bartal, G., Fishman, S. and Segev, M. (2007), Transport and Anderson localization in disordered two-dimensional photonic lattices, *Nature* **446**, 52–55. 4, 31

Segev, M., Crosignani, B., Yariv, A. and Fischer, B. (1992), Spatial solitons in photorefractive media, *Phys. Rev. Lett.* **68**, 923–926. 42

Segev, M., Silberberg, Y. and Christodoulides, D. N. (2013), Anderson localization of light, *Nature Photon.* **7**, 197–204. 3, 10, 31

Shah, R. R., Kim, D. M., Rabson, T. A. and Tittel, F. K. (1976), Characterization of iron doped lithium niobate for holographic storage applications, Technical report, Department of Electrical Engineering, Rice University. 42, 44

Shandarova, K., Rüter, C. E., Kip, D., Makris, K. G. and Christodoulides, D. N. (2009), Experimental observation of Rabi oscillations in photonic lattices, *Phys. Rev. Lett.* **102**, 123905(4pp). 10

Shechtman, D., Blech, I., Gratias, D. and Cahn, J. W. (1984), Metallic phase with long-range orientational order and no translational symmetry, *Phys. Rev. Lett.* **53**, 1951–1954. 5, 6

Sigler, L. E. (2002), *Fibonacci's Liber Abaci: A translation into modern English of Leonardo Pisano's Book of Calculation*, Springer-Verlag New York, Inc. 5

Siviloglou, G. A., Broky, J., Dogariu, A. and Christodoulides, D. N. (2007), Observation of accelerating Airy beams, *Phys. Rev. Lett.* **99**, 213901(4pp). 11

Sperling, T., Bührer, W., Aegerter, C. M. and Maret, G. (2013), Direct determination of the transition to localization of light in three dimensions, *Nature Photon.* **7**, 48–52. 22, 23

Szameit, A. and Nolte, S. (2010), Discrete optics in femtosecond-laser-written photonic structures, *J. Phys. B: At. Mol. Opt. Phys.* **43**, 163001(25pp). 27

Taketomi, Y., Ford, J. E., Sasaki, H., Ma, J., Fainman, Y. and Lee, S. H. (1991), Incremental recording for photorefractive hologram multiplexing, *Opt. Lett.* **16**, 1774–1776. 48

Toet, D., Potemski, M., Wang, Y. Y. and Maan, J. C. (1991), Experimental observation of Landau levels in nonperiodic (Fibonacci) superlattices, *Phys. Rev. Lett.* **66**, 2128–2131. 7

Trompeter, H., Pertsch, T., Lederer, F., Michaelis, D., Streppel, U. and Bräuer, A. (2006), Visual observation of Zener tunneling, *Phys. Rev. Lett.* **96**, 023901(4pp). 10

Trompeter, H., Peschel, U., Pertsch, T., Lederer, F., Streppel, U., Michaelis, D. and Bräuer, A. (2003), Tailoring guided modes in waveguide arrays, *Opt. Exp.* **11**, 3404–3411. 27

Vassallo, C. and Collino, F. (1996), Highly efficient absorbing boundary conditions for the beam propagation method, *J. Lightwave Technol.* **14**, 1570–1577. 37

Vazquez, R., Ewbank, M. and Neurgaonkar, R. (1991), Photorefractive properties of doped strontium-barium niobate, *Opt. Commun.* **80**, 253–258. 42

Verbin, M., Zilberberg, O., Lahini, Y., Kraus, Y. E. and Silberberg, Y. (2015), Topological pumping over a photonic Fibonacci quasicrystal, *Phys. Rev. B* **91**, 064201(4pp). 8

Wartak, M. S. (2013), *Computational photonics: an introduction with MATLAB*, Cambridge University Press. 33

Weaver, R. L. (1990), Anderson localization of ultrasound, *Wave Motion* **12**, 129–142. 3

Wiersma, D. S., Bartolini, P., Lagendijk, A. and Righini, R. (1997), Localization of light in a disordered medium, *Nature* **390**, 671–673. 4, 23

Wood, G. L., Clark, W. W., Miller, M. J., Sharp, E. J., Salamo, G. J. and Neurgaonkar, R. R. (1987), Broadband photorefractive properties and self-pumped phase conjugation in Ce-SBN:60, *IEEE J. Quant. Elect.* **23**, 2126–2135. 42

Xu, C., Huang, W., Chrostowski, J. and Chaudhuri, S. (1994), A full-vectorial beam propagation method for anisotropic waveguides, *J. Lightwave Tech.* **12**, 1926–1931. 34

Yablonovitch, E. (1987), Inhibited spontaneous emission in solid-state physics and electronics, *Phys. Rev. Lett.* **58**, 2059–2062. 2

Yablonovitch, E. and Gmitter, T. J. (1989), Photonic band structure: the face-centered-cubic case, *Phys. Rev. Lett.* **63**, 1950–1953. 2

Yamaguchi, A. A., Saiki, T., Tada, T., Ninomiya, T., Minawa, K., Kobayashi, T., Kuwata-Gonokami, M. and Yao, T. (1990), Transport properties of photoexcited carriers in a Fibonacci superlattice, *Solid State Commun.* **75**, 955–961. 7

Yeh, P. (1989), Two-wave mixing in nonlinear media, *IEEE J. Quant. Electron.* **25**, 484–519. 41

Yeh, P. (1993), *Introduction to photorefractive nonlinear optics*, John Wiley & Sons, Inc. 39, 41

Zarkov, B., Grujić, D. and Pantelić, D. (2012), High-resolution dot-matrix hologram generation, *Phys. Scr.* **T149**, 014021(3pp). 44

Zhu, S. N., Zhu, Y. Y. and Ming, N. B. (1997), Quasiphase-matched third-harmonic generation in a quasi-periodic optical superlattice, *Science* **278**, 843–846. 9

Zhu, S. N., Zhu, Y. Y., Qin, Y. Q., Wang, H. F., Ge, C. Z. and Ming, N. B. (1997), Experimental realization of second harmonic generation in a Fibonacci optical superlattice of $LiTaO_3$, *Phys. Rev. Lett.* **78**, 2752–2755. 9

Zoorob, M. E., Charlton, M. D. B., Parker, G. J., Baumberg, J. J. and Netti, M. C. (2000), Complete photonic bandgaps in 12-fold symmetric quasicrystals, *Nature* **404**, 740–743. 7

Biography

Nemanja M. Lučić was born in Priboj, Serbia, on February 16th, 1983. After graduating from VI Belgrade Gymnasium in 2002, he enrolled in the School of Electrical Engineering at the University of Belgrade. He graduated from the Department of Physical Electronics in 2008, with the GPA of 8.97 (out of 10.00). In 2010 he received his master degree from the Department of Signals and Systems of the School of Electrical Engineering. He entered the Nanoelectronics and Photonics Ph.D. program at the same university in 2011.

N. M. Lučić has been working as a research assistant in the Photonics Center at the Institute of Physics Belgrade since 2011, participating in national research project "Generation and characterization of functional nano-photonic structures in bio-medicine and informatics"(III45016). In 2013/2014 he spent three months working as a visiting student in the Institute for Applied Physics, Westfälische Wilhelms-Universität Münster, Germany, participating in DAAD project "Light propagation and light localization in complex photonic lattice systems".

The most important research results of the Ph.D. candidate Nemanja M. Lučić are summarized in eight articles published in international journals.

List of publications

1. M. Boguslawski, N. M. Lučić, F. Diebel, D. V. Timotijević, C. Denz, and D. M. Jović Savić, Light localization in optically induced deterministic aperiodic Fibonacci lattices, *arXiv*:1501.04479v2 (2016) - *accepted for publication in Optica*

2. N. M. Lučić, D. M. Jović Savić, A. Piper, D. Ž. Grujić, J. M. Vasiljević, D. V. Pantelić, B. M. Jelenković, and D. V. Timotijević, Light propagation in quasiperiodic Fibonacci waveguide arrays, *J. Opt. Soc. Am. B* **32** 7 1510-1513 (2015) (doi: 10.1364/JOSAB.32.001510)

3. S. N. Nikolić, M. Radonjić, N. M. Lučić, A. J. Krmpot, and B. M. Jelenković, Transient development of Zeeman electromagnetically induced transparency during propagation of Raman-Ramsey pulses through Rb buffer gas cell, *J. Phys. B: At. Mol. Opt. Phys.* **48**, 045501(11pp) (2015) (doi:10.1088/0953-4075/48/4/045501)

4. S. N. Nikolić, M. Radonjić, N. M. Lučić, A. J. Krmpot, and B. M. Jelenković, Optical Ramsey fringes observed during temporal evolution of Zeeman coherences in Rb buffer gas cell, *Phys. Scr.* **T162** 014038(4pp) (2014) (doi:10.1088/0031-8949/2014/T162/014038)

5. N. M. Lučić, B. M. Bokić, D. Ž. Grujić, D. V. Pantelić, B. M. Jelenković, A. Piper, D. M. Jović, and D. V. Timotijević, Defect-guided Airy beams in optically induced waveguide arrays, *Phys. Rev. A* **88**, 063815(4pp) (2013) (doi: 10.1103/PhysRevA.88.063815)

6. S. N. Nikolić, A. J. Krmpot, N. M. Lučić, B. V. Zlatković, M. Radonjić, and B. M. Jelenković, Effects of laser beam diameter on electromagnetically induced transparency due to Zeeman coherences in Rb vapor, *Phys. Scr.* **T157** 014019(4pp) (2013) (doi:10.1088/0031-8949/2013/T157/014019)

7. S. N. Nikolić, M. Radonjić, A. J. Krmpot, N. M. Lučić, B. V. Zlatković, and B. M. Jelenković, Efects of laser beam profile on Zeeman electromagnetically induced transparency in Rb buffer gas cell, *J. Phys. B: At. Mol. Opt. Phys.* **46**, 075501(10pp) (2013) (doi:10.1088/0953-4075/46/7/075501)

8. S. N. Nikolić, V. Đokić, N. M. Lučić, A. J. Krmpot, S. M. Ćuk, M. Radonjić and B. M. Jelenković, The conection between electromagnetically induced transparency in the Zeeman configuration and slow light in hot rubidium vapor, *Phys. Scr.* **T149**, 014009(3pp) (2012) (doi:10.1088/0031-8949/2012/T149/014009)

Прилог 1.

Изјава о ауторству

Потписани-а Немања М.Лучић

број индекса 11/5054

Изјављујем

да је докторска дисертација под насловом

Пропагација светлости у детерминистичким апериодичним низовима таласовода

(Light propagation in deterministic aperiodic waveguide arrays)

- резултат сопственог истраживачког рада,
- да предложена дисертација у целини ни у деловима није била предложена за добијање било које дипломе према студијским програмима других високошколских установа,
- да су резултати коректно наведени и
- да нисам кршио/ла ауторска права и користио интелектуалну својину других лица.

Потпис докторанда

У Београду, _____

Немања Лучић

Прилог 2.

Изјава о истоветности штампане и електронске верзије докторског рада

Име и презиме аутора Немања М Лучић

Број индекса 11/5054

Студијски програм Наноелектроника и фотоника

Наслов рада Пропагација светлости у детерминистичким апериодичним низовима таласовода (Light propagation in deterministic aperiodic waveguide arrays)

Ментор др Дејан М. Гвоздић, др Јасна В. Црњански

Потписани/а Немања М Лучић

Изјављујем да је штампана верзија мог докторског рада истоветна електронској верзији коју сам предао/ла за објављивање на порталу **Дигиталног репозиторијума Универзитета у Београду.**

Дозвољавам да се објаве моји лични подаци везани за добијање академског звања доктора наука, као што су име и презиме, година и место рођења и датум одбране рада.

Ови лични подаци могу се објавити на мрежним страницама дигиталне библиотеке, у електронском каталогу и у публикацијама Универзитета у Београду.

Потпис докторанда

У Београду, _____

Немања Лучић

Прилог 3.

Изјава о коришћењу

Овлашћујем Универзитетску библиотеку „Светозар Марковић“ да у Дигитални репозиторијум Универзитета у Београду унесе моју докторску дисертацију под насловом:

Пропагација светлости у детерминистичким апериодичним низовима таласовода

(Light propagation in deterministic aperiodic waveguide arrays)

која је моје ауторско дело.

Дисертацију са свим прилозима предао/ла сам у електронском формату погодном за трајно архивирање.

Моју докторску дисертацију похрањену у Дигитални репозиторијум Универзитета у Београду могу да користе сви који поштују одредбе садржане у одабраном типу лиценце Креативне заједнице (Creative Commons) за коју сам се одлучио/ла.

1. Ауторство
2. Ауторство - некомерцијално
3. Ауторство – некомерцијално – без прераде
4. Ауторство – некомерцијално – делити под истим условима
5. Ауторство – без прераде
6. Ауторство – делити под истим условима

(Молимо да заокружите само једну од шест понуђених лиценци, кратак опис лиценци дат је на полеђини листа).

Потпис докторанда

У Београду, _____

_____

1. Ауторство - Дозвољавате умножавање, дистрибуцију и јавно саопштавање дела, и прераде, ако се наведе име аутора на начин одређен од стране аутора или даваоца лиценце, чак и у комерцијалне сврхе. Ово је најслободнија од свих лиценци.

2. Ауторство – некомерцијално. Дозвољавате умножавање, дистрибуцију и јавно саопштавање дела, и прераде, ако се наведе име аутора на начин одређен од стране аутора или даваоца лиценце. Ова лиценца не дозвољава комерцијалну употребу дела.

3. Ауторство - некомерцијално – без прераде. Дозвољавате умножавање, дистрибуцију и јавно саопштавање дела, без промена, преобликовања или употребе дела у свом делу, ако се наведе име аутора на начин одређен од стране аутора или даваоца лиценце. Ова лиценца не дозвољава комерцијалну употребу дела. У односу на све остале лиценце, овом лиценцом се ограничава највећи обим права коришћења дела.

4. Ауторство - некомерцијално – делити под истим условима. Дозвољавате умножавање, дистрибуцију и јавно саопштавање дела, и прераде, ако се наведе име аутора на начин одређен од стране аутора или даваоца лиценце и ако се прерада дистрибуира под истом или сличном лиценцом. Ова лиценца не дозвољава комерцијалну употребу дела и прерада.

5. Ауторство – без прераде. Дозвољавате умножавање, дистрибуцију и јавно саопштавање дела, без промена, преобликовања или употребе дела у свом делу, ако се наведе име аутора на начин одређен од стране аутора или даваоца лиценце. Ова лиценца дозвољава комерцијалну употребу дела.

6. Ауторство - делити под истим условима. Дозвољавате умножавање, дистрибуцију и јавно саопштавање дела, и прераде, ако се наведе име аутора на начин одређен од стране аутора или даваоца лиценце и ако се прерада дистрибуира под истом или сличном лиценцом. Ова лиценца дозвољава комерцијалну употребу дела и прерада. Слична је софтверским лиценцама, односно лиценцама отвореног кода.